A Dissertation

entitled

Biomedical Applications of Magnesium Phosphate Nanoparticles

by

Maryam Nabiyouni

Submitted to the Graduate Faculty as partial fulfillment of the requirements for the

Doctor of Philosophy Degree in Engineering

_____
Dr. Sarit B. Bhaduri, Committee Chair

_____
Dr. Arunan Nadarajah, Committee Member

_____
Dr. Scott C. Molitor, Committee Member

_____
Dr. Beata Lecka-Czernik, Committee Member

_____
Dr. Eda Yildirim-Ayan, Committee Member

_____
Dr. Patricia R. Komuniecki, Dean
College of Graduate Studies

The University of Toledo

December 2014

An Abstract of

Biomedical Applications of Magnesium Phosphate Nanoparticles

by

Maryam Nabiyouni

Submitted to the Graduate Faculty as partial fulfillment of the requirements for the
Doctor of Philosophy Degree in
Engineering

The University of Toledo

December 2014

The focus of this dissertation is synthesis and biomedical applications of magnesium phosphate nanoparticles. Phosphates of alkaline earths such as calcium phosphates (CaPs; also synonymously referred to as apatites) have long been known as biocompatible orthopedic substituents. Like calcium, magnesium belongs to the alkaline earths. However, magnesium phosphates (MgPs) are not as well studied as the CaPs even though they are effective scaffold materials and potential nonviral DNA carriers. Hence, it is important to investigate MgPs in depth. Relatively open structures of apatites provide them with possibilities for various substitutions.

Present research focuses on the applications of magnesium phosphate nanoparticles as promising biomaterials with a focus towards orthopedic uses. The relevance of these apatite nanoparticles in biomedical applications depends on the efficiency and speed of the synthesis process as well as the biocompatibility since the ease of production method and lack of cytotoxicity are some of the most crucial factors for mass production of biomaterials. Consequently, as explained below, the goal of this study is to provide an efficient production method for these apatites via a novel microwave assisted synthesis

method (MAS), investigate their bioactivity, and examine their applications as scaffolds in orthopedics, and carriers in gene delivery.

Amorphous magnesium phosphate nanoparticles were synthesized utilizing a novel, and rapid microwave assisted synthesis (MAS) method. In this methods, the household microwave generated rapid heating and cooling to promote generation of nanoparticles. The ability to control the heating time and power, and speed are some advantages of the applied methods for quick production of nanoparticles of interest.

The as-synthesized materials were characterized using Scanning Electron Microscopy (SEM), Transmission Electron Microscopy (TEM), X-ray Diffraction (XRD), and Fourier Transform Infrared Spectroscopy (FTIR). In vitro studies were conducted on mouse osteoblasts using CytoTox96 assay. The fluorescent microscopy was used as the imaging method.

The goal of this study is to investigate the application of MgPs as orthopedic scaffolds, stimulator of osteoblastic proliferation, and gene delivery vectors. To evaluate the applicability of MgPs in orthopedics, first, magnesium phosphate nanoparticles were compared to commonly used calcium phosphates, and magnesium substituted calcium phosphate nanoparticles. Subsequently, amorphous magnesium phosphates (AMP) mixed with the electrospun polylactic acid (PLA) fibers demonstrated the ability to stimulate a series of cell responses leading to proliferation and differentiation of preosteoblasts. Later, the ability of AMP nanoparticles to transfect the mouse osteoblasts were studied via fluorescent microscopy. Plasmid vectors containing green fluorescent protein (GFP) were used to examine the nanoparticles as efficient gene carriers.

To my parents, Masoumeh and Hossein

Acknowledgements

I would like to express my gratitude to my advisor, Dr. Sarit B. Baduri, for giving me the opportunity to work under his supervision. His support, motivation, enthusiasm, and knowledge helped me throughout this study. Also, I am thankful for the other members of my dissertation committee, Dr. Beata Lecka-Czernik, Dr. Scott Molitor, Dr. Arunan Nadarajah, and Dr. Eda Yildirim-Ayan for their guidance.

I would like to indicate appreciation for my friend and colleague Dr. Huan Zhou for providing me with the guidance in different parts of this dissertation.

Also, I am thankful for Tamara (Tammy) L. Phares in the Bioengineering undergraduate lab. Her expertise, enthusiasm, and passion for helping students has played a crucial role in completing this dissertation.

Finally, I am most indebted to my family and friends especially my parents, Hossein and Masoumeh, my sister, Nasim, and my brother, Ehsan, for their love and support throughout my life.

Table of Contents

List of Tables

List of Figures

List of Abbreviations

α-MEM.....alpha minimum essential medium

AMP.....Amorphous magnesium phosphate

ACP.....Amorphous calcium phosphate

BMP-2.....Bone Morphogenic Protein-2

CaP.....Calcium phosphate

CMP.....Calcium magnesium phosphate

DMF.....Dimethylformamide

DSC.....Differential scanning calorimetry

FBS .....Fetal Bovine Serum

FTIR.....Fourier transform infrared spectroscopy

HA.....Hydroxyapatite

HSA.....12-hydroxysteric acid

ICDD.....International Center for Diffraction Data

MAS.....Microwave assisted synthesis

MgP.....Magnesium phosphate

ORF .....Open Reading Frame

PDF .....Powder Diffraction File

PLA.....Poly lactic acid

SBF .....Simulated body fluid

SEM .....Scanning electron microscopy

Tc .....Crystallization temperatures

Tg .....Glass transition temperature

Tm .....Melting temperature

TCP .....Tricalcium phosphate

TEM .....Transmission electron microscopy

TGA .....Thermogravimetric analysis

XRD .....X-ray diffraction

Chapter 1

Introduction

1.1 Overview

Bone deficiency caused by trauma and various diseases affect millions of people world wild, every year. Parallel to an increase in the human life span, it is expected to observe a larger population of elderlies who suffer from different skeletal disorders such as osteoporosis, arthrodesis, lower back pain, etc. The ideal treatment method consists of the replacement of the defective hard tissue with the materials that can promote the growth of healthy bone. Autologous bone transplants are used in majority of cases. However, this method is not ideal as it does not eliminate the need for a second surgery and it may cause other complications like extending the recovery time, infections, long-lasting pains, and higher cost. As a result, the scientific community's quest is to find bone graft substitutes which are capable of promoting the bone growth while eliminating the need for a second surgery. Numerous materials such as polymers, ceramic-polymer composites, metals, glasses, and ceramics have been tested as the potential bone graft substitutes. However, majority of these substitutes failed to provide characteristics which are similar to the natural bone such as the adequate strength and biodegradability. As a result, many researchers have

considered calcium phosphates (CaP), especially hydroxyapatites (HA; $Ca_5(PO_4)_3OH$), β-tricalcium phosphate (β-TCP; $Ca_3(PO_4)_2$), and biphasic calcium phosphates (BCP), as an effective bone substitute due to the presence of carbonated apatites (65%) in human bones.

Although calcium apatites have shown great potential as bone substitutes, they are not the only potential candidates. Over the last few years, magnesium substitution in the structure of calcium phosphates have been shown to enhance the mechanical properties, biocompatibility, and biodegradability of the resulting magnesium substituted calcium phosphates [1, 2]

Despite the lack of sufficient number of studies, pure magnesium phosphates have been introduced as an alternative to CaPs for orthopedic applications. Previously, magnesium was used as a dopant for calcium based biomaterials. However, recent studies demonstrated that magnesium phosphate based biomaterials can be directly applied in orthopedics [3].

Higher biocompatibility and faster degradation rate of magnesium phosphates compared to the CaPs [3] make them advantageous over the commonly used CaPs for various clinical purposes. Magnesium phosphates' injectability, high strength, and suitable setting time can be applied in production of bone cements [4], while magnesium phosphate nanoparticles can be used in production of magnesium phosphate-polymer composite scaffolds, and as gene and drug delivery vehicles.

Rest of this dissertation is organized as following: Chapter 2 presents a comprehensive review of the state-of-the-art developments on magnesium based bioceramics and their applications in orthopedics. The results reported in Chapter 3 compares the physical and biological characteristics of pure magnesium phosphate,

magnesium substituted calcium phosphates, and pure calcium phosphates. A variety of material characterizations, degradation and biological testing are executed to confirm different properties of the studied materials. Subsequently chapters 4 and 5 present two important applications of magnesium phosphate nanoparticles. Chapter 4 presents magnesium phosphate nanoparticles in composition with polylactic acid (PLA) polymers as orthopedic scaffolds, while chapter 5 shows the application of magnesium phosphates as plasmid DNA carriers.

Chapter 2

Magnesium-based Bioceramics in Orthopedic Applications: A Review

2.1 Abstract

Magnesium-based bioceramics include a large group of magnesium containing compounds such as oxides, phosphates and silicates, that are involved in orthopedic applications like bone cements, bone scaffolds, implant coating, and even as DNA carriers. Magnesium ions are directly involved in numerous biological mechanisms; for example, Mg^{+2} ions play an important part in the regulation of ion channels, DNA stabilization, enzyme activation, and stimulation of cell growth and proliferation. This alkaline earth metal has gained great popularity in orthopedic applications in recent years. However, a comprehensive review on different magnesium-based bioceramics including different production methods and orthopedic applications is still missing in the literature. This paper presents a comprehensive review of magnesium containing materials for biomedical applications. In this paper, the magnesium-based bioceramics are divided into three major systems based on their compositions and applications. Magnesium phosphates (MgO-P_2O_5), calcium magnesium phosphates (CaO-MgO-P_2O_5), and magnesium glasses (SiO_2-MgO) are the major systems reviewed here. Prior to presenting different Mg-containing

bioceramic systems, biological roles of magnesium are discussed. The remainder of the paper is organized into three main sections according to the three classes of materials described above. Each main section contains sub-sections such as materials and synthesis aspects, applications (e.g., bone cements, gene delivery, etc.) and ends with the future directions section.

2.2 Introduction

Human bones have multiple functions in our bodies and are crucial components of the skeleton. Support, movement, protection, blood cell production, storage, endocrine regulation, and sexual dimorphism are the main functions of human bones. Although human bones are naturally designed for their sophisticated functions, and are capable of physiological remodeling, removal and self-healing, they are unable to cope with the negative effects of extensive defects, and large-scale fractured bones are rarely self-healed. Bone problems such as numerous fractures, low back pain, osteoporosis, scoliosis and other musculoskeletal problems affect millions of people worldwide. Indeed, the percentage of people over 50 years of age suffering from bone and joint diseases is predicted to double by 2020 [5]. These statistical data confirm the great need of the scientific and clinician communities for inventing novel, efficient ways to address the bone and joint problems of this growing population.

Currently, autografts, allografts and xenografts are the most common methods of bone treatment [6, 7]. Even though these methods are reasonably effective in many cases, they are associated with certain limitations. For instance, providing adequate autografts is challenging in large defective areas such as in the case of spinal arthrodesis [8]. Allografts

are great alternatives in some procedures; however, they are associated with other issues like the immunologic problems, low osteogenicity, and higher rate of resorption compared to the autogenous bones [9]. The invasive nature of these methods makes them susceptible to possible infection, rejection, and disease transmission [8, 10]. High cost of graft supply and surgery procedures is some of the financial burdens limiting their use in the orthopedic applications [8, 11].

A great need for bone substitutes and the aforementioned limitations of the already existing materials encourage scientists in their quest for more reliable bone substitutes with biological and physical properties comparable to human bones. In seeking the "Holy Grail" in biomaterials research, three different generations are identified: bioinert materials (first generation), bioactive and biodegradale materials (second generation), and materials designed to stimulate specific cellular responses at the molecular level (third generation) [12]. Among bone substitute materials, first-generation materials are still successfully used in a wide range of applications while third-generation materials can open new possibilities of treatments and applications, but they are not meant to replace materials from previous generations [5]. In general, recent bone substitutes consist of metals, ceramics, biological or synthetic polymers, and their composites, all either bioinert or bioactive in nature. The ideal basic premise, is that the materials will be resorbed and replaced over time by, and in tune with, the body's own newly regenerated biological tissues [13]. A case in point is the recent development of biodegradable magnesium and its alloys [14, 15]. To put the subject in proper perspective, Figure 2-1 represents the results of a bibliographical search using Scopus database with key phrases such as "Magnesium Biomaterials", "Magnesium Alloy Biomaterials", "Magnesium Phosphate Biomaterials", and "Magnesium Phosphate

Bioceramics". The rationale here is that the first keyword represents an all-inclusive picture while the second phrase represents magnesium alloys *per se,* while the last two phrases are directly associated with magnesium phosphates, the key focal point here.

Figure 2-1 summarizes a few key trends in the growth of Mg-containing biomaterials. First, the data are collected from 1990 up until this year. The single reason for choosing 1990 as the initial year is that there was no activity around that time. Between 1990 and 2000, there have been some sporadic activities, while there is some growth between 2000 and 2006. Since 2006, there has been exponential growth in research, with the year 2012 representing the current maximum. It is expected that this year will experience a further growth of activities beyond the level of 2012. Second, from the data, it is obvious that the bulk of the activities take place in Mg-alloys. Third, it is interesting to note that along with the growth in activities in Mg-alloys, Mg-phosphates are also attracting the attentions of researchers. As opposed to the number of papers published in Mg-alloys, the number of papers in Mg- phosphates is about half. Nevertheless, there is an increasing trend in activities. We suspect that this increasing growth rate in activities is tied to the developments that are taking place in Mg-alloys.

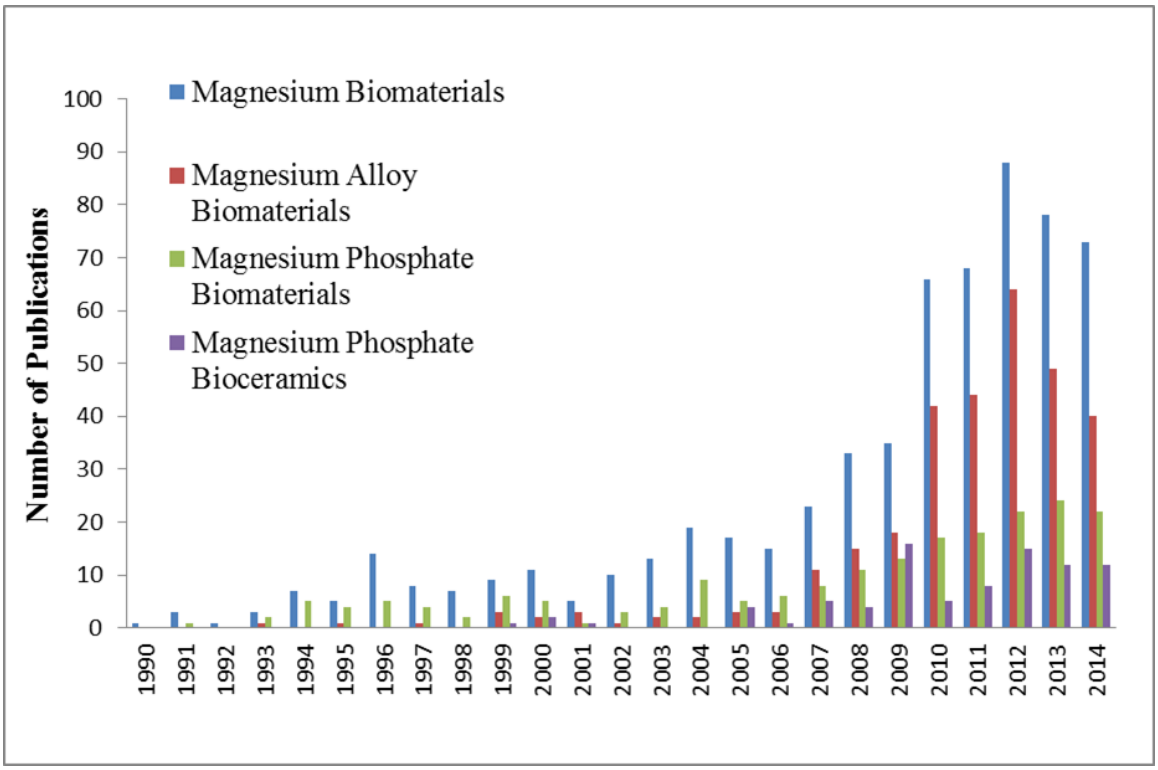

Figure 2-1: Key words and quantity of magnesium-related studies over the last 20 years (1990-2014) [16].

Because of this growth in research activities, there are some excellent review papers on biodegradable Mg-alloys. References [17-24] represent some of the important review papers. The paper by Witte gives a nice perspective of the historical aspects of these alloys [25, 26]. The global activities in the development of Mg-alloys are reviewed in references [17, 18, 20]. Interestingly, to the best of our knowledge, there is no such review available on Mg-containing bioceramics including Mg-phosphates. Hence, this review is presented to emphasize that all of these materials have applications in orthopedics and dentistry.

This review attempts a comprehensive review of all Mg-containing bioceramics. The motivation behind this review is the absence of any published effort of this kind. Secondly, as mentioned before, the research in Mg-containing bioceramics is complementary to the

research in Mg-alloys. For the purpose of this review, it covers three different important classes of Mg-containing bio ceramics: 1) $MgO–P_2O_5$ resulting in magnesium phosphates; 2) $CaO\text{-}MgO\text{-}P_2O_5$ resulting in calcium magnesium phosphates; and $MgO\text{-}SiO_2$ which are magnesium silicate glasses. Rest of the paper is organized as follows. Section 2 discusses the role of Magnesium in the human body. Section 3 comprehensively discusses various aspects of the magnesium phosphates, starting off with materials aspects. For example, section 3.1 is followed by applications such as in cements (section 3.2.1) and gene delivery (section 3.2.2). This section concludes with future directions of development (section 3.2.3). The two other main topics are also laid out following a similar format.

2.2.1 Role of Magnesium in the Human Body

In order to emphasize the potential of magnesium containing ceramics in orthopedic applications, a thorough understanding of the physiological roles magnesium plays in human body is addressed first.

Magnesium ions are the fourth most abundant cations in mammalians behind sodium, potassium, and calcium, and also the second most prevalent intracellular cation [18, 19]. Inside mammalian cells magnesium plays multiple essential roles including: regulation of calcium and sodium ion channels, stabilizing DNA, cofactor and catalyzer for many enzymes, and stimulating cell growth and proliferation [19-21].

On average, adult human bodies contain 1000 mmol [18] or about 24.00 g [22] of magnesium, mostly stored in the bones [18], although it decreases by age [22]. More than one half the magnesium supply of adult humans is stored in their bones [23, 24]. One third is stored in muscles, and a small amount (about 1%) is present in the extracellular space

[23]. Table 2.1 illustrates the total distribution of magnesium in human body. Serum concentration of magnesium varies. It normally ranges between 0·75 and 0·95 mmol/L [18].

Table 2.1: Total distribution of magnesium in the human body **[22, 27]**

Location	**Percent of total**	**Magnesium content* (mg)**
Bone	53	12,720
Muscle	27	6,480
Soft tissue	19.2	4,608
Erythrocyte	0.5	120
Serum	0.3	72
Total	100	24,000

*Data For 70-kg adult humans

Inside the cell, magnesium cations are mostly found in Mg-ATPase complexes, bound to the mitochondria and the extracellular membrane, bound to a variety of proteins and enzymes, in endoplasmic reticulum, and even inside the nucleus [21]. The intracellular magnesium is illustrated in Figure 2-2. As a result, the concentration of free magnesium is very low in the intracellular space [22]. Although the concentration of magnesium is not regulated by specific hormones as opposed to calcium and sodium, it is tightly regulated via the gastro-intestinal tract and the kidneys [27, 28]. In case of deficiency, magnesium can be released from the bones and the muscles [23]. Magnesium deficiency can be due to decreased intake or increased loss via thiazide diuretics [29].

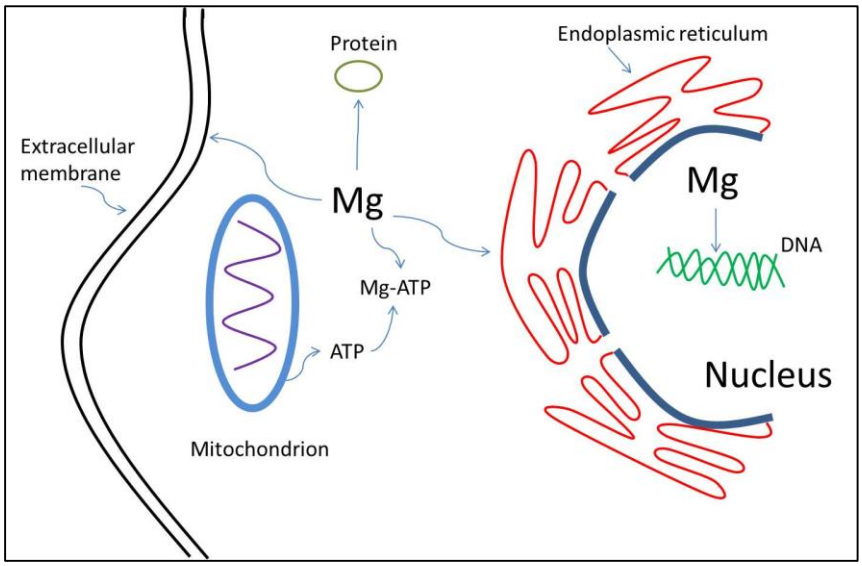

Figure 2- 2: Major roles of intracellular magnesium

Magnesium uptake is crucial for growth and maintenance of human tissues as shown in Table 2.2. Its deficiency leads to numerous health problems. According to the U.S. Food and Nutrition Board the Recommended Dietary Allowance (RDA) for

magnesium for adult males is 420 mg/day and for adult females is 320 mg/day [30]. Magnesium deficiency can lead to multiple disorders.

Table 2.2: Illustrates a list of health issues directly related to magnesium depletion [18]

Neuromuscular	**Cardiovascular**	**Metabolic**	**Bone**
Trousseau and Chvostek signs	Widening of QRS complex	Carbohydrate intolerance	Osteoporosis and osteomalacia
Carpopedal spasm	prologation of PR interval	Hyperinsulinism	
Seizures	inversion of T wave, U waves	Atherosclerosis	
Vertigo and ataxia	Severe ventricular arrhythmias		
Muscular weakness	Sensitivity to cardiac glycosides		
Depression, psychosis			

Magnesium content is 0.44wt% of enamel, 1.24wt% of dentin and 0.72wt% of bone in an adult human [31]. Magnesium deficiency is linked to low bone mass, reduced bone growth, osteoporosis, and increased skeletal fragility [30]. Studies in humans and rat models demonstrated magnesium deficiency can cause three phenomena: 1) low serum parathyroid hormone (PTH) and calcitriol, the hormonally active form of vitamin D, levels, which may contribute to reduced bone formation; 2) an increase in substance P, a neuropeptide, which in turn stimulates production of cytokines to intensify osteoclastic bone resorption; 3) a decrease in osteoprotegerin (OPG) and an increase in receptor activator of nuclear factor *kB* ligand (RANKL) favoring an increase in bone resorption [32]. Another key role of Mg in bone is related to adhesion and growth of osteoblastic cells [22]. The interactions between osteoblast cells and biomaterial surfaces are thought

to be mediated primarily by membrane-associated adhesion receptors belonging to the integrin superfamily, which are transmembrane proteins consisting of noncovalently associated α and β subunits [33]. The extracellular domain of the α-subunit needs to bond to divalent cations such as Mg^{2+} and Ca^{2+} and the change of extracellular ions can modify the integrin affinity to their respective ligands [34, 35]. Thus, Mg is an essential element in human body and its addition to bioceramics can play an important role in the bioceramics bone interaction and bone tissue development. Hence, the importance of bioceramics such as magnesium phosphates, which are discussed in details in the following.

2.3 $MgO-P_2O_5$ System

2.3.1 Materials and Synthesis Aspects

This section introduces the $MgO-P_2O_5$ system, which forms the core of this review. Compared to the $CaO-P_2O_5$ (Ca-P) system, the $MgO-P_2O_5$ (Mg-P) system has been studied to a much lesser extent. For example, two facts have motivated the development of range of calcium-phosphate-based orthopedic cements. First is the well-known fact that mammalian bone minerals consist of calcium phosphates. The second and not so well appreciated reason is that the cement-forming ability of calcium phosphates has been utilized in traditional high-temperature refractories for more than five decades [36, 37]. Likewise, the compounds of the Mg-P system have been used in agricultural, environmental, and civil engineering fields [38-42], yet unlike their Ca-P counterpart, Mg-P did not receive their well-deserved attention in the biomedical fields, perhaps due to the overwhelming attention given to Ca-P and lesser appreciation of the role of Mg in the human body.

A summary of important magnesium phosphate compounds is given in Table 2.3 [43-48], in a format allowing comparison to their well-known calcium phosphate counterparts, which are presented in the same format in Table 2.4.

Table 2.3: Magnesium phosphate phases with potentials in orthopedic applications [49]

Compound	**Chemical Formula**	**Crystal System**	**Lattice Parameter (Å)**	**Solub. 37 ˚C pK_{sp}**	**Den. (g/cm^3)**	**Mg/P**
Dimagnesium phosphate trihydrate (Newberite)	$MgHPO_4.\ 3H_2O$	Ortho.	10.203, 10.678, 10.015	5.8	2.122	1
Dimagnesium ammonium phosphate hexahydrate (Struvite)	$MgNH4PO_4.6H_2O$	Ortho.	6.9660, 6.1420, 11.217	13.27	1.698	1
Amorphous magnesium phosphate (AMP)	$Mg3(PO_4)_2$ (Amorphous)	N/A	N/A	15.9	N/A	1.5
Trimagnesium phosphate octahydrate (Bobierrite)	$Mg_3(PO_4)_2.8H_2O$	Mono.	4.6670, 27.926, 10.067	25.2	2.133	1.5
Trimagnesium phosphate docosahydrate (Cattiite)	$Mg_3(PO_4)_2.22H_2O$	Tri.	6.9020, 6.9610, 15.982	23.1	1.639	1.5

Table 2.4: Properties and crystallographic data of calcium phosphates [31]

Compound	**Chemical Formula**	**Crystal System**	**Lattice Parameter (Å)**	**Solub. 37˚C pK_{sp}**	**Den. (g/cm^3)**	**Ca/P**
Monocalcium phosphate monohydrate (MCPM)	$Ca(H_2PO_4)_2.H_2O$	Tri.	5.6261, 11.8891, 6.4731	N/A	2.23	0.5
Monocalcium phosphate anhydrate (MCPA)	$Ca(H_2PO_4)_2$	Tri.	7.5577, 8.2531, 5.5504	N/A	2.58	0.5
Dicalcium phosphate dehydrate (DCPD, brushite)	$CaHPO_4.2H_2O$	Mono.	5.8120, 15.1800, 6.239	6.63	2.32	1
Dicalcium phosphate anhydrate (DCPA, monetite)	$CaHPO_4$	Tri.	6.9100, 6.6270, 6.998	7.02	2.89	1
Octacalcium phosphate (OCP)	$Ca_8(HPO_4)_2(PO_4)_4.5H_2O$	Tri.	19.6924, 9.5232, 6.8352	95.9	2.61	1

α-tricalcium phosphate (α-TCP)	α-$Ca_3(PO_4)_2$	Mono.	12.8870, 27.2800, 15.219	25.5	2.86	1.5
β-tricalcium phosphate (β-TCP)	β-$Ca_3(PO_4)_2$	Rhombo.	10.4391, 10.4391, 37.3756	29.5	3.07	1.5
Amorphous calcium phosphate (ACP)	$Ca_x(PO4)_y.nH_2O$	N/A	N/A	N/A	N/A	1.2-2.2
Calcium deficient hydroxyapatite (CDHA)	$Ca_{10-x}(HPO_4)_x(PO_4)_{6-x}(OH)_{2-x}$ $(0<x<1)$	N/A	N/A	85.1	N/A	1.5-1.67
Hydroxyapatite (HA)	$Ca_{10}(PO_4)_6(OH)_2$	Hexa.	9.4302, 9.4302, 6.8911	117.2	3.16	1.67
		Mono.	9.8421, 19.6842, 6.8814			
Tetracalcium phosphate (TTCP)	$Ca_4P_2O_9$	Mono.	7.0230, 11.9860, 9.4730	37-42	3.05	2

Important similarities and dissimilarities are easily discernible from these two tables. It is seen that the most important compounds in the Mg-P system have Mg/P ratios of 1 and 1.5. Likewise, in the Ca-P system, Ca/P ratios of 1 and 1.5 are related to important compounds of orthopedic significance such as dicalcium phosphate anhydrous DCPA (monetite), dicalcium phosphate dihydrate DCPD (brushite), and tri-calcium phosphate (TCP). It is well known that, in the Ca-P system, Ca/P ratios can vary from 0.5 to 2.0. Compounds with very low Ca/P ratios (0.5) are too acidic to be of any importance. An important compound in the Ca-P system, hydroxyapatite (HA), with a Ca/P ratio of 1.67, does not occur in the Mg-P system. Other than brushite, and octa-calcium phosphate (OCP), other calcium phosphates do not have water of crystallization in their structures. In contrast, most of the magnesium phosphates are hydrated at low temperature. These compounds ($Mg(H_2PO_4)_2 \cdot xH_2O$ (x = 4, 2, 0), $MgHPO_4 \cdot yH_2O$ (y = 3, 7), and $Mg_3(PO_4)_2 \cdot zH_2O$ (z = 8, 22) can be synthesized via precipitation in aqueous solutions [49, 50]. The complex phase relationship between these hydrated phases has been reported by Brown *et al*., as shown in

Figure 2-3 [49]. Reference 44 is the most comprehensive phase diagram and mostly agrees with the previously reported Russian results [51, 52].

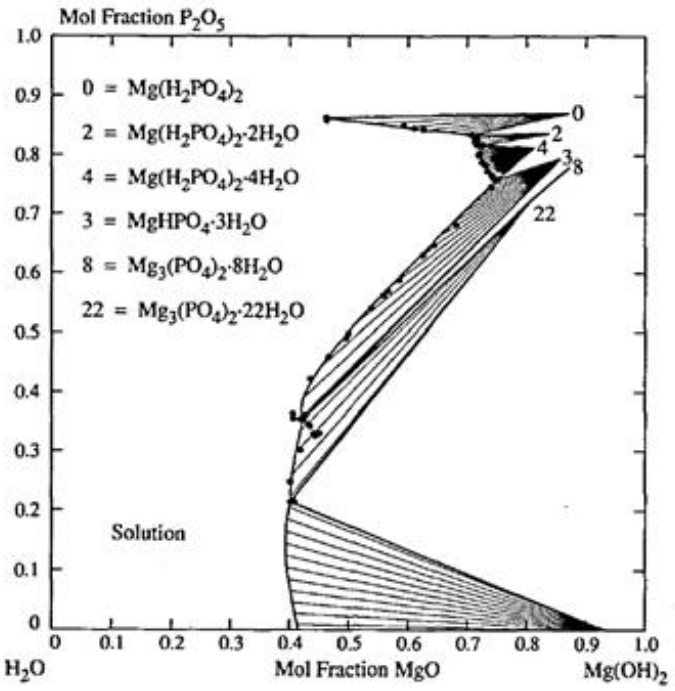

Figure 2-3: Ternary System $MgO-P_2O_5-H_2O$ at 25 °C [49]

The important features of this diagram are follows. The diagram is drawn according to the convention devised in the construction of previously complied $CaO-P_2O_5-H_2O$ phase diagram [53]. This involves plotting the concentrations as $(\text{mole fraction})^{1/2}$. This plotting scheme enables simultaneously presenting the solubility data over several orders of magnitude while also indicating the crystallization paths. An important conclusion is that with the exception of newberyite, most of the Mg-phosphates show incongruent solubility. The diagram shows six different hydrated Mg-phosphates with varied amounts of water of crystallization. The data show greater solubility range for x = 2 as opposed to y = 3, an important piece of information for the setting reactions in cements. As an example, the dissolution of cattiite yields a solution saturated with newberyite but unsaturated with cattiite and results in the precipitation of the latter. The diagram also presents a conclusive

resolution of a controversy to prove that incongruent dissolution of bobierrite to cattiite is not possible.

The high-temperature calcination can convert these materials into either magnesium pyrophosphate ($Mg_2P_2O_7$) or magnesium orthophosphate ($Mg_3(PO_4)_2$) [54, 55]. Like the Ca-P compounds, compounds in the Mg-P system can accept other cations such as NH_4^+, Na^+, and K^+ to result in new materials with modified physical properties [54, 56-59]. Finally, all of the compounds listed in

Table 2.3 are resorbable and therefore are very important for orthopedic applications. Newberyite is as reactive as monetite and brushite, while bobierrite and cattiite have solubility similar to that of TCP. Since the biodegradability of monetite, brushite and TCP are well known, the Mg-P compounds can be as effective as their Ca-P counterparts, and with additional benefits such radio-opacity and high strength.

Unlike in the Ca-P system, compounds containing NH_4^+ occur in the Mg-P system, and their uniqueness has been noted in the literature. Such compounds include dittmarite (dimagnesium ammonium phosphate monohydrate, $MgNH4PO_4.6H_2O$), schertelite (dimagnesium ammonium phosphate tetrahydrate, $MgNH4PO_4.4H_2O$) and struvite (dimagnesium ammonium phosphate hexahydrate, $MgNH4PO_4.6H_2O$). Some of these phases result in better mechanical properties e.g., struvite-containing compositions. There is no equivalent phase in the Ca-P system [57].

2.3.2 Applications

Though magnesium phosphates are components of minerals such as kidney stone and bone, there is limited work studying the interactions between magnesium phosphates and bone

cells. Few researchers like Tamimi *et al.* [60] and Zhou *et al.* [61] have studied the impact of magnesium phosphate on osteoblastic cells.

2.3.2.1 Bone Cements

As previously mentioned, the motivation for the formation of orthopedic CPCs came from traditional ceramic industries [58, 62]. Likewise, MPCs have been studied in civil engineering. U.S. patent 2,391,493, issued in 1942, is related to the development of the first MPC for repairing concrete, albeit without addressing much in the way of scientific issues [63]. This cement actually used a reaction between MgO and ammonium phosphate. More specifically, most MPCs with civil engineering applications use either ammonium dihydrogen phosphate or diammonium hydrogen phosphate. Abdelrazig *et al.* [64] and Popovics *et al.* [65] made some important early scientific contributions on the first kind of NH_4^+-containing cements. Recent developments toward the understanding of the setting process and microstructure development are provided in references [66, 67]. Wagh and Jeong made important scientific contributions toward understanding the setting reactions of MPCs [68, 69]. Briefly, the hardening of MPCs takes place by an acid-base reaction between magnesia (MgO) and some compounds containing ammonium and phosphate ions [42, 57]. Soudee *et al.* investigated the setting mechanism of magnesium phosphate cement based on MgO and monoammonium dihydrogen phosphate. MgO is dissociated to MgO^{2+} and reacts with six water molecules resulting in $Mg(H_2O)_6^{2+}$ complexes. These complexes are big enough to avoid adsorption of water molecules to the MgO surface. Crystallization of struvite structure takes place with PO_4^{3-}, NH^{4+} and $Mg(H_2O)_6^{2+}$ bound together with hydrogen bonds [66]. Figure 2-4 illustrates the struvite crystal development process [66,

67]. Diammonium hydrogen phosphates reacting with MgO can also harden, but the mechanical properties are not ideal [70, 71]. The important features of NH_4^+-containing cements are as follows. First, while the primary phase developed in most cases is struvite, newberyite can also be present in the MPC structure as a by-product, since struvite is not very stable [62]. Other phases such as dittmarite and schertelite can also form. Second, the formation of the phase assemblage is dictated by the liquid to powder (L/P) ratio. Third, most of these cements form exothermically, with temperatures reaching 60°C to 80°C with rapid setting, which is indeed an undesirable property. In order to counteract it, boric acid or borax has been added in small amounts as retarders. The retardation of the setting has been explained by the formation of a thin coat on the surfaces of MgO particles with lunebergite ($Mg_3B_2(PO_4)_2(OH)_6.6H_2O$) [72]. Finally, most of the MPCs have significantly higher strengths than CPCs [71, 73, 74]. A possible explanation could be the reduction of porosities in the cement and/or formation of non-equiaxed (e.g., needle-like/plate-like) morphologies [66].

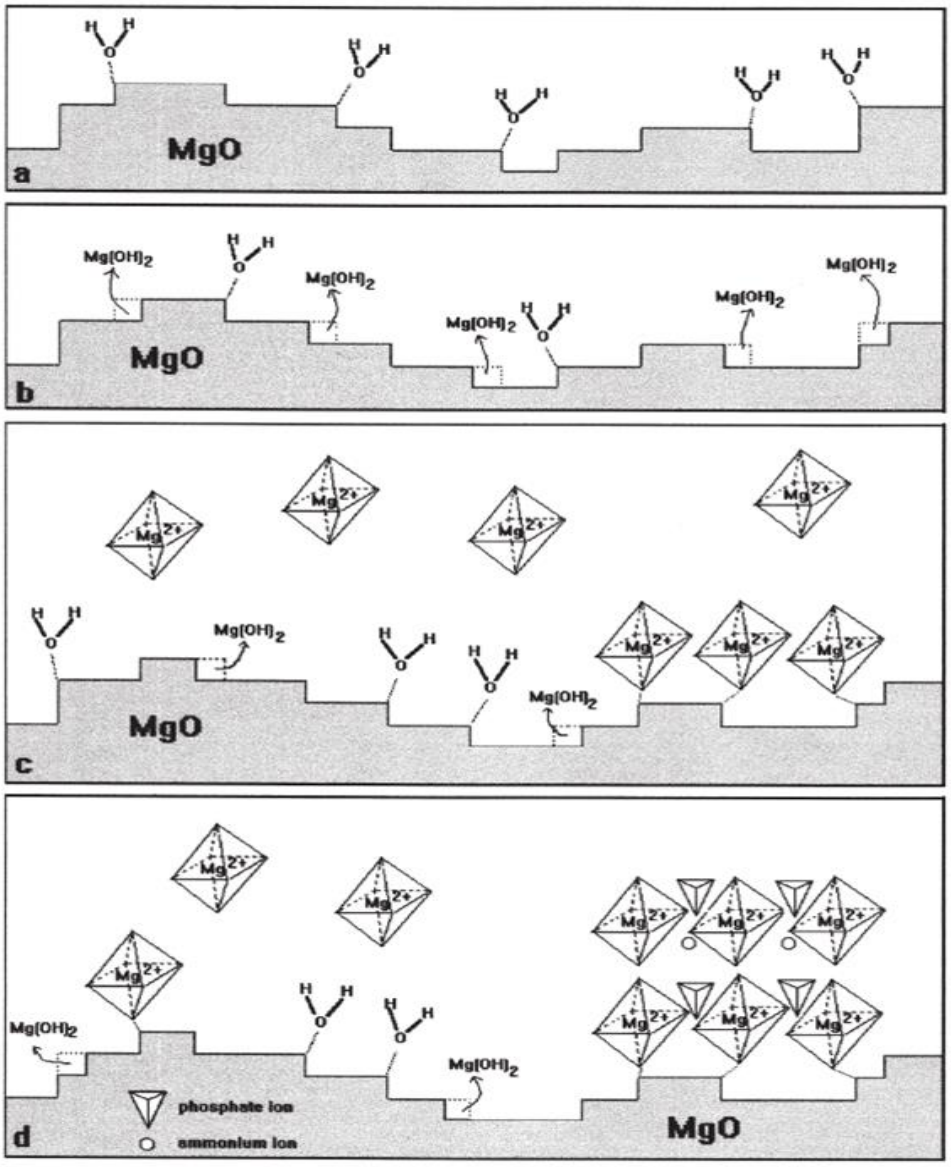

Figure 2-4: Development process of struvite crystal [66, 67]

As far as orthopedic applications of MPCs are concerned, the Barcelona group in 1995 reported an MPC based on the reaction of monetite (DCPA, $CaHPO_4$), MgO, and hayesite ($MgHPO_4.2H_2O$) [75]. The obvious cue was given by CPCs. The predominant phase was bobierrite, with brushite dispersed in it. Strictly speaking, this was a composite of CPC and MPC. This MPC composition could induce bone formation after 8 weeks of

implantation in rats. However, this cement was not as strong as CPCs. Since that initial work, little progress was made for the next two decades until the publications of recent papers. Waselau *et al.* compared biocompatibility and bone adhesive characteristics of MPC, CPC, and sham samples in horses [76]. Seven weeks after implantation, it was observed that MPC secured fragments significantly closer to parent bone, compared with a CPC. Callus amount and bone remodeling and healing were significantly greater with MPC than with CPC. MPC in general exhibits greater early/final strength, comparable biocompatibility, and a higher dissolution rate than CPCs. With regard to mechanical strength, MPC shows enhanced values compared to CPCs. In Germany, Moseke *et al.* prepared an MPC of struvite and newberyite via the reaction between farringtonite and diammonium hydrogen phosphate ($(NH_4)_2HPO_4$) [77]. The prepared MPC exhibited an average compressive strength of 64.55 MPa after 24 hours setting. However, there are two limitations of the product: 1) the setting is an exothermic process with a temperature rise of the cements to 58–72˚C during setting; 2) the setting time is too short for clinical applications. In newer contributions from Barcelona, Mestres and Ginebra prepared an MPC by mixing magnesium oxide (MgO) with either sodium dihydrogen phosphate (NaH_2PO_4) or ammonium dihydrogen phosphate ($NH_4H_2PO_4$), or an equimolar mixture of both [78, 79]. After 2 hours setting, MPCs reached a compressive strength of 30-50 MPa, much higher than that of the CPC control (5 MPa). The ammonium-containing MPC resulted in struvite as the major reaction product, whereas the MPC prepared with sodium dihydrogen phosphate resulted in an amorphous product. Unreacted magnesium oxide was found in all the formulations. Except for demonstrating greater early strength, this work introduces two concepts in developing MPCs. First, the addition of borax to MPC can

decrease the maximum temperature (e.g., 110 to 42˚C) and improve setting time. Second, excessive MgO in MPC can improve compressive strength and provide antibacterial properties. In our realm of activities, our group has developed a microwave assisted technology that can significantly reduce maximum temperature of MPCs [80]. In this process, the template MPC was produced by the reaction of $Mg(OH)_2$ and phosphoric acid, showing maximum temperature of 65 ˚C and compressive strength of 13 MPa after 24 hours setting. In the new process, the as-mixed MPC paste was treated via microwave to form solid MPC powders. These as-prepared MPC powders can further become solid after subsequent exposure to water, with a maximum generated temperature of 25 ˚C and compressive strength of 30 MPa after 24 hours setting. This phenomenon is attributed to two facts: 1) the hydrogel of PO_4^{3-}, H^+ and $Mg(H_2O)_6^{2+}$ for newberyite network construction in MPC paste can be temporarily dehydrated by microwave irradiation, while preserving the activity of this mixture; 2) the rapid reaction between acidic and basic sources can result in a network with high porosity since partial reactants are isolated from local acid attack by the formed network. This causes reduction in final strength of cement and formation of AMP phase. In the new process, the crushing and subsequent mixing with water of as-prepared MPC powders can re-construct the cement crystal network, reduce AMP content and reduce the porosity of the cement structure, thus resulting in higher compressive strength.

For the aspects of biocompatibility and dissolution, some *in vitro* and *in vivo* studies are published in the literature. Klammert *et al.,* in Germany, reported a 15-month *in vivo* study of newberyite, struvite, and brushite (DCPD, $CaHPO_4.2H_2O$) cement implants [3]. After 15 months, struvite presented the highest loss of mechanical performance (95%),

followed by newberyite (67%), and brushite (41%). This work has demonstrated that the magnesium phosphate compounds such as struvite and newberyite do not only chemically dissolve in a physiological environment, but also present remarkable changes of their phase composition, in which newberyite converted into low-crystalline whitlockite ($Ca_3(PO_4)_2$), and struvite became a mixture of farringtonite ($Mg_3(PO_4)_2$) and whitlockite. Yu *et al.* evaluated the toxicology of MPC, including a gene mutation assay (Ames test), chromosome aberration assay (micronucleus test), and DNA damage assay (unscheduled DNA synthesis test) [81]. The results clearly indicated biocompatibility of MPC. Ewald *et al.* provided further proof of bioactivity [82]. As briefly mentioned above, antibacterial properties are another advantage of magnesium phosphate cements (MPCs). In an *in vitro* study, Mestres and Ginebra demonstrated the antibacterial effect of Na^+-containing MPCs in cultures of *Streptococcus sanguinis* [78], a common bacteria involved in dental plaque formation [78].

In summary, there are many papers on NH_4^+-containing MPCs with applications in civil engineering. Struvite is the principal phase with other NH_4^+-containing phases such dittermite, or non-NH_4^+-containing phases such as newberyite also present. Taking the cue from the previous studies, a few reports in the current literature evaluated the biocompatibility and biodegradability of struvite-containing cements. Some of the signatures of these cements are as follows: they all set rapidly with the simultaneous generation of high temperatures. The rapid setting kinetics, however, has been controlled by the addition of boron-based compounds. All of the compositions result in compressive strength values 2-5 times greater than those of CPCs. In animal studies, both struvite and

newberyite have been proven to be biocompatible and biodegradable. Needless to say, due to the dominant presence of magnesium, MPCs are all radio-opaque.

2.3.2.2 Gene Delivery

Another potential application of magnesium phosphates is in gene and drug delivery. Currently, there are two approaches for gene delivery: viral and non-viral [83]. Since viral gene delivery can be associated with problems such as unintentional infection of host cells via insertion of undesired viral genetic materials, many investigators favor the non-viral approach. The inorganic non-viral particles are easy to store due to their resistance against the microbial attack. Also, they can be prepared in an inexpensive way with large quantities produced at a low temperature [84]. It is interesting to note that Bhakta *et al.* reported 100% efficiency in transfection of HeLa cells as a result of DNA loaded magnesium phosphate nanoparticles compared to that of polyfect [84]. Their continued work evaluated magnesium phosphate nanoparticles encapsulating pSVbetagal and pEGFP *in vitro* and *in vivo* [85]. Both tests showed magnesium phosphate nanoparticles were nontoxic. Similar results were also obtained in *in vitro* transfection in COS-7 cells with magnesium phosphate nanoparticles, as compared to commercial transfecting reagent polyfect as well as calcium phosphate nanoparticles. More recently DNA-encapsulated magnesium phosphate nanoparticles were suggested as a safer and more stable DNA vaccine [86]. Magnesium phosphate scaffolds are also capable of effective drug delivery [87].

2.3.2.3 Future Directions

Understanding applications of magnesium phosphates in orthopedic is still in an early stage, though the materials have been known for decades. In cement related applications, compared to the well-developed CPC system, there is still much room for improving the properties of MPCs. Some possibilities are: 1) composition modification such as removal of NH_4^+ and optimizing MgO content; 2) preparation of composite cements such as adding polymers to create porosity and improve biological responses; 3) evaluation as a drug delivery vehicle; 4) improving handling properties and setting behavior etc. In addition, the beneficial role of Mg^{2+} in gene delivery is rarely studied and magnesium phosphates' potential applications in gene delivery have not been compared to their calcium phosphates counterpart. Magnesium phosphate scaffolds for tissue engineering applications have been scarcely studied [88], although magnesium phosphates exhibit much higher mechanical strength and dissolution rate than calcium phosphates. In addition, in the era of 3D printing, magnesium phosphates in the form of injectable cements or loose fine powders need more comprehensive investigations to be applied as construct scaffolds.

2.4 CaO-MgO-P_2O_5 System

2.4.1 Material and Synthesis Aspects

CaO-MgO-P_2O_5 system mainly refers to magnesium substituted calcium phosphates. In bone structure, the amount of Mg associated with apatite minerals is higher at the beginning of the calcification process, and decreases with increasing calcification [89, 90]. This change results in an increase in crystallinity, as well as thermal stability.

Therefore, it is logical to assume that with more Mg^{2+} content, there is a higher probability to achieve amorphous or nanocrystalline structures with lesser stability and greater dissolution. This section simultaneously addresses the effects of Mg^{2+} substitution into the lattice of calcium phosphates and their synthesis via aqueous media. Synthesis of these compounds in aqueous media is common in the literature, hence this organization. The discussion is based on Mg^{2+} substitution of some of the structures listed in Table 2.4 [31] but not all, since in some cases there have been no reports of Mg^{2+} substitution in those structures. In many cases, the substitution of Mg^{2+} into calcium phosphates can be disruptive to the long range order of the crystalline lattice, resulting amorphous phases which can result in different biological responses.

It is believed that the presence of Mg^{2+} ions can initially retard the nucleation and growth of HA in the biological mineralization process from the precursors ACP and OCP, via blocking of active growth sites through adsorption of Mg^{2+} ions at the crystal surface [91-96]. On the other hand, Abbona *et al.* suggest that magnesium ions can be incorporated into the ACP clusters and HAP pre-nuclei and absorbed on to the surface of ACP and HAP crystallites [97]. Figure 2-5 demonstrates the decrease of Mg/Ca ratios in solid phases with time [97]. It is also noted that, when excessive Mg^{2+} ions are present in aqueous Ca^{2+}, Mg^{2+}, and PO_4^{3-} containing solution, brushite and whitlockite can also form as end products. Boistelle *et al.* studied precipitation of calcium phosphates at 37˚C in urine or aqueous solutions, with calcium and magnesium concentrations close to those of urine [98]. They found that although the solutions are supersaturated with respect to all calcium phosphates, only an amorphous phase (ACP) and brushite precipitate at time zero [98]. Later, ACP transforms either into whitlockite or into apatite depending on the solution composition.

Cheng *et al.* kept neutral aqueous solutions containing [$CaCl_2$] = 1 or 3 mM, [$MgCl_2$] = 0-9 mM, [Na_2HPO_4] = 0.1-90 mM, and NaCl (total 300 mosM) at 37˚C for 21 days [99]. In all solutions containing 1 mM Ca^{2+} ions and in solutions with Ca^{2+} = 3 mM and PO_4^{3-} less than 10 mM, heterogeneous nucleation of OCP (for Mg/Ca less than or equal to 1) or brushite (for Mg/Ca greater than 1) was observed; the former transforming into apatite with time. In contrast, homogeneous nucleation of an unstable amorphous calcium magnesium phosphate occurred in solutions with Ca^{2+} = 3 mM and PO_4^{3-} greater than or equal to 10 mM, transforming into apatite, brushite, and whitlockite (and newberyite) depending on Mg/Ca and PO_4^{3-} values [99].

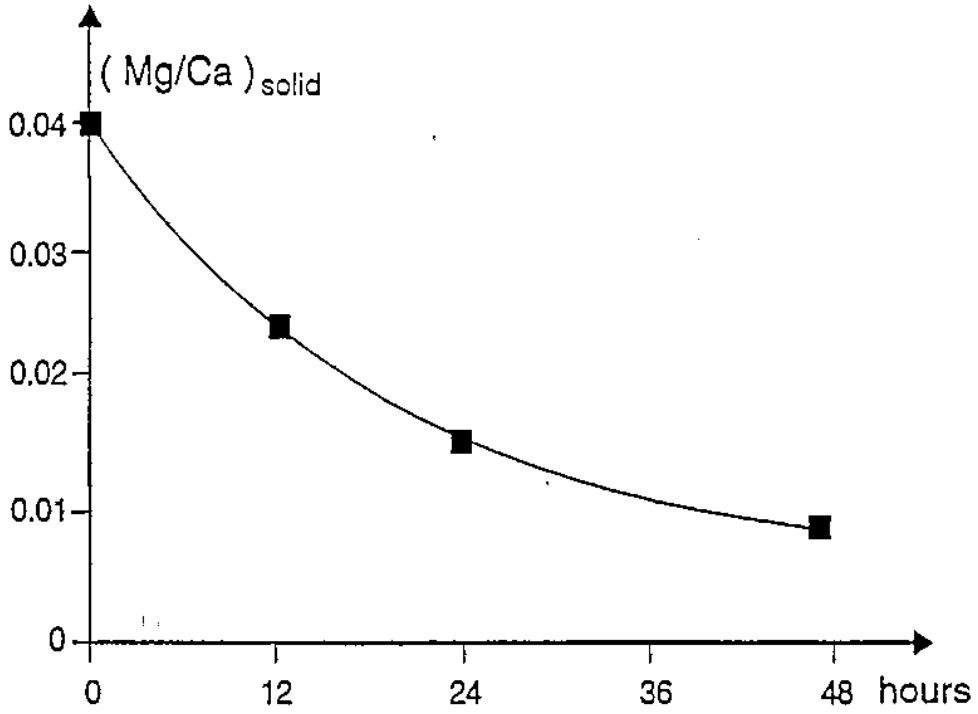

Figure 2-5: Change of the Mg/Ca atom ratio in the solid phases with time [97]

As far as aqueous synthesis of Mg^{2+} substituted HA is concerned, the substitution occurs only for Ca^{2+} in a limited composition range (up to about 10 at.%) [100, 101]. In

line with its smaller ionic radius (0.065 nm), Mg^{2+} substitution for Ca^{2+} causes a reduction in the lattice parameters of HA [102]. Moreover, the degree of crystallinity of Mg-substituted HA decreases with increasing Mg content [100, 101]. In contrast, the total amount of Mg present in the apatitic phases precipitated from aqueous solution can amount to up to 30 at.%, with the excess being in the amorphous phase and/or on the crystal surface [100-102]. Mg-doped HA displays increased solubility with respect to stoichiometric HA, which may be related to reduced crystallinity and/or increased surface hydration [102, 103]. Near-infrared (NIR) and medium-infrared (MIR) spectroscopic data indicated that the samples enriched with Mg^{2+} ions retained more water at their surface than the Mg-free sample, both at the level of H_2O coordinated to cations and adsorbed in the form of multilayers [104]. Additionally, the H-bonding network in defective subsurface layers was also noticeably modified, indicating that the Mg^{2+}/Ca^{2+} exchange was not limited to the surface. After calcination, the Mg doped HA can be converted into HA (eg. Mg<1mol% Ca) or biphasic calcium phosphate (BCP) phases of HA and β-TCP (eg. Mg>1mol% Ca) [105, 106]. In this case the β-TCP structure type increases with the content of Mg^{2+} and at the same time the quantity of the HA phase diminishes [105, 106]. The doped Mg^{2+} can be either incorporated into BCP phases, or segregated as free MgO [105, 107].

Substitution of Mg^{2+} in TCP structure is also interesting. The presence of Mg^{2+} can stabilize β-TCP at high temperature, suppressing the transformation of β-TCP to α-TCP [108, 109]. Magnesium-containing calcium phosphates like β-TCMPs are formed via different methods. In aqueous systems precipitation or hydrolysis of monetites are some of the common techniques. Kumta *et al.* precipitated β-TCMP by adding Ca^{2+} and Mg^{2+} containing solutions into a NaH_2PO_4 containing solution in a dropwise manner [110]. The

initial pH of the system was 5 and the system was kept at 95-100 ^{o}C for 5 hours. Hydrolyzing monetite in a stirred Ca^{2+} and Mg^{2+} containing solution at pH of 5 at 95-100 ^{o}C for 8 hours results in β-TCMPs as well. [111] Furthermore, doping of Mg^{2+} improved densification behavior of TCP, increased compressive strength but reduced TCP dissolution [112].

Magnesium substitution of brushite has been reported in the literature. Pure brushite in physiological condition is unstable and converts into HA over time. Lee *et al.* synthesized magnesium doped brushite via reacting Na_2HPO_4, $CaCl_2$, and $MgCl_2$ in aqueous solution with different Mg/(Ca+Mg) ratios (0, 14%, 50%) [113]. The doping of magnesium can stabilize brushite. However, similar to HA, the substitution of Mg in brushite structure is limited. Once excessive Mg^{2+} is added, it is most likely that the incorporated magnesium remains in the interstitial sites of the brushite structure. Mg^{2+} substitution distorts the lattice to be weakly crystalline rather than exhibiting other phases. It is also possible for this excess amount of Mg to contribute to disorder resulting in the formation of some amorphous phase. In this situation Mg distorts the structure considerably, and prohibits the crystallization of the hexagonal shaped brushite platelets, lowering the surface energy of the platelets, thus intensifying the formation of nanospherical particles. Additionally bobierrite appears to crystallize out from the brushite phase during the 12 hour aging period, probably as the amorphous phase, which crystallizes out to form magnesium phosphate during the aging process.

In summary, Mg^{2+} substitution affects different calcium phosphate phases in different ways resulting in crystalline structures of different stabilitiers, and biological and

physical properties. Overall, it is believed that incorporation of Mg^{2+} in calcium containing apatites disrupts the nucleation and growth of crystals and reduces the lattice size.

2.4.2 Applications

Calcium phosphate based materials have been used as bone substitutes for many years. To enhance the biological and mechanical properties of these substitutes, many investigators have doped them with elements like magnesium (Mg), strontium (Sr), manganese (Mn), zinc (Zn), etc. with magnesium as the most important metal; following is an overview of the potential orthopedic applications for magnesium containing calcium phosphates.

2.4.2.1 Bone Cements

Incorporation of Mg^{2+} ions in the calcium phosphate cements (CPCs) in the CaO-MgO-P_2O_5 systems significantly improves CPCs' limitations. CPCs have been used as bone substitutes for many years. Hydroxyapatite (HA), β-tricalcium phosphate (β-TCP), brushite based compositions, all have been commercially available [114]. Their clinical applications are limited due to their short setting times, low mechanical strength, and low biodegradability [110, 115]. For instance, setting time of magnesium-substituted β-tricalcium phosphate cements increases to 8-11 minutes from 2 minutes in magnesium-free β-TCP cements, which is advantageous for surgical applications since 6-9 minutes is efficient for insertion of cement in defective bones [115, 116]. Additionally, magnesium addition doubled the compressive strength of set cements from 19 MPa to more than 40 MPa after one day of wet storage [110]. Similar results were observed in a study by Jia *et al.* which reported a rapid setting for the magnesium calcium phosphate cements [2]. This

group fabricated the magnesium calcium phosphate cements (MCPCs) by mixing magnesium oxide (MgO) powders with calcium dihydrogen phosphate ($Ca(H_2PO_4)_2 \cdot H_2O$). The setting time of 7 minutes and compressive strength of 43 MPa was reported after 1 hour. The acid-base reaction involved magnesium oxide and calcium dihydrogen phosphate in a 2:1 molar ratio, which produced $Mg_3(PO_4)_2$ and $Ca_3(PO_4)_2$ as the final products. Later, the MCPCs were tested for degradability and biocompatibility. MCPCs were shown to be degradable in Tris-HCl solution and the degradation was significantly improved when compared to magnesium-free calcium phosphate cements (CPCs) due to the fast dissolution rate of MCPCs. Cell proliferation rate of human fibroblast cells (MG_{63}) cultured on magnesium calcium phosphate cements (MCPCs), calcium phosphate cements (CPCs), and tricalcium phosphate (TCPs) were reported at 1, 3, and 5 days as shown in Figure 2-6 [2].

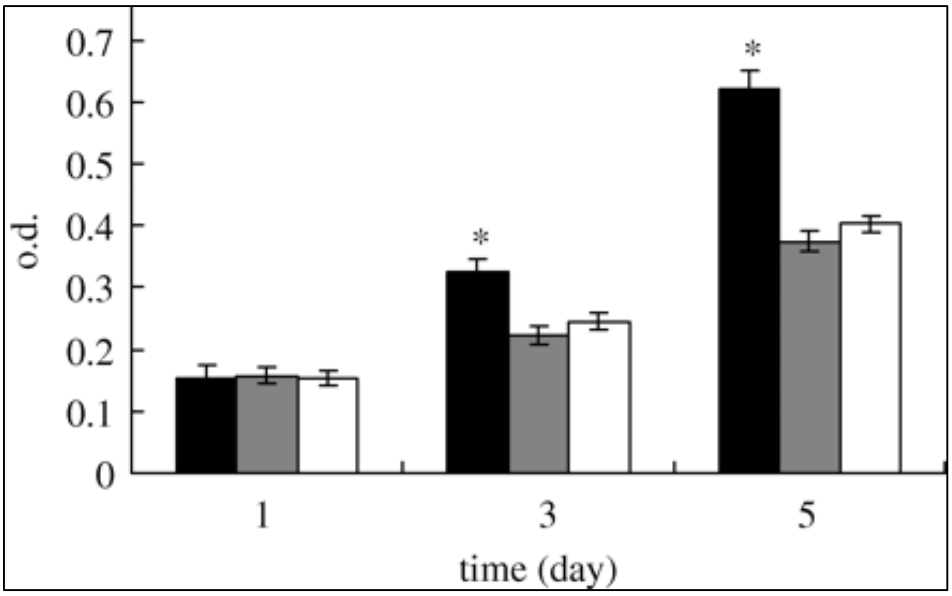

Figure 2-6: Proliferation rate of MG63 cell cultures on MCPC, CPC, and control TCP at 1, 3, and 5 days. Black, grey, and white represent MCPC, CPC, and TCP respectively. (*) indicates $p < 0.05$ [2]

The MG_{63} growth rate was higher on MCPCs than CPCs and TCPs. Scanning electron microscopy images shown in Figure 2-7 illustrate the high attachment of MG_{63} to MCPCs and their high proliferation rate at 1, 3 and, 5 days [2]. *In vivo* studies of MCPCs exhibited high biodegradability and osteoconductivity in rabbit bone tissues along with lack of inflammation and necrosis [115]. High degradation rate is attributed to rapid dissolution of $NH_4MgPO_4.6H_2O$. Two months of monitoring of implanted rabbits further indicated that MCPCs are capable of forming direct bonds with the host bones without interrupting the surrounding connective tissues, and they exhibit higher osteogenesis [115].

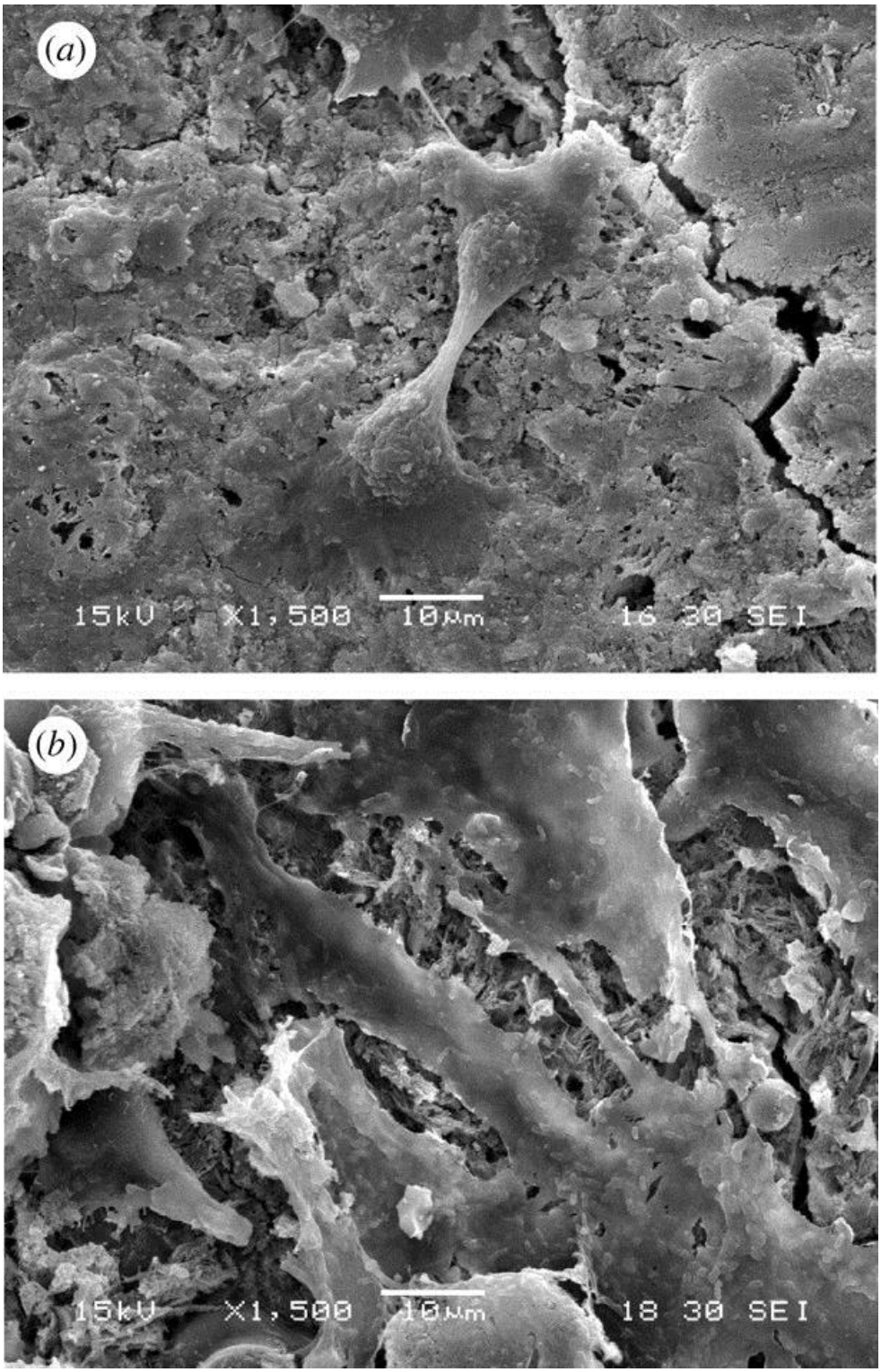

Figure 2-7: SEM images of the MG63 cells cultured on MCPCs for 3 (a), and 5 (b) days [2]

In summary, incorporation of Mg^{2+} ions in CaO-MgO-P_2O_5 systems improves many of its limitations as biological cements like expanding the setting time, increasing the compressive strength, improving the biodegradability and biocompatibility of forming apatites.

2.4.2.2 Scaffolds for Bone Regeneration

Magnesium substituted calcium phosphate cements (MCPC) have additional applications as tissue engineering micro/macroporous scaffolds. Various methods are used to form MCPC porous scaffolds. Kim *et al.* presented an in situ coprecipitation method and rotary spray drying atomization process to synthesize the MCPC scaffolds [117]. To fabricate the MCPCs calcium nitrate tetrahydrate ($Ca(NO_3)_2{\cdot}4H_2O$) and magnesium nitrate hexahydrate ($Mg(NO_3)_2{\cdot}6H_2O$) were used with the Mg/Ca molar ratio of 0.01. Next, Diammonium hydrogen phosphate ($(NH_4)_2{\cdot}HPO_4$) was gradually added to the solution. This study reports the formation of spherical MCPC scaffolds which are capable of supporting the growth and proliferation of human adipose tissue-derived mesenchymal stem cells (hAT-MSCs). *In vitro* and *in vivo* results showed the osteogenic differentiation and proliferation of the stem cells cultured on MCPC scaffolds [117]. Wei *et al.* introduced a hierarchically structured 3D microporous/macroporous magnesium–calcium phosphate scaffold fabricated via the setting of magnesium ammonium phosphate hexahydrate ($NH_4MgPO_4.6H_2O$) and hydroxyapatite ($Ca_{10}(PO_4)_6(OH)_2$) as reactants with sodium chloride added as a space holder for creating porosity. In a different study, Wei *et al*. observed an increased degradation rate in Tris-HCl solution compared with the magnesium-free calcium phosphate scaffolds [118]. The *in vitro* and *in vivo* results were

in complete agreement with the previous studies. The MCPC scaffolds exhibited bone regeneration, high biocompatibility, and effective osteogenesis in MG_{63} cell cultures and in implants in rabbit femora [118, 119]. Hussain *et al.* reported magnesium calcium phosphate containing gelatin scaffolds showing enhanced physical and mechanical properties when compared to the pure gelatin scaffolds. The crucial mechanical and biological properties of MCP were tested in a system where gelatin scaffolds contained different levels of MCPs like 0, 25, 50, 75, and 90 wt%. Mechanical testing such as the resistance to the volume change indicated that there is significant improvement of MCP containing gelatin scaffolds compared with their Mg-free counterparts. As in previous studies, the bone marrow mesenchymal stem cells showed much higher proliferation and osteogenic differentiation in the MCP containing gelatin scaffolds [120].

Overall, magnesium substituted calcium phosphate ceramics can be used as bone scaffolds. Such scaffolds show bone regeneration, biocompatibility, and higher physical and mechanical properties compared to their magnesium-free counterparts.

2.4.2.3 Coatings

In recent years, the addition of magnesium has become very popular for bioceramic coatings like hydroxyapatite (HA), tricalcium phosphate (TCP) and self-setting cements, bone substitutes, and many biomedical implants [121, 122]. It has been argued that magnesium has the ability to strengthen the coating/substrate interface in experimental materials. Also, magnesium ions present in the $CaO\text{-}MgO\text{-}P_2O_5$ system slows down the dissolution of calcium ions from the Mg/Ca coatings [123]. Magnesium incorporation on the surface of implants increases osteoconductivity [124] and magnesium bound integrin

positively affects the adhesion ability of cells to the orthopedic or dental implants [125]. For example, Qi *et al.* synthesized magnesium-substituted calcium apatite coatings on Ti_6Al_4V substrates via sol-gel dip-coating method [123]. They indicated that apatites coated with magnesium in the CaO-MgO-P_2O_5 systems improve adhesion, proliferation and metabolic activation of Mesenchymal stem cells (MSCs) and MG_{63} cells in comparison with the magnesium-free hydroxyapatites [123]. Another study by Revell *et al.* confirmed that magnesium-substituted calcium phosphate coating on titanium alloy implants enhances the bone bonding *in vivo* systems [126] .

2.4.2.4 Gene Delivery

Similar to the MgO-P_2O_5 system, the CaO-MgO-P_2O_5 system provides potential DNA carriers. For this application magnesium doped calcium phosphates Mg^{2+} ions are used to replace calcium phosphate particles and inhibit precipitation of large structures, consequently promoting synthesis of fine particles, which are specifically desirable for DNA delivery [127]. For example, substitution of Ca^{2+} ions present in the calcium phosphates like tricalcium phosphate (β-TCP) by Mg^{2+} can result in formation of magnesium-containing tricalcium phosphates (β-TCMP) [110]. Adding greater than 14% magnesium to the CaP structure results in the formation of more stable nano-spherical structures with high surface area (~200 m^2/g). Higher surface area provides more attachment sites for DNA molecules. The presence of phosphate groups *in situ* facilitates the condensation of DNA at the binding sites. Consequently, the high surface area and more condensed CaP-DNA composites enable the particles to interact with the cell membranes and eventually enter the cells [110].

2.4.2.5 Future Directions

There is still room for further development in the CaO-MgO-P_2O_5 system. First, the effects of Mg^{2+} substitution in several calcium phosphate phases such as monetite and calcium pyrophosphate are not clear. Second, though Mg^{2+} is supposed to accelerate calcium phosphate dissolution rate and improve substance biocompatibility, the potential of using MgO-CaO-P_2O_5 as carrier is not well studied yet. Third, similar to MgO-P_2O_5, these materials can be great candidates for 3D printing. Lastly, there has not been much effort in understanding the synergistic relationship between Ca^{2+} and Mg^{2+} and even the interaction of other possible dopants on tissue response and material properties. A recent study is one of a few that mentioned that Mg^{2+} can buffer the toxicity of excessive Sr^{2+}, while Ca^{2+} has no impacts at all [128].

2.5 SiO_2-MgO system

2.5.1 Material Aspects

SiO_2-MgO system mainly refers to the magnesium containing bioactive glasses. Diba *et al.* provides a comprehensive list of more than 100 MgO containing silicate systems [22, 129]. MgO is reported to have different roles in the glass network such as the modifier [130, 131], intermediate oxide [132], and the exhibiter of anomalous properties [133]. MgO is shown to act as an intermediate oxide in the $49.5SiO_2$-$1.1P_2O_5$-(23.0(1 - x))CaO-xMgO-$26.4Na_2O$ (mol%) system. In the region where $0 \leq x \leq 1$, MgO_4 tetrahedral structures form [133]. MgO addition to the SiO_2-Na_2O-CaO-MgO, SiO_2-K_2O-MgO-BaO, and SiO_2-CaO-K_2O-MgO systems cause a decrease in hardness, elastic modulus, and brittleness. However, the fracture toughness improves by increasing MgO content [134]. This can be

attributed to the substitution of CaO, BaO, and SiO_2 by MgO, which leads to a higher Poisson's ratio, elastic modulus, and hardness [135]. In addition, the Mg^{2+} ions donated by MgO can create a tighter glass network due to their high Dietzel's ionic field strength [22]. MgO-containing silicate glasses have lower transition temperatures, which can be caused by the formation of Si-O-Mg bonds instead of Si-O-Si bonds [133]. However, the MgO addition inhibits the crystallization and increases the crystallization temperature in the MgO-containing glasses [136]. As a result, MgO-containing glasses have larger processing window, which enables them to be processed as bioactive glasses without the formation of crystals [133].

Crucial biomedical applications of MgO-containing glasses are attributed to the presence of Mg^{2+} along with their SiO_2 content. Since Mg^{2+}, as a divalent cation, plays key roles in human body and binds the extracellular domain of α-subunit of the integrin superfamily [137], it is mainly responsible for the interactions between the osteoblasts and the biomaterial surfaces covering the implants [33]. Some of the beneficial effects of Mg^{2+} addition on the MgO-containing glasses are: higher thermal stability and surface reactivity [136], higher antibacterial activities resulting from the increased pH caused by MgO content [138], higher glass dissolution via disruption of silica glass network [139], and stimulation of bone cell proliferation [140, 141]. The well-known glasses for biomedical applications have been summarized in literature, by Diba *et al.* (Table 2.5)[22].

Table 2.5: Mg-O containing glasses with potentials in biomedical applications [22]

Number	Chemical Formula	Biomedical Applications	Ref.
1	$MgO\text{-}CaO\text{-}P_2O_5\text{-}SiO_2$	Glass degradation rate, Apatite formation	[142]
2	$MgO\text{-}CaO\text{-}P_2O_5\text{-}SiO_2\text{-}CaF_2\text{-}Na_2O$	Not Mentioned	[143]
3	$MgO\text{-}CaO\text{-}P_2O_5\text{-}SiO_2\text{-}CaF_2\text{-}SrO$	Not Mentioned	[144]
4	$MgO\text{-}CaO\text{-}P_2O_5\text{-}\ SiO_2\text{-}Na_2O\text{-}K_2O$	Higher expression of collagen type 1, and alkaline phosphatase in human fibroblasts	[136], [145]
5	$MgO\text{-}CaO\text{-}P_2O_5\text{-}SiO_2\text{-}CaF_2\text{-}B_2O_3$	Not Mentioned	[143]
6	$MgO\text{-}CaO\text{-}P_2O_5\text{-}\ SiO_2\text{-}K_2O$	Glass stability	[136]
7	$MgO\text{-}CaO\text{-}P_2O_5\text{-}SiO_2\text{-}Na_2O$	Not Mentioned	[133]
8	$MgO\text{-}CaO\text{-}P_2O_5\text{-}SiO_2\text{-}Na_2O\text{-}K_2O\text{-}B_2O_3$	Antibacterial properties	[138]
9	$MgO\text{-}CaO\text{-}P_2O_5\text{-}SiO_2\text{-}Na_2O\text{-}B_2O_3$	Not Mentioned	[146]
10	$MgO\text{-}CaO\text{-}P_2O_5\text{-}SiO_2\text{-}Na_2O\text{-}B_2O_3\text{-}Y_2O_3$	Not Mentioned	[147]
11	$MgO\text{-}CaO\text{-}P_2O_5\text{-}SiO_2\text{-}Na_2O\text{-}K_2O\text{-}B_2O_3\text{-}Y_2O_3$	Not Mentioned	[147]
12	$MgO\text{-}CaO\text{-}P_2O_5\text{-}SiO_2\text{-}CaF_2\text{-}Na_2O\text{-}K_2O\text{-}Ta_2O_5\text{-}La_2O_3$	Not Mentioned	[148]
13	$MgO\text{-}CaO\text{-}P_2O_5\text{-}SiO_2\text{-}CaF_2\text{-}Na_2O\text{-}K_2O\text{-}ZnO\text{-}Nb_2O_5$	Not Mentioned	[148]
14	$MgO\text{-}CaO\text{-}P_2O_5\text{-}SiO_2\text{-}CaF_2\text{-}Na_2O\text{-}K_2O\text{-}ZnO\text{-}SrCO_3$	Not Mentioned	[148]
15	$SiO_2\text{–}CaO\text{–}P_2O_5\text{–}MgO\text{–}K_2O\text{–}Na_2OAl_2O_3$	Higher expression of collagen type I, II, and V in human osteoblasts	[149]

The MgO-containing bioactive glasses are suggested to induce the formation of hydroxyapatite and interact with the bone tissues via following steps in Table 2.6 [150, 151].

Table 2.6: Suggested steps for bioactive glasses-bone interaction [151]

1	Formation of silanol groups (Si-OH)
2	Formation of silanol groups (Si-OH)
3	Formation of silica-rich layer by Polycondensation of Silanols
4	Amorphous HA-layer formation by adsorption of $Ca+PO_4$
5	Crystallization of HCA-layer by incorporation of CO_3
6	Adsorption of biological moieties on HCA surface
7	Action of macrophages
8	Attachment of stem cells
9	Differentiation of stem cells
10	Generation of bony matrix
11	Crystallization of matrix

It is suggested that the cations covering the bioactive glasses rapidly become replaced by the hydrogen ions from the body, leading to the formation of silanol groups. These sites later become adsorption sites for the growth factors and lead to *de novo* bone generation [151]. This effect might be caused by the electrical stimulation initiated by the presence of Mg^{2+} ions [152]. For example, sources of magnesium like magnesium hydroxide are known to improve osteoblast activity through release of Mg^{2+} ions [152]. Furthermore, in semi-biological systems like the simulated body fluid, Mg^{2+} ions are shown to form complexes with OH^- and result into weak buffers [136]. In summary, the presence of MgO causes formation of a tighter glass network, a larger glass temperature network in SiO_2-MgO systems, and leads to higher biocompatibility and antibacterial activities of such systems. MgO-containing bioactive glasses are associated with many biomedical applications. The following section aims to introduce some of these applications.

2.5.2 Applications

Bone cements, tissue engineering scaffolds, and coatings of implants are some of the biomedical applications of biocompatible MgO-containing bioglasses. To better understand the effect of Mg^{2+} ions involved in the bioglasses, results of many investigations have been presented [153-156].

Biocompatibility is a crucial characteristic of any of the reported bioactive glasses. *In vivo* studies are conducted in different SiO_2-MgO systems to demonstrate the potential of these compositions in orthopedics. For example, *in vivo* studies of 26 different bioactive glasses in MgO-CaO-P_2O_5-SiO_2-Na_2O-B_2O_3 system showed no inflammatory responses and formation of new bones in intramuscular and intraosseus implants [157]. Higher MgO content of the bioactive glasses in MgO-SiO_2-P_2O_5-CaO system was shown to increase the glass surface and decrease the pore sizes. Consequently, MgO accelerated the formation of hydroxyapatites on the glasses, making them more biocompatible by providing more sites for cell attachment [158]. The same results were observed in the MgO-SiO_2-CaO-P_2O_5-Na_2O-K_2O where the implanted materials stimulated osteoconductivity and bone colonization through the macroporous structure of bioactive glasses [159]. Osseous tissue proliferation, implant disaggregation and reabsorption are some of the other effects which are provided by the addition of magnesium to the bioactive glasses.

In addition to biocompatibility, this review summarizes the bone proliferation effects of MgO-containing bioactive glasses applications as bone cements, bone scaffolds, and implant coating.

2.5.2.1 Bone cements

MgO-containing bioactive glasses are used as bone cements to stimulate integration between the implants and their surrounding tissues. Bioactive glass cements have been produced in different forms such as powder and beads with diverse compositions in the MgO-CaO-P_2O_5-SiO_2 and MgO-CaO-P_2O_5-SiO_2 -CaF_2 systems with or without additives like starch, cellulose, acetate, poly(methyl methacrylate) (PMMA), phosphoric ester, and N,N dimethyl-P-toluidine [159-162]. In general, the MgO-containing bioactive glass cements are meant to set in a few minutes and have high compressive strength while getting bonded to the surrounding osseous tissue. Addition of MgO in the MgO-CaO-P_2O_5-SiO_2-CaF_2 system seems to decrease the compressive strength via formation of crystalline magnesium ammonium phosphate hexahydrate ($MgNH_4PO_4.6H_2O$) and inhibiting HA formation in SBF [163]. However, MgO-containing bioglasses increase the compressive strength in MgO-CaO-P_2O_5-SiO_2 system when polyacrylic acid (PAA) is present. The change in the compressive strength depends on the crosslinking of the PAA carboxyl groups with the Ca^{2+} and Mg^{2+} ions present in the glass powder [164]. Even though the mechanical properties of glass bone cements are improved by polymers like PAA, the bioactivity of these materials can limit their biomedical applications. The lower bonding interfaces in systems like 3CaO-P_2O_5-SiO_2-MgO and higher glass degradation rate can lead to lower bioactivity [165]. However, higher MgO content of bioactive glass cements can be beneficial in biological systems since it releases alkaline-earth ions like Mg^{2+} that can act as a buffer as it interacts with the H^+ and H_3O^+ products of acidic agents like the acrylic acid which are used in bone cements [161].

2.5.2.2 Bone Scaffolds

MgO-containing glass scaffolds must provide suitable surface chemistry, biocompatibility, biodegradability, porosity, physical and thermal stability, reproducibility, and scalability in order to be applicable in bone tissue engineering [153-156]. Multiple studies on MgO-containing glass scaffolds reported all or some of these properties in the investigated systems. For instance, the bioactive glass which was prepared via glass sintering and slip casting in MgO-CaO-P_2O_5-SiO_2-Na_2O-K_2O system showed mechanical, physical and thermal stability, *in vitro* bioactivity and degradation when compared to the control groups. *In vivo* studies of the same composition revealed enhanced cell proliferation in different cell lines [166-172]. The foam replica technique was used to fabricate Mg-containing glass in the MgO-CaO-P_2O_5-SiO_2 system and led to products with chemical and physical stability and cell proliferation properties [173]. The same method was used to synthesize a porous scaffold, a 0.1 wt% MgO-containing bioactive glass (1806), in the SiO_2–CaO–Na_2O–MgO–B_2O_3 system.

Robocasting and sintering of ground glasses are two other methods used in the MgO-CaO-P_2O_5-SiO_2-Na_2O-K_2O and in MgO-CaO-P_2O_5-SiO_2-Na_2O-B_2O_3 systems that provide the MgO containing scaffolds with chemical, physical, and mechanical properties along with biodegradable properties *in vitro* environments [174, 175]. MgO presence in silicate-based bioactive glass scaffolds gives them a manufacturing advantage. Glasses which contain 5 wt% MgO can be used to fabricate porous structures without crystallization [168]. Furthermore, Fu *et al.* showed that MgO-containing glass scaffolds are able to promote HA formation on bioglasses and stimulate bone-implant interactions, although the HA layer formation is slower when it is compared to the traditional 45S5

bioglasses [168]. Addition of zinc, copper, and biopolymers like poly(D, L lactic) acid (PDLLA) as coating materials can enhance the mechanical properties of MgO-containing bioglass, and improve their fracture toughness. A more comprehensive section on bioglass scaffolds is presented by Diba *et al.* [22].

2.5.2.3 Implant Coating

Protection against corrosion, interaction between implant and surrounding tissues, and induction of bioactivity are three main purposes for production of coating materials [176]. Consequently, MgO-containing bioactive glasses must provide high bioactivity and mechanical stability in order to be applicable as bioactive coating substances. Currently, most MgO-containing bioactive glasses are produced in MgO-CaO-P_2O_5-SiO_2-Na_2O systems via enameling, pulsed laser deposition, magnetron sputtering, and plasma spraying methods with K_2O, CaF_2, B_2O_3, ZnO, or SrO additives [177-180]. Resulting coating materials have been tested for their mechanical and thermal properties along with *in vitro* and *in vivo* bioactivity. Pazo *et al.* showed that SiO_2 and MgO content of bioactive glasses enhance the resistance against temperature change in glasses by reducing their thermal expansion coefficient (TEC). This might be due to the role SiO_2 plays as a site for creation of new networks [181].

MgO-containing bioglass coating materials, especially those with higher Mg content, have limitations in biomedical applications due to their lower bioactivity when compared to other available materials like 45S5 bioglasses®. However, the bioactivity issues can be overcome by maintaining the SiO_2 level of MgO-containing glasses to <60

wt% since higher ratios inhibit the formation of HA layer on bioglass surfaces which results in lower bioactivity [182].

2.5.2.4 Future Directions

There are numerous new compositions of magnesium containing bioactive glasses which release different ions over time; however, many of them still lack the properties suitable for orthopedic applications like the compressive strength and biocompatibility. On the other hand, these compositions are still limited due to the bone-bonding properties of Mg^{2+} containing bioactive glasses. Finally, the application of these bioactive glasses as carriers of DNA molecules and therapeutic drugs is still poorly explored [183, 184].

2.6. Summary

Magnesium-containing bioceramics are promising candidates for applications in orthopedics and dentistry due to their mechanical, bioreactive, biocompatible, and osteoconductive properties. In particular, they can be manufactured into different formats such as cements, scaffolds, powders, and coatings to satisfy specific needs. This paper reviews recent progress in existing magnesium based bioceramics. Recent work is more focused on the composition study and evaluation of these ceramic materials. It is expected that these ceramics can act as carriers for different bioactive molecules and therapeutic drugs to enhance the bone regeneration strategies in future. In addition, development of new composites of magnesium containing functional bioceramics and other biomaterials should also be carried out in the future to overcome the brittle nature of ceramics.

Chapter 3

Magnesium Substitution in the Structure of Orthopedic Nanoparticles: a Comparison Study

3.1 Abstract

As biocompatible materials, magnesium phosphates have received a lot of attention for orthopedic applications. During last decade multiple studies have shown advantages for magnesium phosphate such as lack of cytotoxicity, biocompatibility, strong mechanical properties, and high biodegradability. Present study investigates the role of Mg^{+2} and Ca^{+2} ions in structure of magnesium phosphate and calcium phosphate nanoparticles. To directly compare the effect of Mg^{+2} and Ca^{+2} ions on structure of nanoparticles and their biological behavior, three groups of nanoparticles including amorphous magnesium phosphates (AMPs) which released Mg^{+2}, calcium magnesium phosphates (CMPs) which released Mg^{+2} and Ca^{+2}, and hydroxyapatites (HAs) which release Ca^{+2} were studied. SEM, TEM, XRD, and FTIR were used to evaluate the morphology, crystallinity, and chemical properties of the particles. AMP particles were homogeneous nanospheres, whereas CMPs were combination of heterogeneous nanorods and nanospheres, and HAs which contained heterogeneous nanosphere particles. Cell viability was monitored in all groups to determine the cytotoxicity effect of particles on studied MC3T3-E1 preosteoblasts. AMPs showed

significantly higher attachment rate than the HAs after 1 day and both AMPs and CMPs showed significantly higher proliferation rate when compared to HAs after 7 days. Amount of Mg^{+2} ions present in the cell culture media was monitored daily and low amount of remaining Mg^{+2} ions in the AMPs cell culture media suggested that absorption of Mg^{+2} played a crucial role in increasing the MC3T3-E1 preosteoblast proliferation rate. Gene expression level of osteoblastic markers ALP, COL I, OCN, OPN, RUNX2 were monitored and they were normalized to GAPDH housekeeping gene. Beta actin expression level was monitored as the second housekeeping gene to confirm the accuracy of results. In general, AMPs and CMPs showed higher expression level of osteoblastic genes after 7 days which can further confirm the stimulating role of Mg^{+2} and Ca^{+2} ions in increasing proliferation rate, differentitation, and mineralization of MC3T3-E1 preosteoblast.

3.2 Introduction

Over the last few years magnesium phosphates have gained some attention, albeit a lot less than they deserve, for their potential applications in the biomedical field specifically in orthopedics. To appreciate the prospects of magnesium phosphates in such applications, an understanding of the physiological roles of magnesium in the human body is essential. It is well known that magnesium ions are the fourth most abundant cations in mammals after sodium, potassium, and calcium [1,2]. Also, magnesium is the second most prevalent intracellular cation [1,2]. Inside mammalian cells magnesium plays multiple essential roles including: regulation of calcium and sodium ion channels, stabilizing DNA, cofactor and catalyzer for many enzymes, and stimulate cell growth and proliferation [2,3].

There are three major reasons that justify application of magnesium phosphates in orthopedics: 1) magnesium can easily substitute calcium in body minerals due to their chemical similarities [4]; 2) presence of Mg^{2+} ions in bone minerals and body fluid can influence the bone mineral metabolism, formation and crystallization processes [5], [6]; 3) magnesium phosphates have higher dissolution rate than the calcium phosphates [7], [8]. During the last several decades, reports on investigations on the calcium phosphates with orthopedic applications have been numerous, as opposed to a handful of reports on magnesium phosphates [9], [10]. Magnesium phosphates are components of minerals such as kidney stone and bone, however most of magnesium related studies have been on orthopedic cements [9], [10].

There is limited work studying the interactions between magnesium phosphates and bone cells. Tamimi *et al.* reported that newberyite ($MgHPO_4 \cdot 3H_2O$) and cattiite ($Mg_3(PO_4)_2.22H_2O$) demonstrated biocompatibility with osteoblast cultures and induced osteoblast adhesion and differentiation [11]. Ewald *et al.* showed that osteoblast activity was higher on brushite ($CaHPO_4 \cdot 2H_2O$) and struvite ($NH_4MgPO_4 \cdot 6H_2O$) cements than the calcium deficient hydroxyapatite ($Ca_9(PO_4)_5HPO_4OH$) cements when cell activity was normalized to cell number [12]. They showed that highest survival rate and cell activity belonged to osteoblasts cultured on magnesium phosphate, struvite-based cements [12]. Expression levels of osteoblastic specific proteins on calcium and magnesium phosphate surfaces were determined. Collagen (COL), osteopontin (OPN), bone sialoprotein (BSP), alkaline phosphatase (ALP), and ostecalcein (OCN) expression level were monitored, and all except COL showed higher expression level in brushite than other groups [12]. Osteoblasts cultured on struvite showed higher osteobalstic characteristics when compared

to their counterparts seeded on polystyrene [12]. However, this study did not include calcium-magnesium phosphate biomaterials and their impact on osteoblastic markers expression level.

Calcium magnesium phosphates (CMPs) are mostly referred to magnesium doped calcium phosphates. Products of Mg^{2+} ion substitution into calcium phosphates can be either in the amorphous phase or in the crystal structures which can cause a series of changes to the biological and physical properties of hosts. Presence of magnesium ions is believed to retard the nucleation and growth of hydroxyapatite (HA) in biological mineralization process via blocking of active growth sites through adsorption of Mg^{2+} ions at the crystal surface [6], [13]–[15]. In the chemical synthesis of Mg^{2+} substituted HA using aqueous solution, Mg^{2+} substitution for Ca^{2+} in the structure of HA occurs only over a limited composition range (up to about 10 at.%) [16], [17]. It has been reported that Mg^{2+} substitution for Ca^{2+} causes a reduction in the lattice parameters of HA [18]. Moreover, the degree of crystallinity of Mg-substituted HA decreases with increasing Mg^{2+} content [16], [17]. Mg-doped HA displays increased solubility with respect to stoichiometric HA, which may be related to reduced crystallinity and/or increased surface hydration [18], [19].

Previously, our group used a microwave assisted technique to synthesize amorphous magnesium phosphate (AMP) in a nanospherical form from an aqueous solution containing Mg^{2+} and HPO_4^{2-}/PO_4^{3-} [20]. The as-prepared AMP was shown to assist the proliferation of preosteoblasts [20]. Our group demonstrated that sustained release of magnesium and phosphate ions incorporated into the AMP and polylactic acid (PLA) structure could stimulate a series of cell responses. Magnesium ions in the AMP nanospheres additionally

promoted the expression level of bone formation markers such as alkalin phosphatase (ALP), type I collagen (COL I), ostecalcein (OCN), and osteopontin (OPN) [21].

Although previous studies confirm the stimulating effect of Mg^{2+} on osteoblast proliferation, there is a lack of comparative studies analyzing the effect of simultaneous presence of magnesium and calcium ions on osteoblast growth and differentiation rate. As a result, there is a need for comparative studies like the present one. To the best of our knowledge, this study is the first one that specifically compares the effect of Mg^{2+} and Ca^{2+} ions on preosteoblast proliferation and differentiation. Here, the hypothesis tested was that Mg^{2+} and Ca^{2+} ions significantly increase proliferation rate of preosteoblasts and directs them towards osteoblastic differentiation via regulation of osteoblastic genes.

In this study, AMP particles were used as the Mg^{2+} source, and for the first time CMPs with Mg^{2+}/Ca^{2+} ratio of 1:1 were used as the source for Mg^{2+} and Ca^{2+} ions. Commercial HAs were used to provide preosteoblasts with Ca^{2+} ions. Cell viability and up-regulation of osteobalstic gene markers (ALP, Col I, OCN, OPN, RUNX2) were monitored and normalized to GAPDH housekeeping genes. Beta actin expression level was measured to confirm the accuracy of the results. Concentration of remaining Mg^{2+} ions in media was used to confirm the correlation between higher osteoblastic cell proliferations with increased Mg^{2+} ion intake.

3.3 Experiments

3.3.1 Microwave Assisted Phosphate Synthesis

All chemicals were purchased from Fisher Scientific (Fair Lawn, NJ, USA) and used without further purification. The synthesis of AMP, CMP nanoparticles using

microwave assisted method has been reported in our previous publication [20]. Commonly used commercial hydroxyapatite was purchased from Fisher Scientific (Fair Lawn, NJ, USA) and was used as a control. Briefly, the reaction solutions were prepared by orderly stirring the reagents in Table 3.1.

Table 3.1: Compositions of reaction solutions

	AMP	**CMP**
DI Water (mL)	10	10
$NaNO_3$ (g)	0	5
$Ca(NO_3)_2.4H_2O$ (g)	0	1
$Mg(NO_3)_2.6H_2O$ (g)	0	0.910
$NaHCO_3$ (g)	0.680	0
$MgCl_2.6H_2O$ (g)	0.623	0
KH_2PO_4 (g)	0.408	0.345
HNO_3 (mL)	0	0.5

The solutions were then placed in onto 10 × 10 × 1 cm alumina insulating fiberboards and covered with an upside down 250 ml-capacity glass beaker. The entire assembly was later placed into a household microwave (MW) oven (Emerson, 800 W, 2450

MHZ, Hackensack, NJ, USA) for 5 min. Once microwave heating was completed, the beakers were left to cool in the microwave for 15 minutes prior to the transportation to the cold water bath for further cooling. The precipitates were magnetically stirred at 400 rpm in 500 ml of de-ionized water until the entire precipitates were dissolved. Finally, the solutions were washed with approximately 2 L of de-ionized water and filtered using a filter paper (Whatman Grade 4, 1004- 055). The filtrates were then placed in an 80 ^{o}C oven overnight to dry. The synthesized AMP, CMP powders were then crushed and used for the analysis. The Mg/P molar ratio in AMP solution was set to 1 since the Mg/P molar ratio in human plasma/serum ranges from 3:2 to 2:3 [1], [22]. The Mg^{2+}/ Ca^{2+} ratio in CMP was 1:1.

3.3.2 Characterization

The morphological features of the as-synthesized particles were visualized by scanning electron microscope (SEM, S4800, Hitachi, Japan). Element compositions were acquired from single particles using the Oxford X-Max EDS detector (Oxford INCA software). Sample characterization was performed using X-ray diffraction (XRD) (Ulitma III, Rigaku, Woodlands, TX) with monochromated Cu Kα radiation, operated at voltage 40 kV and 44 mA setting over a 2θ range from 10 to 45 at a scanning speed of 1˚ per minute. Nano-structures of particles were investigated using transmission electron microscopy (TEM, HD-2300, Hitachi, Japan) with a voltage 200 kV.

Fourier transform infrared spectroscopy (FTIR, UMA-600 Microscope, Varian Excalibur Series, Holliston, MA, USA) was applied for chemical analysis of AMPs, CMPs, and

commercial HAs. The transmittance of each sample was recorded with 256 scans with resolution of 4 cm^{-1} between 4000 and 700 cm^{-1}.

3.3.3 SBF Incubation

To examine stability of particles in physiological conditions, the particles were incubated in simulated body fluid (SBF) in 37°C, and 5% CO_2 environment. SBF was prepared based on the recipe reported previously [185], with an ionic composition similar to human body plasma. The composition is shown in Table 3.2. The reagents were dissolved in solution one by one in the order listed in Table 3.2 and stored at 4˚C when not in use. The as-synthesized AMPs, CMPs, and HA particles were incubated in a 37˚C and 5% CO_2 environment for 7 days with SBF replenished every 48 hours. The incubated particles were rinsed using DI water and dried in oven 80˚C for SEM characterization.

Table 3.2: Composition of 1L test SBF

Order	Reagent	SBF
1	NaCl	6.546 g
2	$NaHCO_3$	2.269 g
3	KCl	0.373 g
4	Na_2HPO_4	0.142 g
5	$MgCl_2.6H_2O$	0.304 g
6	1M HCl	10.0 mL
7	$CaCl_2.2H_2O$	0.3881 g
8	Na_2SO_4	0.072 g
9	Tris-Base	6.063 g
10	1M HCl	33.3 mL

3.3.4 Cytocompatibility Study

Preosteoblast cells (MC3T3-E1, CRL-2593™, ATCC, USA) were used to study the biological effect of AMPs, CMPs, and HAs on preosteoblast proliferation and differentiation. Cells were initially grown at 37 °C and 5% CO_2 in alpha minimum essential medium (α-MEM, Thermo Scientific HyClone), augmented by 10% Fetal Bovine Serum (FBS, Thermo Scientific HyClone, USA), and 1% antimycin and penicillin (Sigma-Aldrich, USA). The culture medium was replenished every other day until the cell reached 90% confluency. To study cell proliferation, MC3T3-E1 cells were seeded to wells (Flacon™ 12 wells cell culture plates, BD Biosciences, USA) at a density of 20,000 cells/well. Cell density was measured after 24 hours, and 7 days using CytoTox 96® Non-Radioactive Cytotoxicity Assay kit (Promega, USA). For statistical analysis, all experiments were performed at least in triplicate, and t-test analysis was applied for data analysis.

3.3.5 Titration

To study the effect of magnesium ions on preosteoblast proliferation, the cell culture media was refurbished and the $[Mg^{+2}]$ was measured in cell culture wells daily. The $[Mg^{+2}]$ was measured using the complexometric titration method. Briefly, the large Ethylenediaminetetraacetic acid (EDTA) molecule is used to form a complex with calcium and magnesium ions and the blue Eriochrome Black T (ErioT) dye is used as the indicator. The indicator forms a complex with calcium and magnesium ions and changes color to pink. During the process, the cell culture medium containing Mg^{+2} reacts with excessive EDTA. Since the bond between ErioT-Mg^{+2} is less stable then the EDTA-Mg^{+2}, the

indicator remains blue when added to the mixture of cell culture medium and EDTA. Later, magnesium chloride solution is added to carry out a back titration reaction. This process leads to formation of magnesium-EDTA. The remaining Mg^{+2} will then complex with the ErioT indicator which will change the color to pink. Via complexometric titration method total calcium and magnesium ions are measured first, later calcium ions are subtracted to determine the magnesium ions concentration in a sample.

3.3.6 Polymerase Chain Reaction

To study cell differentiation, MC3T3-E1 cells were cultured in wells containing AMP, CMP, and HA nanoparticles at a density of 20,000 cells/sample. At the end of 7 days incubation, cells were lysed using Trizol® reagent following the manufacturer's protocol and the total RNA was extracted and quantified by reading the optical density at 260 nm. Total RNA (2 μg for each sample) was reverse transcribed to cDNA using a high-capacity M-MLV reverse transcriptase enzyme (Promega, Madison, WI, USA). The resulting cDNAs were used for real-time polymerase chain reaction (PCR). Reactions were carried out in a 7500 Real-time PCR System (Applied Biosystems, Carlsbad, CA, USA) for 40 cycles. A cycle threshold (Ct) value for each reaction was calculated using Applied Biosystems' sequence detection software and the relative ratio of expression was determined. For statistical analysis, all experiments were performed at least in triplicate. Primers used to amplify specific targets are shown in Table 3.3.

Table 3.3: Sequences of forward and reverse primers

Primer	**Forward 5′-3′**	**Reverse 5′-3′**	**Ref.**
GAPDH	TGTGTCCGTCGTGGATCTGA	CCTGCTTCACCACCTTCTTGA	[186]
ALP	ATCTTTGGTCTGGCTCCCATG	TTTCCCGTTCACCGTCCAC	[187]
Col I	GGAGAGAGCATGACCGATGGA	GGTGGACATTAGGCGAGGAA	[188]
OCN	GCAATAAGGTAGTGAACAGACTCC	GTTTGTAGGCGGTCTTCAAGC	[187]
OPN	CTTTCACTCCAATCGTCCCTAC	GCTCTCTTTGGAATGCTCAAGT	[189]
RUNX2	CGCCCCTCCCTGAACTCT	TGCCTGCCTGGGATCTGTA	[190]
Beta actin	GAGAAGATCTGGCACCACACCT	CAGGATTCCATACCCAAGAAGG	[191]

3.4 Results

Scanning electron microscopy images of the synthesized particles are presented in Figure 3-1. The microwave assisted apatite synthesis resulted in production of homogeneous nanosphere shaped AMP particles. Based on the SEM images, diameter of each nanosphere was approximately 300 nm. CMP particles were heterogeneous with the combination of larger nanorods (≈50%) with the length ranging 700 nm to 5 μm<, and smaller nanospheres (≈50%) with diameters about 250 nm. Commercial HAs were heterogeneous with a combination of nanosphere particles with diameters ranging from 200-2000 nm.

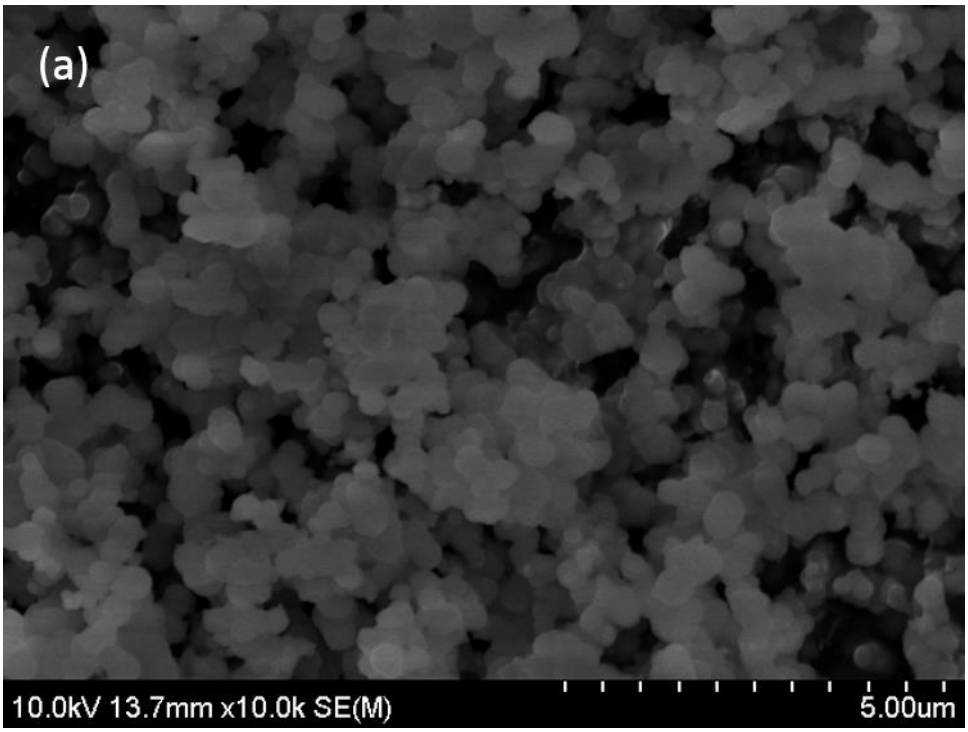

Figure 3-1: SEM characterization at 10k magnifications: (a) AMPs

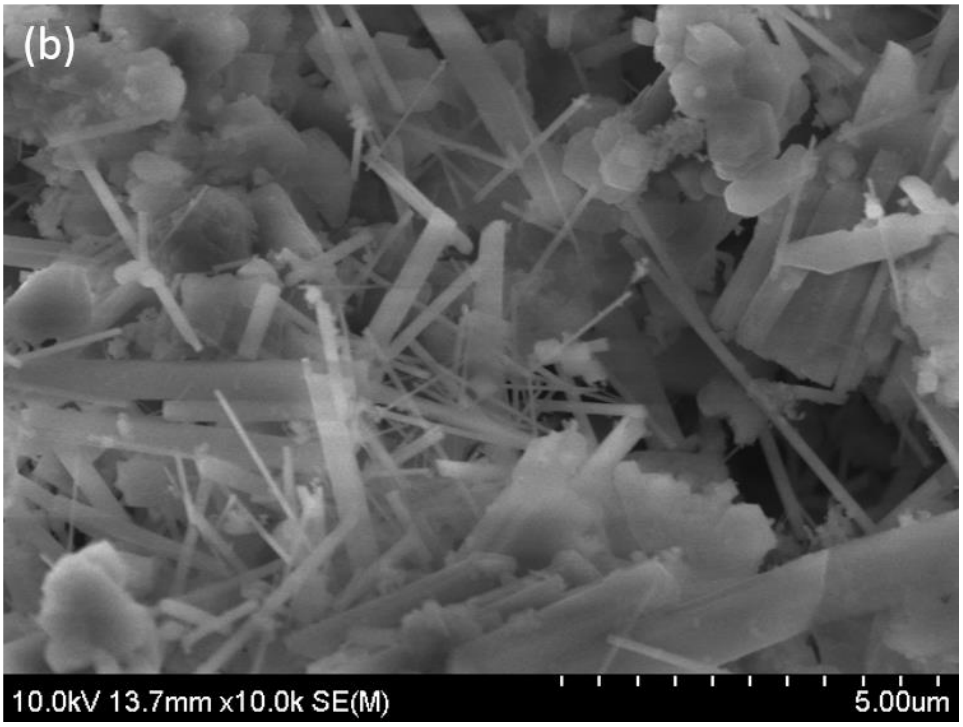

Figure 3-1: SEM characterization at 10k magnifications: (b) CMPs

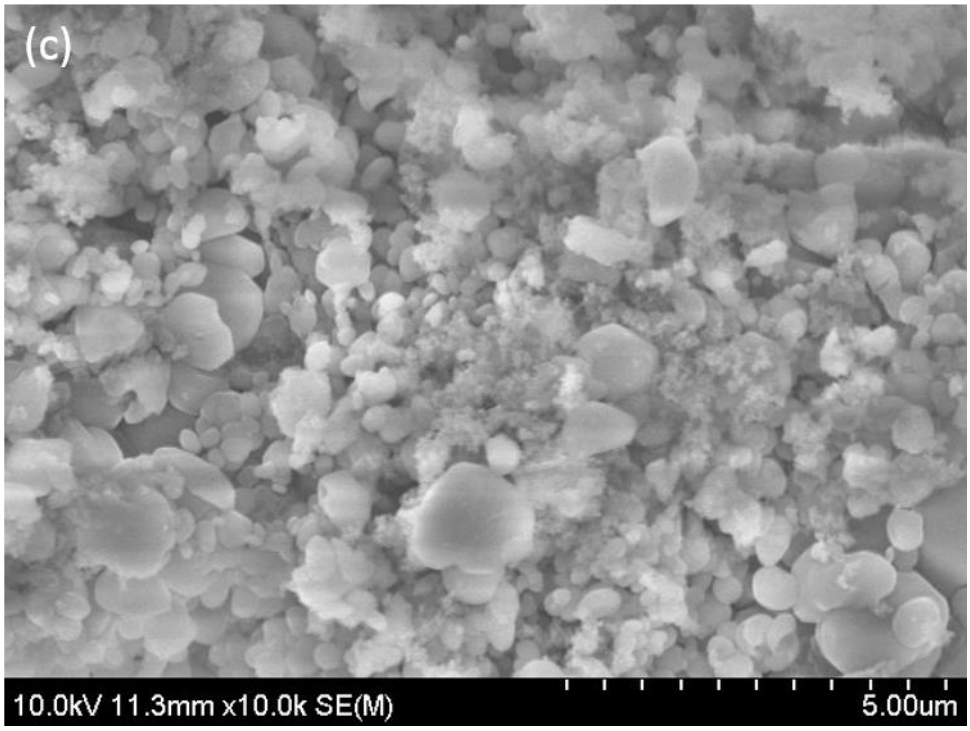

Figure 3-1: SEM characterization at 10k magnifications: (c) HAs

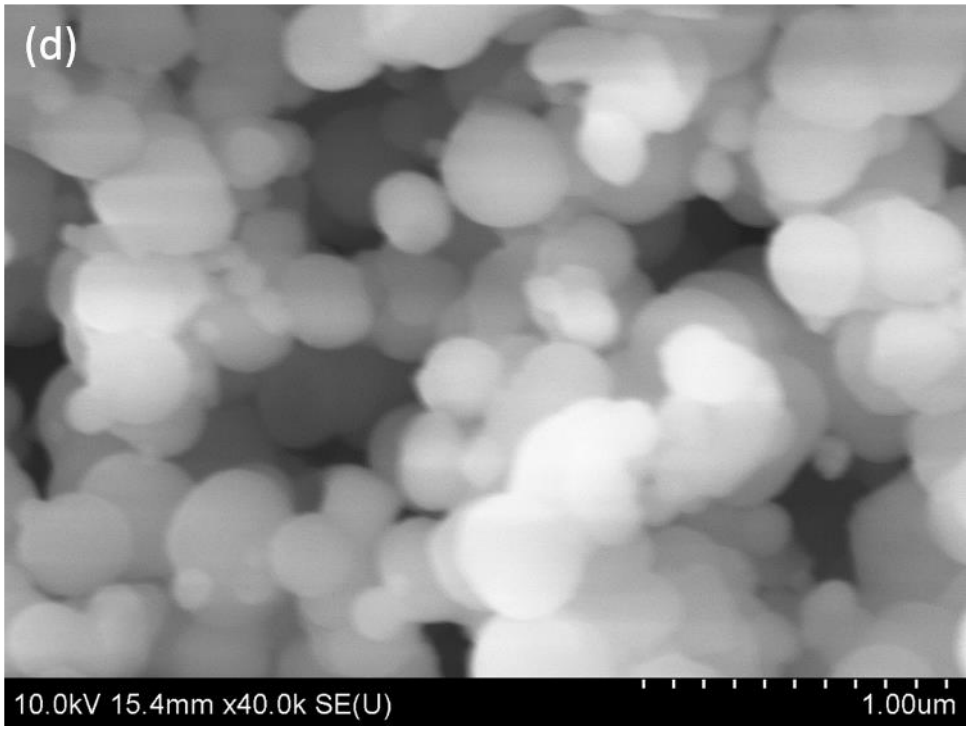

Figure 3-1: SEM characterization at 40k magnifications: (d) AMPs

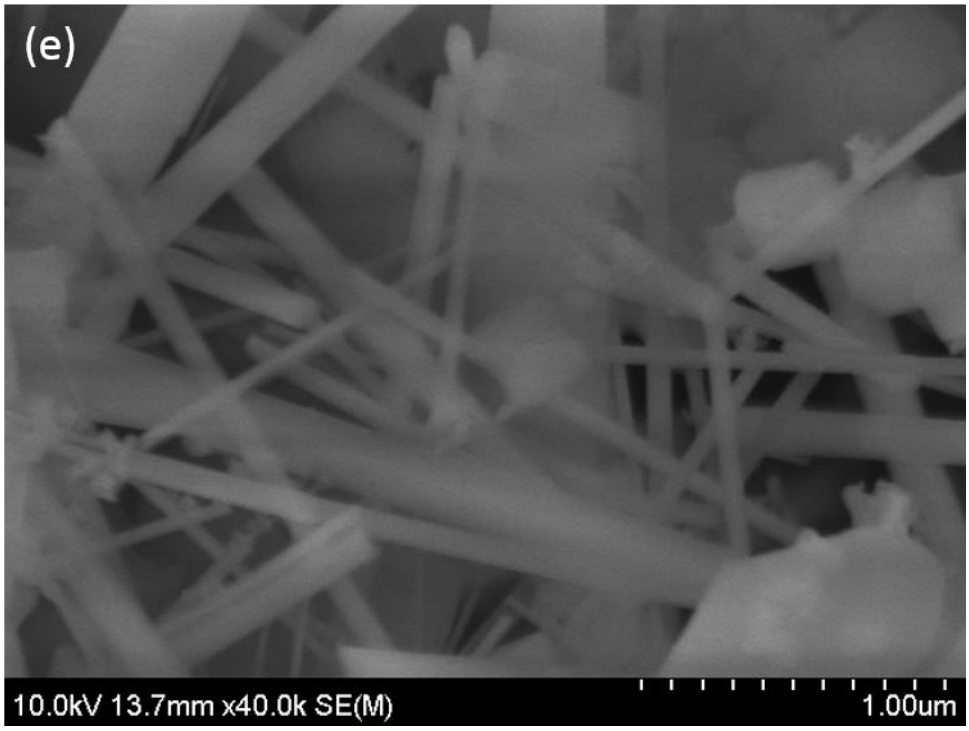

Figure 3-1: SEM characterization at 40k magnifications: (e) CMPs

Chemical compositions of single particles were determined via the Oxford X-Max EDS detector. Magnesium and calcium composition of studied groups are shown in Table 3.4.

Table 3.4: Magnesium and calcium composition of AMP, CMP, and HA particles

	Magnesium (%)	**Calcium (%)**
AMP	19.63	0
CMP	3.62	39.55
HA	0	81.16

Transmission electron microscopy was used to collect detailed images of each as-synthesized particles as shown in Figure 3-2. In TEM images, AMPs are presented as dense nanospheres, CMPs are mostly less dense, elongated nanorods; HAs are also less dense nanospheres.

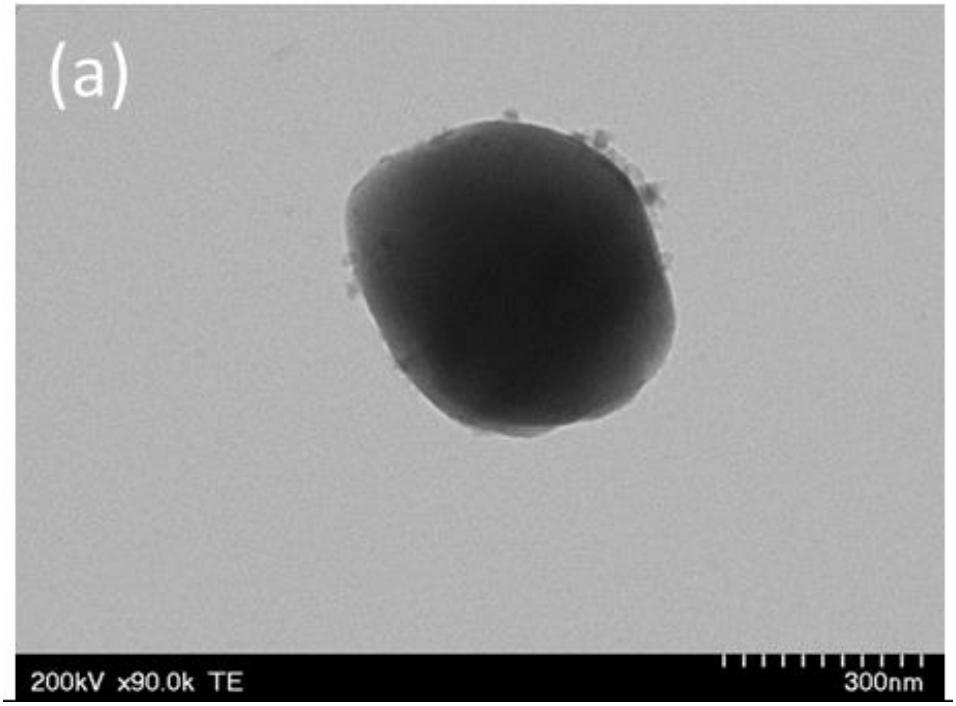

Figure 3-2: TEM images of: (a) AMPs

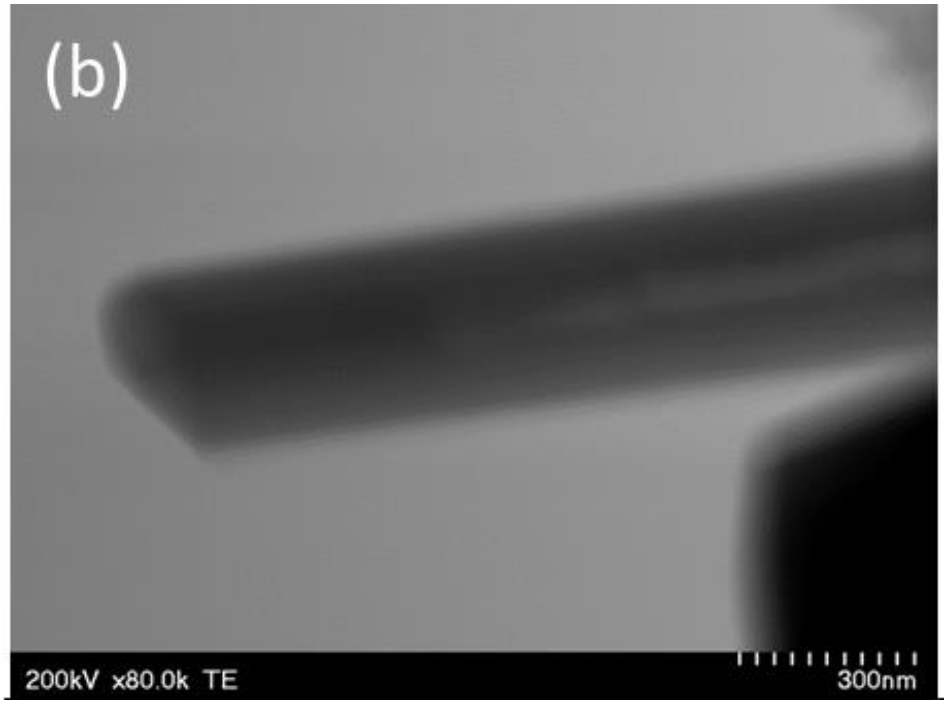

Figure 3-2: TEM images of: (b) CMPs

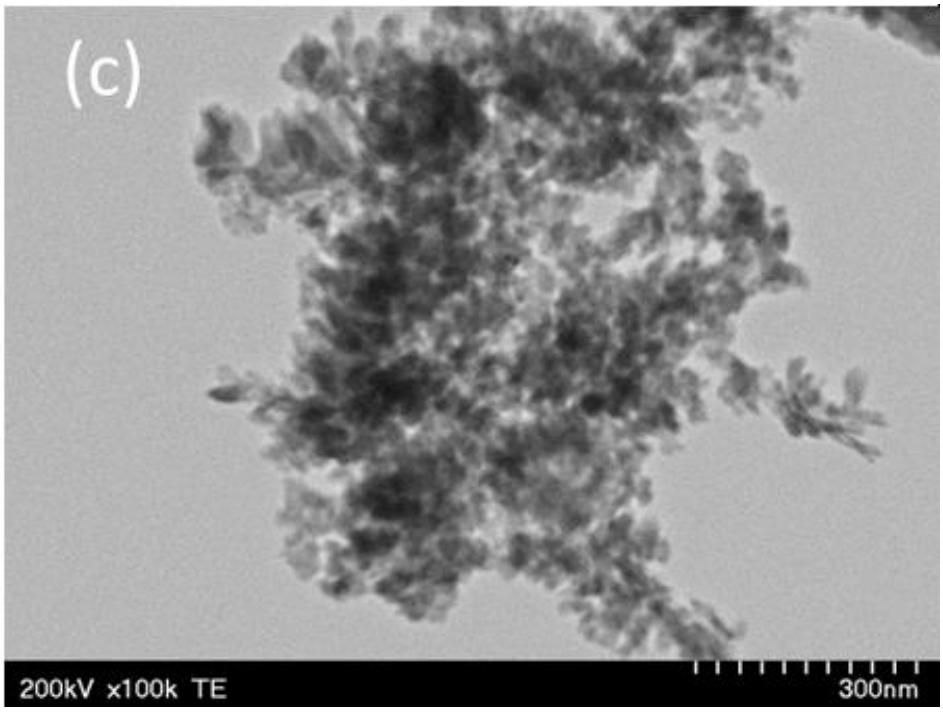

Figure 3-2: TEM images of: (c) HAs

X-ray diffraction pattern of AMPs, CMPs, and HAs are shown in Figure 3-3. To identify the phases present in the sample, the XRD pattern of the sample was compared with calculated patterns in a Powder Diffraction File (PDF) database from the International Center for Diffraction Data (ICDD). Using the search-match capabilities of XRD software JADE (MDI, USA) and the ICDD-PDF database, all phases present in the samples were identified. AMP peaks were similar to the peaks collected from Newberyite, $Mg(PO_3OH)•3(H_2O)$ with PDF# 98-000-0328, CMP peaks were a combination of Hydroxyapatite $Ca_{10}(PO_4)6(OH)$ with PDF# 97-028-9993, and Magnesite $Mg(CO_3)$ with PDF# 97-006-7812. Hydroxyapatite $Ca_5(PO_4)3(OH)$ was found in the database with PDF# 98-000-0251. XRD patterns confirmed lack of crystallinity in AMPs where CMPs showed strong peaks in different angles especially 33º-35º and 42º. HA particles showed similar peaks at the 33º-35º range.

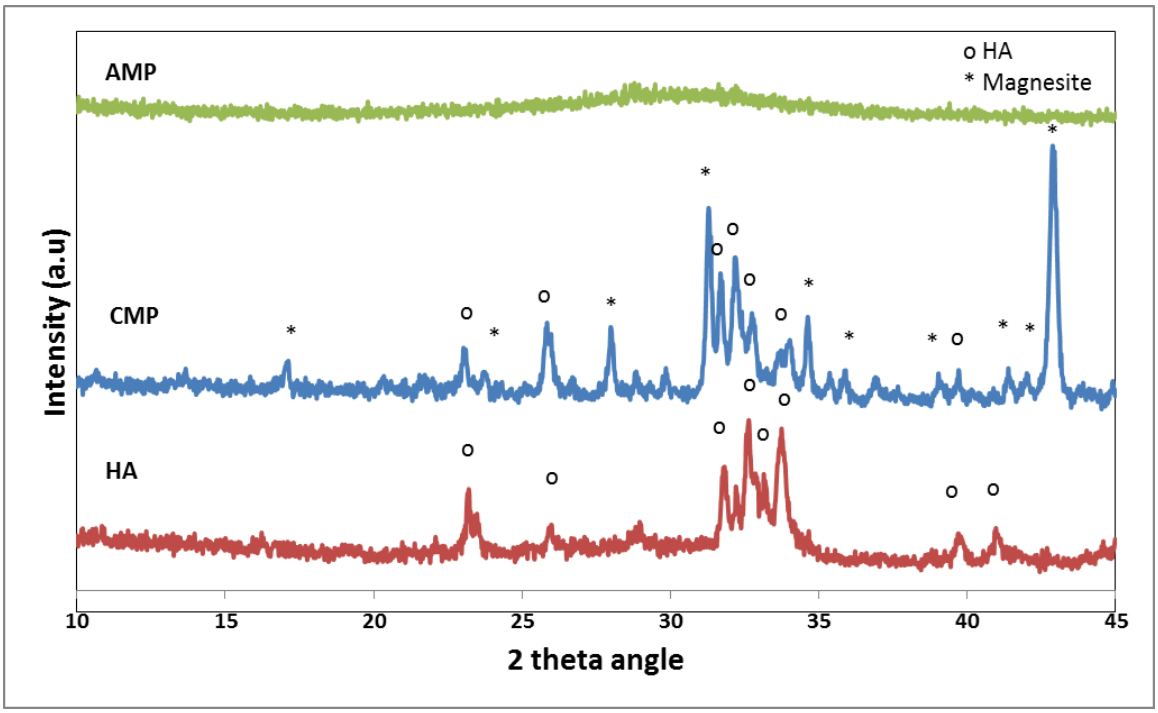

Figure 3-3: XRD patterns of: (a) AMPs; (b) CMPs; (c) HAs. (o) Hydroxyapatite peaks; (*) Magnesite peaks are represented.

The FTIR spectra of AMPs, CMPs, and HA particles are illustrated in Figure 3-4. In all groups similar peaks were observed at wavenumbers of 1040-1100 cm^{-1} or wavelength of 9.6 μm, confirming the presence of PO_4^{3-} groups.

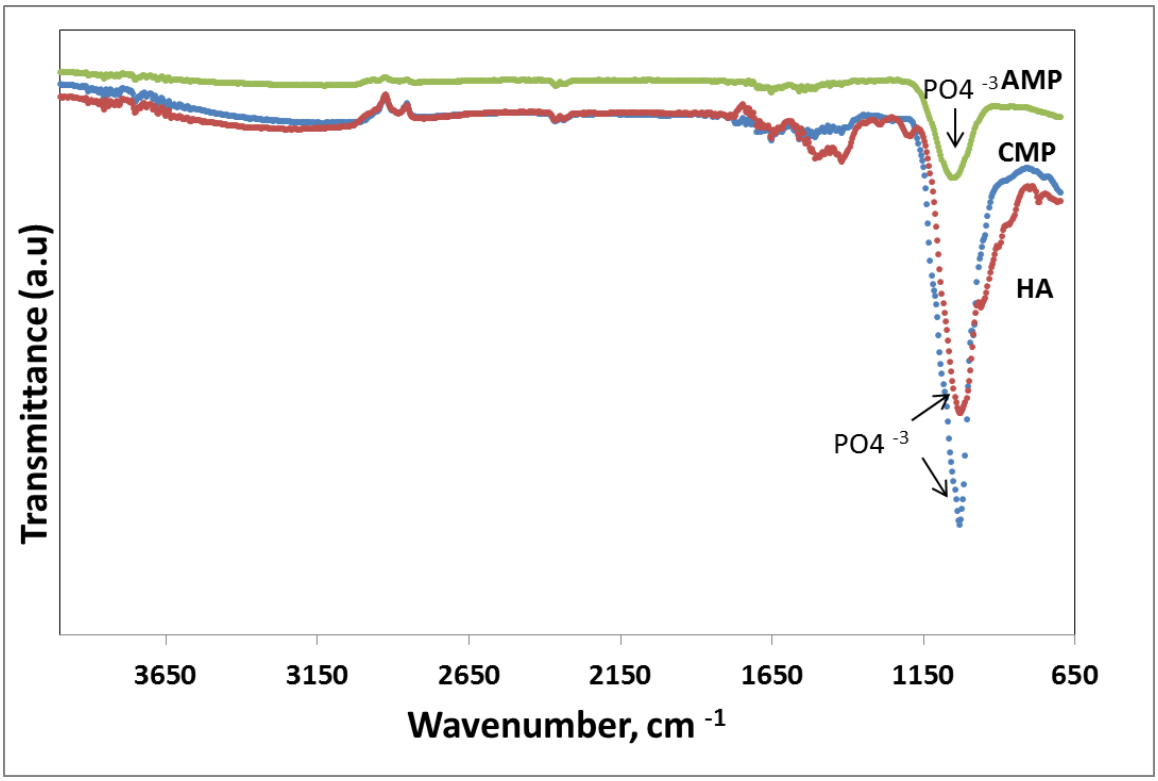

Figure 3-4: FTIR spectra of: (a) AMPs; (b) CMPs; (c) HAs

Apatite formation was monitored in all three examined groups and the images are presented in Figure 3-5. As illustrated the AMPs show highest apatite formation after 7 days of incubation in SBF. CMPs and HAs show similar apatite formation.

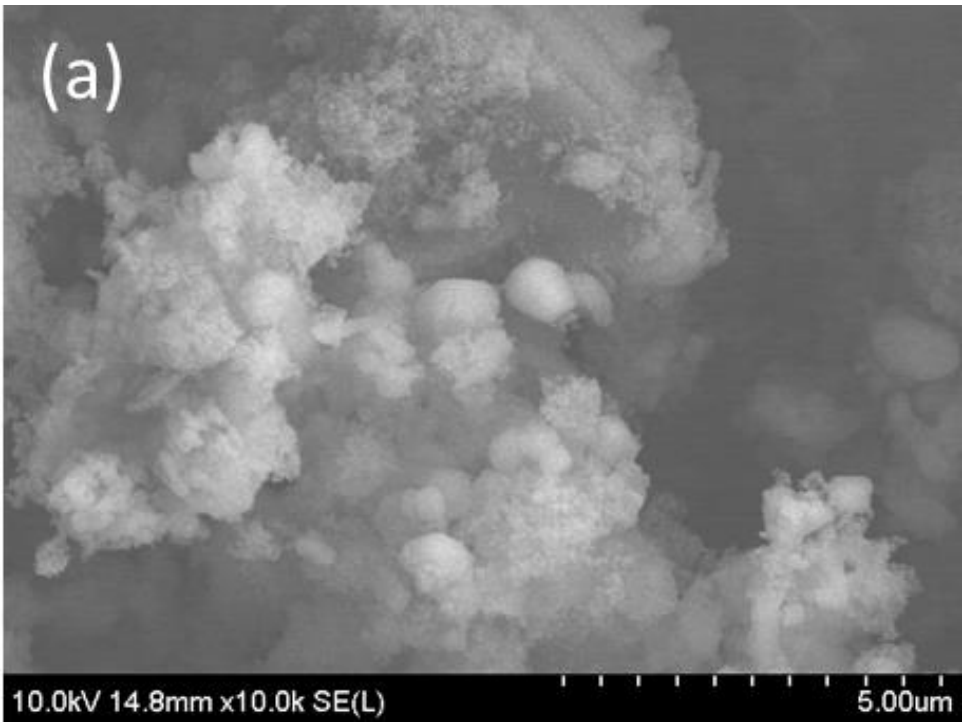

Figure 3-5: SEM images of particles after 7 days of incubation in SBF at 10k magnifications: (a) AMPs

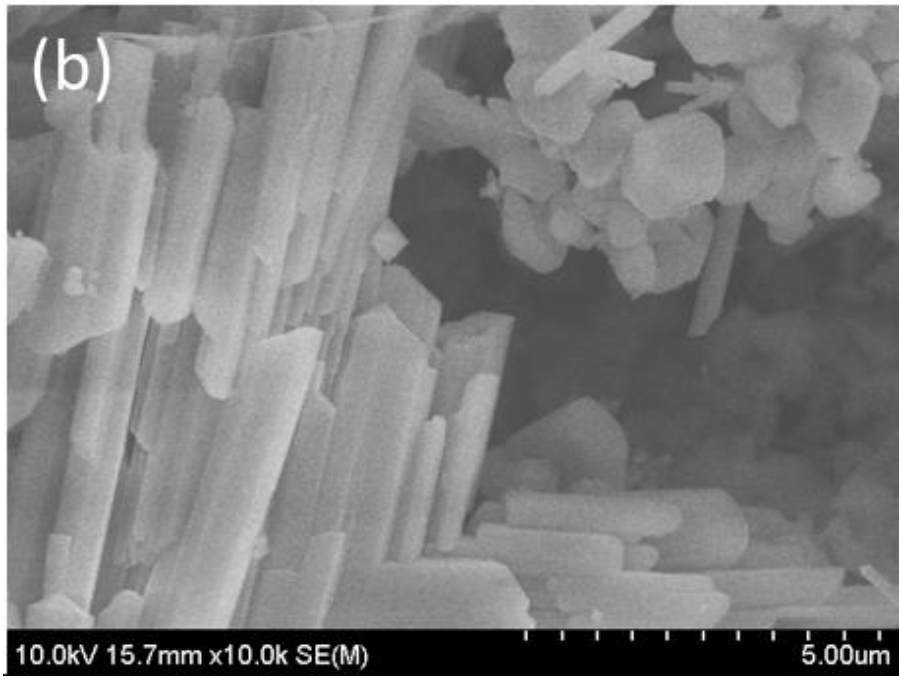

Figure 3-5: SEM images of particles after 7 days of incubation in SBF at 10k magnifications: (b) CMPs

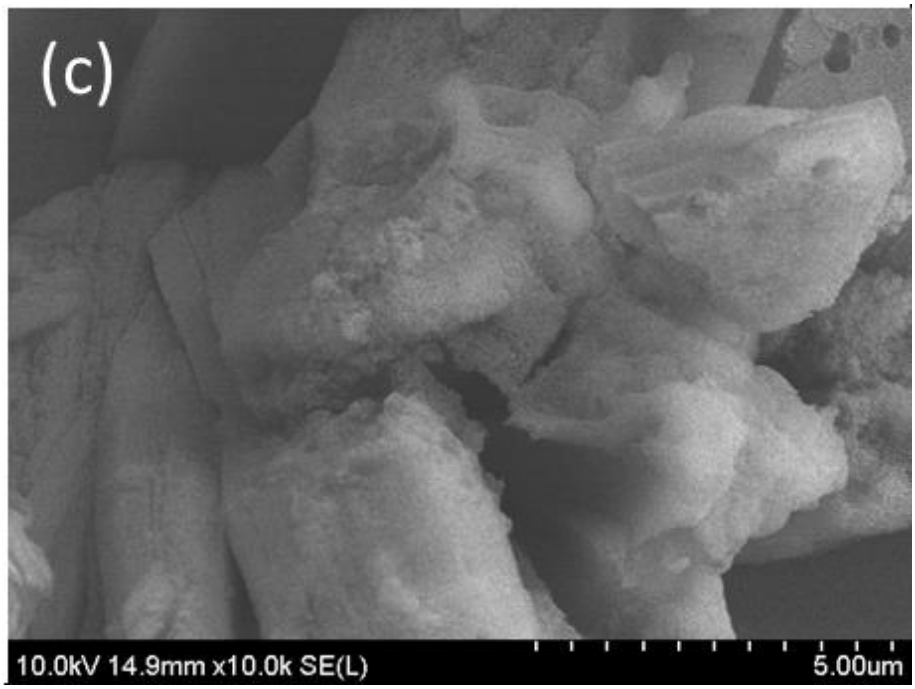

Figure 3-5: SEM images of particles after 7 days of incubation in SBF at 10k magnifications: (c) HAs

Cytocompatibility results are revealed in Figure 3-6. AMPs illustrate significantly higher cell compatibility rate after 1 day when compared to HAs ($p < 0.05$). Compatibility rate of CMPs was not significantly different than the HAs ($p > 0.05$). 7 days results showed significantly higher proliferation rate for AMPs ($p < 0.05$) and CMPs ($p < 0.05$) when compared to the HAs.

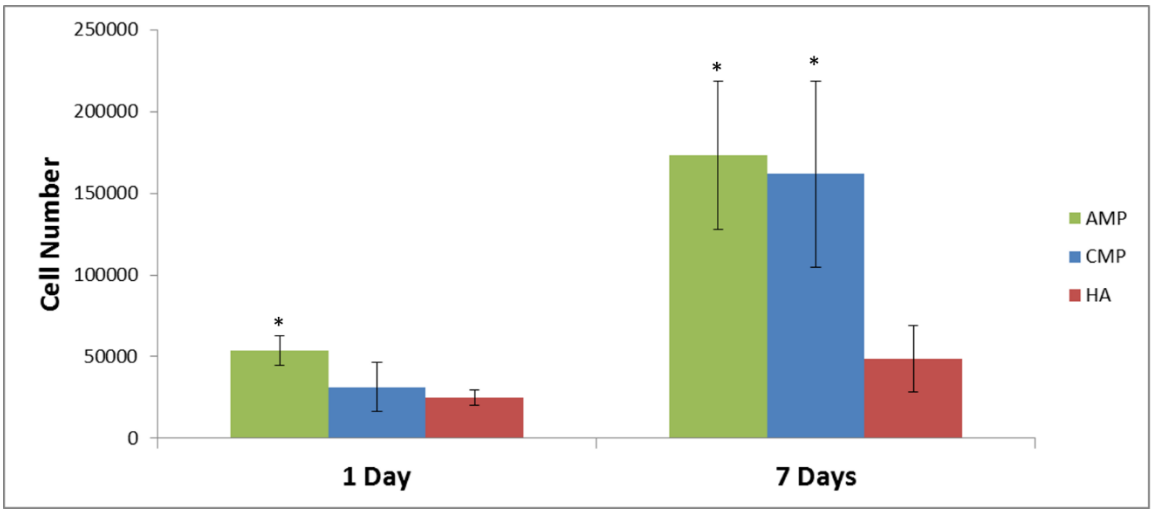

Figure 3-6: Number of MC3T3-E1 preosteoblast cells grown on (a) AMPs; (b) CMPs; (c) HAs after 1 day and 7days. 20,000 cells were seeded on Day 0. Groups were studied in at least triplicates. Statistical analysis was performed using t-test. (*) indicates $p < 0.05$ for AMPs and CMPs cell numbers when compared to the control group (HA).

Concentration of $[Mg^{+2}]$ was measured in cell culture media daily and the results are shown in Figure 3-7. Magnesium concentration was significantly lower in media obtained from the cell cultures containing AMPs when compared to the fresh media after 2, 3, 4, 5 and 6 days ($p < 0.05$). Media obtained from the cells containing CMPs showed significantly lower $[Mg^{+2}]$ after 2 and 3 days ($p < 0.1$) and after 4, 5, and 6 days ($p < 0.05$) when compared to the fresh media. Media obtained from the cells containing HAs showed significantly lower $[Mg^{+2}]$ after 2 and 3 days ($p < 0.1$) when compared to the fresh media.

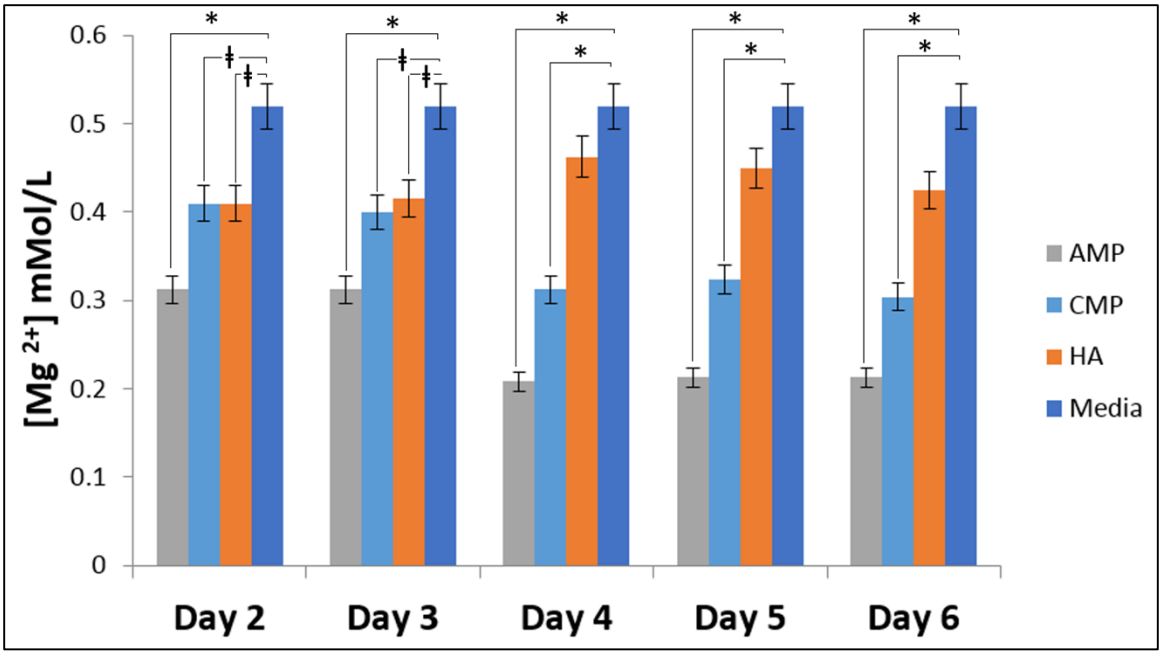

Figure 3-7: Magnesium concentration (mMol/L) in the α-MEM media obtained from the environment of MC3T3-E1 preosteoblasts cultured on (a) AMPs; (b) CMPs; (c) HAs (d) Media (control) after 6 days. Groups were studied in at least triplicates. Statistical analysis was performed using t-test. (*) indicates $p < 0.05$, (ł) indicates $p < 0.1$.

Expression level of multiple osteoblast-indicator genes such as GAPDH, ALP, COL I, OCN, OPN, RUNX2 are measured in MC3T3-E1 cells cultured on AMPs, CMPs, and HAs and the results are illustrated in Figure 3-8. Gene expression levels are normalized to the expression level of GAPDH. Significantly different expression levels are determined by comparing the expression level of each osteoblast-indicator gene in cells growing on AMPs, CMPs, or HAs to the expression level of the GAPDH gene in cells growing in the AMPs, CMPs, and HAs respectively.

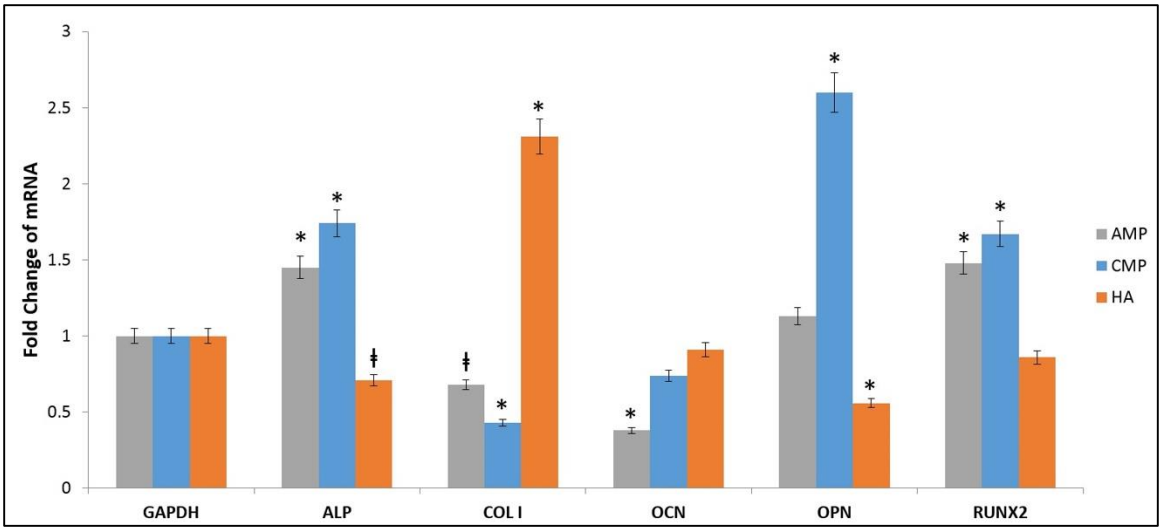

Figure 3-8: RT PCR results of expression level of ALP, COL I, OCN, OPN, RUNX2 on MC3T3-E1 preosteoblast cells cultured on AMP, CMP, and HA nanoparticles. Data is normalized to the GAPDH housekeeping gene and illustrates the fold change in expression. Significantly different expression levels are determined by comparing the expression level of each osteoblast-indicator gene in cells growing on AMPs, CMPs, or HAs to the expression level of the GAPDH gene in cells growing in the AMPs, CMPs, and HAs respectively. Groups were studied in at least triplicates. Statistical analysis was performed using t-test. (*) indicates $p < 0.05$, (ǂ) indicates $p < 0.1$.

3.5 Discussion

The overall results of the effect of magnesium and calcium on proliferation rate and differentiation of preosteoblasts indicated that both ions significantly increased proliferation rate of preosteoblasts. Remaining magnesium level in the media in the AMP group was much lower than the other groups while the cell viability of the AMP group was the highest. It was suggested that magnesium ions played a crucial role in increasing the attachment and proliferation rate of the studied preosteoblasts.

Small, homogeneous structure of AMP nanoparticles play an important role in facilitating the attachment of preosteoblasts, while larger, heterogeneous CMPs and larger

HA particles might delay the attachment process (Figure 3-1). These results are in agreement with the previous study by Lipski *et al.* confirming that MC3T3-E1 preosteoblast cells exhibit larger cell attachment areas and higher prolifertation rate in surfaces with smaller nanoparticles [23]. Lipski *et al.* showed that surface roughness promoted the development of long, thick F-actin fibers aligning with the long axis of each cell [23].

Transmission electron microscopy images of different compositions are shown in Figure 3-2. These results can be compared and contrasted with the XRD results. X-ray diffraction showed the amorphous nature of AMP, broad peaks for CMP and crystallinity for HA (Figure 3-3). Both AMP and CMP present featureless structures in TEM. Thus both TEM and XRD results confirmed the amorphous structure of the AMP nanoparticles. Results are also unambiguous for crystalline HA. Indeed, Panda et al. previously reported similar peaks in HA nanoparticles [24]. However, for CMP, the results differ presumably because of the local structural response provided by the TEM and bulk properties determined by the XRD.

Fourier transform infrared spectroscopy of AMP, CMP, and HA nanoparticles in Figure 3-4 showed an absorption band at 1040-1020 cm^{-1} which belonged to the PO_4^{-3} group. There were no bands observed at 1470-1420 cm^{-1} and 875 cm^{-1} confirming the absence of carbonate groups.

Biodegradation and apatite formation on nanoparticles were examined in the SBF incubation experiment (Figure 3-5 a). AMP was previously known as a highly degradable material [21]. Mg^{2+} ions that are released from the AMP nanoparticles promote formation

of amorphous calcium phosphate which creates deposition sites for further deposition of apatites [21]. Bachra reported that magnesium ions negatively affect the precipitation of calcium phosphates by delaying the transformation of amorphous precipitates into poorly crystalized apatites [25]. Another study by the same researcher confirms that presence of Mg^{2+} ions in biological apatites also contributes to their low crystallinity [26]. Ca^{2+} and phosphate ions are crucial for apatite formation (Figure 3-5 b and c). Soaking in SBF induces dissolution on calcium and phosphate ions. Weng *et al.* reported that as the concentration of calcium and phosphate ions increase in the SBF solution due to the dissolution of calcium and phosphate ions from the hydroxyapatite coatings, it leads to higher supersaturation of these ions in the solution, which results to formation of nucleation sites and growth of apatites [27].

Developing degradable biomaterials with the ability to induce proliferation and differentiation of preosteoblasts is a major goal in orthopedics. Cell compatibility results presented in this study showed that AMP group provided the best condition for preosteoblast cell compatibility compared to the CMPs and HAs on day 1 (Figure 3-6). AMPs also showed higher proliferation rate than the HAs on day 7. These results suggest that Mg^{2+} ions do not have cytotoxicity effects on preosteoblasts and stimulate preosteoblast cell proliferation which was in consistent with previous studies [28]–[32].

Higher proliferation rate of the preosteoblasts in the AMP group seems to be directly influenced by Mg^{2+} ion concentration in the surrounding environment. As our results show, remaining Mg^{2+} ion concentration was the lowest in AMPs amongst the three studied groups (Figure 3-7) suggesting that Mg^{2+} ions can be involved in multiple

preosteoblastic proliferation pathways. It seems that Mg^{2+} ions were provided by the dissolution and degradation of AMPs, were used by the preosteoblasts and stimulated subsequent preosteoblast cell growth in the AMP groups. On the other hand, lesser amount/no amount of Mg^{2+} ions were provided by CMP or HA groups, respectively. This might be due to the lower dissolution rate in these groups which failed to provide similar concentration of Mg^{2+} ions to preosteoblasts in CMPs. Significantly higher amount of the remaining magnesium in the AMP media in day 2 and 3 compared to the following days can be due to the doubling time of the MC3T3-E1 cells (approximately 38 hours). Consequently, improving effect of higher Mg^{2+} ion concentration is observed after completion of the first doubling time as expected. Presence of Mg^{2+} ions was previously known to stimulate preosteoblast cell responses [32]. These results are in agreement with prior reports that showed addition of Mg^{2+} ions in fluorapatite promoted osteoblast differentiation [31] and Mg^{2+} ions induced osteoblast proliferation and differentiation [29].

To determine the mechanism of osteoblast proliferation and differentiation on examined nanoparticles it is crucial to monitor the expression level of genes associated with the osteoblast phenotypes. Sequence of gene expression defines three distinct phases in osteoblastic cells: 1) growth or proliferation and extracellular matrix biosynthesis; 2) extracellular matrix development, maturation, and organization; and 3) extracellular matrix mineralization [33].

Alteration in the expression level of multiple genes including: GAPDH, ALP, COL I, OCN, OPN, RUNX2, and Beta Actin can provide us with valuable information for understanding the mechanism of osteoblast behavior when cultured in AMPs, CMPs, and HAs (Figure 3-8). Overall expression level of osteoblast phenotypic markers like ALP,

OPN, and RUNX2 was higher in nanoparticles like AMPs and CMPs which are capable of releasing Mg^{2+} ions than their HA counterparts [33]–[35]. Although OCN expression level was higher in HAs than other groups, greater expression of ALP and OPN in AMPs and CMPs could provide osteoblastic phenotypes to the cultured cells. ALP is also shown to increase with down-regulation of proliferation [33]. Genes associated with formation of extracellular matrix like COL I, fibronectin, and TGFβ are actively up-regulated during proliferation and gradually decline as the cells proceed to the mineralization stage. Immediately after proliferation stage, extracellular matrix enters a series of modifications leading to higher mineralization [33]. Higher expression level of COL I in cells cultured on HA, and then CMP nanoparticles suggest that Ca^{2+} ions play critical role in mineralization of osteoblasts since these two groups as opposed to the AMPs, contain Ca^{2+} ions. During mineralization OCN and OPN accumulate [35], [36]. Expression level of OPN in AMPs and CMPs show that these groups also stimulate examined cells for active mineralization since OPN is expressed both in proliferation and mineralization stages [33]. In contrast to OPN, OCN is only expressed post-proliferatively [33]. OCN correlates to calcium deposition in osteoblasts [34] which justifies the higher level of OCN expression in calcium containing particles like CMPs and HAs than the non-calcium containing particles like the AMPs. Another study by Zhang *et al.* suggests similar justifications as the release of Ca^{2+} and Si^{2+} ions from calcium silicate, CSP, ($Ca_7Si_2P_2O_{16}$) bioceramics stimulated osteogenic protein expression level of rat bone marrow stromal cells (rBMSCs) [37]. This group monitored expression level of ALP, COL I, OCN, OPN, and RUNX2 in the rBMSCs cultured with the bioceramic disc extracts, and showed that CSP extracts improved the rBMSCs viability. In addition, higher expression level of abovementioned

osteogenic proteins were observed and the up-regulation was shown to be via P-ERK1/2 pathways [37]. Their results suggested that the activation of ERK/RUNX2 pathways might explain the mechanism of up-regultion of these osteogenic genes, since inhibition of this pathway by PD98059, a specific ERK inhibitor, significantly inhibited the up-regulation of protein expression level [37]. AMPs are suggested to up-regulate osteogenic genes via activation of the same pathway.

RUNX2 is a critical osteogenesis transcription factor; it is the product of *Cbfa1* gene, which binds to the osteoblast-specific *cis*-acting element2 (OSE2), and is a key molecule for osteoblast differentiation [38]. RUNX2 is expressed and activated via activation of MAP kinases ERK1 and ERK2 [39] and activates ALP, OPN, and OCN [37]. So, higher RUNX2 level in AMP and CMP after 7 days can suggest even higher expression level of abovementioned genes, especially OCN which is expressed in the later stages of differentiation [37], in the following days Figure 3-8. RUNX2 is an essential factor for osteoblast and hypertrophic chondrocyte differentiation and is expressed during mesenchymal condensations [40]–[43].

As previously reported by Muller *et al.*, RUNX2 expression can be stimulated solely via the calcium phosphate surface or in a combination with osteogenic soluble factors [44] which can justify the similar expression level of RUNX2 in AMPs and CMPs. HAs showed lower level of RUNX2 which might be due to the lower stimulation of either pathway. OCN, COL I, and ALP expression level were previously reported to be more dependent upon the signals from the soluble factors as they were up-regulated when higher biological stimuli were present, whereas RUNX2 regulation was more independent of the environment [44].

Present study provides significant data about direct comparison between AMP nanoparticles, which only provide preosteoblasts with Mg^{2+} ions, CMPs, which provide both Mg^{2+} and Ca^{2+} ions, and HAs, which provide preosteoblasts with Ca^{2+} ions. Although it is important to investigate the effect of these ions on preosteoblasts *in vitro*, lack of *in vivo* studies is one the major limitations of this study since the ultimate goal is to provide orthopedic biomaterials in humans.

3.6 Conclusions

Present study provides valuable evidence on crucial role of Mg^{2+} and Ca^{2+} ions in proliferation, differentiation, and mineralization of preosteoblasts. Our data supports the null hypothesis that presence of Mg^{2+} and Ca^{2+} significantly increases proliferation rate of preosteoblasts and directs them towards osteoblastic differentiation via regulation of osteoblastic genes.

Chapter 4

Fabrication of Novel PLA/AMP Magnesium Phosphate Bionanocomposite Fibers for Tissue Engineering Applications via Electrospinning

4.1 Abstract

Fibrous bionanocomposites consisting of amorphous magnesium phosphate (AMP) nanospheres and polylactic acid (PLA) were fabricated by electrospinning. There are two important signatures of this study. First, AMP, as an alternative to well-known calcium phosphate (CaP) materials, was added to PLA as the second phase. To the best of our knowledge, it was the first attempt to fabricate magnesium phosphate (MgP)/biopolymer composite. This was made possible by our previously reported research on the successful synthesis of AMP nanospheres via microwave processing. Second, the sustained release of magnesium and phosphate ions from PLA matrix could stimulate a series of cell responses. The structure of the composites and their bone-like apatite-forming abilities in simulated body fluid (SBF) were examined. Additionally, the effects on the proliferation and differentiation of preosteoblast cells were evaluated by performing in vitro cell culture and monitoring markers such as Osteocalcin (OCN), Osteopontin (OPN), Alkaline phosphatase (ALP) and Collagen type-I (Col I) using real-time polymerase chain reaction (PCR). For

better dispersion of AMP in the fibers, a surfactant, 12-hydroxysteric acid (HSA), as previously reported in the literature, was used. However, HSA significantly inhibited the proliferation and differentiation of preosteoblast cells, indicating the potential risk in using HSA in the combination of AMP or MgP in tissue engineering applications.

4.2 Introduction

This work was a sequel to our previous efforts on the synthesis of nanocrystalline alkaline earth phosphates and incorporating them into appropriate biopolymer scaffolds [61, 96, 192]. The intended use for such alkaline earth phosphates and related composites was in repairing bone related defects in diverse fields such as orthopedics and dentistry. Previously, nanocrystalline carbonated calcium deficient hydroxyapatite (CDHA) from simulated body fluids (SBF) was synthesized and incorporated into PLA fibers via the process of electrospinning [192]. Here, such composites are referred as "Bionanocomposites", since when nanocomposites have a close connection with biomedical fields, a newer class of materials may be defined by adding the prefix of "bio" to the older class of materials [192, 193].

It is believed that the group of magnesium phosphate compounds (MgP) deserves significant attention as biomaterials. Of all the alkaline earth phosphates, MgP should have importance only second to calcium phosphates (CaP). Yet, unlike CaP, MgP has not received proper attention with the perception that this material is just another alkaline earth phosphate. To justify these assertions, at least two justifications are provided. First, magnesium is the fourth abundant element in human body [194]. Being in the same period (alkaline earth) in the periodic table as calcium, magnesium is one of the key ingredients

of bone mineral. It is known that magnesium ions can influence bone mineral metabolism, formation and crystallization processes [30, 32, 93]. Second, Mg-based biomaterials are becoming more and more popular in biomedical uses such as biodegradable Mg alloys and MgP-based bone cements. In both of these uses, MgP materials play significant roles. Implants made of degradable Mg alloys provide biocompatibility, bioactivity, osteoconductivity, great mechanical performances, and elimination of the need for a second operation for implant removal [24, 195, 196]. Additionally, MgP based coating can be deposited on the surface of Mg alloys to improve the corrosion resistance of Mg alloys [197, 198]. MgP based bone cements are considered as a great alternative to CaP based bone cements, providing positive bone regeneration stimulation, much higher mechanical strength and faster dissolution rate [78, 81]. Furthermore, they can also be combined with CaP cements to modify the mechanical and biological performances of final products [199, 200].

As opposed to hundreds of papers published on CaPs, significantly lesser number of studies was published on MgPs. A few important papers are highlighted in the following. Both magnesium doped CaP and pure MgP exhibit significant biocompatibility and faster biodegradation rate as compared to CaPs [3, 60, 123, 201]. Landi et al. compared 5.7 mol% Mg doped hydroxyapatite (HA) and pure HA [103]. After implantation, Mg-doped HA granules resulted in higher amount of bone in contact with the material as compared to HA, though both materials revealed to be osteoconductive and effective as bone substitutes. They also evaluated mesenchymal stem cells (MSCs) and MG63 osteoblast cells on Mg doped HA (6.5 mol%) and HA, showing Mg doped HA improved the behaviors of MSC and MG-63 cells in term of adhesion, proliferation and metabolic activation compared to

stoichiometric HA [202]. Instead of magnesium doped materials, MgP materials also exhibit great biocompatibility to bone cells. It was reported by Tamimi et al. that both cattiite (Mg3(PO4)2·22H2O) and newberyite ($MgHPO_4 \cdot 3H_2O$) showed low cytotoxicity to MC3T3-E1 cells [60]. In their assessment of expression of osteoblast differentiation markers on MgP phases, the expression of OCN and Col1A1 genes of mouse bone marrow cells (mBMCs) cultured over MgP crystals (newberyite and cattiite) closely matched the expression achieved using calcium phosphates (HA and brushite). Furthermore, it is interesting to notice that Mg^{2+} can have inhibitory effects on the activity of osteoclasts, a function CaP lacks. Janning et al. implanted $Mg(OH)_2$ cylinders into rabbit femur condyles for 2–6 weeks and observed the enhanced bone formation and temporarily decreased bone resorption around the slowly dissolving $Mg(OH)_2$ cylinder resulting in a higher bone mass [152]. Roy et al. reported that 1 wt.% Mg doping in beta tricalcium phosphate (β-TCP) can significantly decrease in initial osteoclast differentiation and restrict osteoclast cell-mediated TCP degradation as compared to pure β-TCP and 1 wt.% strontium doped β-TCP [203].

In human bone minerals, amorphous calcium phosphate (ACP) is of great interest. It is an intermediate phase during the formation process of biological apatites, a highly biodegradable, biocompatible, and bioactive material [204, 205]. In addition, it works alone or as filler in composites to provide sustained release of calcium, phosphate and other doping ions to plasma for the healing and regeneration of hard tissues [204, 206, 207]. Previously, a microwave assisted method to produce nanocrystalline ACP was reported [96]. Under microwave irradiation, the nanospherical form of CaP was the most favored structure. In those experiments, Mg^{2+} ions were observed to be incorporated to the CaP

lattice and the weight ratio of Mg increased with its concentration in aqueous medium. This microwave assisted method was shown to be a strategy to prepare amorphous magnesium phosphate (AMP) nanoparticles. Subsequent research proved this concept with the synthesis of AMP nanospheres using microwave irradiation [61]. The as-synthesized AMP nanospheres were precursors of crystallized bobierrite ($Mg_3(PO_4)_2 \cdot 8H_2O$), converting into microcrystals with a layered structure of ellipses and cylinders after 7 days incubation in SBF, a phenomenon similar to the conversion of ACP to octacalcium phosphate (OCP) and hydroxyapatite (HA) in the formation of CaP materials [208, 209]. Additionally, the presence of MgP has a role in stabilizing ACP, resulting in the formation of poorly crystallized CaP materials [94, 210].

To the best of our knowledge, MgP, to which AMP is a sub-set, has not been used as a potential component of temporary composite scaffolds. One factor limiting the inclusion of MgP in composite scaffolds has been the difficulty in synthesizing nanosized MgP particles, attributed to the high instability of MgP in aqueous medium. Previous reports of MgP synthesis used ionic interaction between Mg^{2+} and PO_4^{3-} in an aqueous medium by controlling reaction conditions such as temperature and ionic composition. This often resulted in the production of large MaP particles [60, 211]. Synthesis of nanosized MgP particles in large scale was a key step to fabricate MgP containing composite scaffold.

Present AMP nanospheres can act as desired fillers for fabrication of composite scaffold with sustained release of magnesium and phosphate ions. Here is the first report of fabricating a composite scaffold using MgP materials as fillers. In this work, polylactic acid (PLA) and AMP were used to make a porous scaffold via electrospinning. PLA was selected as the polymer matrix because it is a FDA approved biodegradable polymer used

for applications as sutures, pins, screws and drug delivery systems [212-214]. Fabrication of PLA based composite for potential bone tissue engineering applications has also been widely investigated, and significant progress was presented in the past decade [6]. Electrospinning was selected due to the fact that it is a simple and versatile technique capable of generating non-woven fibrous mats directly from a variety of polymers and composite materials, providing significant features such as large surface areas, high porosity, and ease of incorporation of functional components [215]. The presence of AMP in PLA matrix was expected to provide sustained release of Mg^{2+} and PO_4^{3-}, thus affecting proliferation and differentiation of osteoblast bone cells.

Thus, the objectives of this study are: 1) to fabricate PLA–AMP bionanocomposite via the process of electrospinning, and 2) to evaluate bioactivity and biocompatibility of as-fabricated composite scaffold.

4.3 Experiments

4.3.1 AMP Synthesis

The synthesis of AMP nanospheres using microwave has been reported in our previous publication [61]. All reagent grade chemicals were purchased from Fisher Scientific (Fair Lawn, NJ, USA) and used without further purification. The reaction solutions were prepared by mixing $MgCl_2 \cdot 6H_2O$ (2.078 g), KH_2PO_4 (1.361 g) and $NaHCO_3$ (2.27 g) in 1 L of DI water in 3 L capacity beaker. The Mg/P molar ratio in solution was set to 1, arguing that the Mg/P molar ratio in human plasma/serum ranges from 3:2 to 2:3 [18, 216]. 150 mL sample beakers with 100 mL as-prepared solution were then placed onto

the 10×10×1 cm alumina insulating fiberboards and covered with an upside down 250 mL-capacity glass beaker. To proceed with microwave-assisted process, the entire assembly was placed into a household microwave (MW) oven (Emerson, 800 W, 2450 MHZ, Hackensack, NJ, USA) for 5 min. At the end of microwave heating, the beaker was moved to a cold water bath to cool down. Finally, the precipitates were collected after centrifugation at 3000 rpm for 5 min. All precipitates were completely dried in 37 °C oven overnight.

4.3.2 PLA/AMP Mixture Preparation

PLA pellets were supplied by Jamplast (Ellisville, MO). The weight average molecular weight (Mw) and polydispersity of PLA are 114,000 and 1.435, respectively. These values were determined by gel permeation chromatography relative to polystyrene standards using Shimadzu LC 10ADVP liquid chromatography equipped with a Shimadzu ELSD-LT ultraviolet (UV) detector (Columbia, MD, USA). Chloroform (CHCl3) and Dimethylformamide (DMF, C3H7NO) were used as solvent for the preparation of electrospinnable mixtures and were purchased from Fisher Scientific (Fair Lawn, NJ, USA). PLA pellets were initially dissolved in chloroform (1 g/10 mL). Subsequently, as-prepared AMP precipitates (25 wt.% of PLA) were added to PLA solution to make the mixture A. To further improve the dispersion and affinity of AMP in PLA, a surfactant 12-hydroxysteric acid (HSA, C18H36O3) was added to PLA–AMP suspension (5 wt.% of AMP) [217], designated as the mixture B. To uniformly disperse AMP particles in PLA solution, mixture was treated by 10 min ultrasonication to destroy any loose AMP

agglomerates. After further addition of DMF (25% volume of chloroform) to the mixture and 4 h of stirring, the mixture was ready for electrospinning.

4.3.3 Electrospinning

A horizontal electrospinning setup was used in this study to fabricate fibrous composite scaffold. It was composed of a high voltage power supply, a pump, a syringe, a flat tip needle and a conducting collector plate. The pumping rate was set to be 1 mL/h, working distance was 20 cm, the tip needle size was gauge 22, and the assigned voltage was 20 kV. Neat PLA fibers were also electrospun with the same operating parameters as control. Fibers were collected and left to dry in a fume hood to remove residual solvents. Once no weight loss of as-produced fibers was observed by using XP105 DeltaRange analysis balance (Mettler-Toledo, Columbus, OH, USA), residual solvents were considered to be totally removed.

4.3.4 Physical Characterization

AMP particles, PLA pellets, and as-fabricated PLA and PLA–AMP fibers were all characterized by X-ray diffraction (XRD, Ultima III, Rigaku, The Woodlands, TX, USA) with monochromated Cu Kα radiation, operated at a voltage of 40 kV and 44 mA setting. All samples were examined at 2θ angles from 10° to 45° at a scanning speed of 1° per minute. Fourier transform infrared spectroscopy (FTIR, UMA-600 Microscope, Varian Excalibur Series, Holliston, MA, USA) was applied for chemical analysis of AMP and fabricated fibers. The transmittance of each sample was recorded with 256 scans with resolution of 4 cm−1 between 4000 and 700 cm−1. The morphological features of AMP

particles and fibers were visualized by scanning electron microscope (SEM, S4800, Hitachi, Japan). Energy dispersive X-ray spectroscopy (EDS) analysis was applied to examine the distribution of precipitates in fibers. Nano-structures of PLA–AMP composites were investigated using transmission electron microscopy (TEM, HD-2300, Hitachi, Japan) with a voltage of 200 kV. Differential scanning calorimetry (DSC, Pyris, Perkin Elmer, Waltham, MA, USA) was applied for thermal analysis of fabricated PLA and PLA–AMP fibers. Thermogravimetric analysis (TGA, Q50, TA Instruments, New Castle, DE, USA) was applied to determine the weight of AMP in PLA matrix.

4.3.5 In vitro Degradation and Bioactivity Testing

PLA and PLA–AMP fibers were electrospun to microscope cover glass (18 mm diameter, Fisher Scientific, Fair Lawn, NJ, USA) for in vitro degradation test. The weight of each glass substrate and sample was recorded and placed in closed tubes containing 40 mL of simulated body fluid (SBF) [218] and incubated in vitro at 37 °C for different periods. The composition of SBF was listed in Table 3.2. The weight changes of samples were measured by using XP105 DeltaRange analysis balance. The incubated fibers were also characterized using SEM.

4.3.6 Preosteoblast Culture

MC3T3-E1 (CRL-2593™, ATCC, Manassas, VA, USA) preosteoblast cells were used to study the effects of additives on preosteoblast proliferation and differentiation. Cells were first grown at 37 °C and 5% CO_2 in alpha minimum essential medium (α-MEM, Thermo Scientific HyClone, Logan, UT, USA), augmented by 10% Fetal Bovine Serum

(FBS, Thermo Scientific HyClone, Logan, UT, USA). The culture medium was replenished every other day until the cell reached a confluence of 90%.

To study cell proliferation, PLA–AMP and PLA–AMP–HSA fibers were first electrospun to microscope cover glass for fiber fixation. PLA fibers and PLA–HA fibers were applied as control. HA was synthesized using $Ca(OH)_2$ and H_3PO_4 and loaded to PLA similar to AMP using electrospinning. All samples were sterilized using 70% ethanol. MC3T3-E1 cells were seeded to wells (Flacon™ 12 wells cell culture plates, BD Biosciences, San Jose, CA, USA) of sterilized samples at a density of 10,000 cells/sample. Cell numbers on samples were counted after 24 h, and 7 days using CytoTox 96® Non-Radioactive Cytotoxicity Assay kit (Promega, Madison, WI, USA). For statistical analysis, all experiments were performed at least in triplicate, and t-test analysis was applied for data analysis. Cell morphology on samples after 7 days was examined using SEM. Prior to SEM, samples underwent a fixation procedure with glutaraldehyde, graded dehydration with ethanol, critical point drying procedure and sputter coating [192, 219-221].

To study cell differentiation, MC3T3-E1 cells were seeded to of sterilized samples (PLA, PLA–AMP, PLA–AMP–HSA) at a density of 10,000 cells/sample. At the end of 10 days incubation, cells were lysed using Trizol® reagent following the manufacturer's protocol and the total RNA was extracted and quantified by reading the optical density at 260 nm. Total RNA (2 μg for each sample) was reverse transcribed to cDNA using a high-capacity M-MLV reverse transcriptase enzyme (Promega, Madison, WI, USA). The resulting cDNAs were used for real-time polymerase chain reaction (PCR). Reactions were carried out in a 7500 Real-time PCR System (Applied Biosystems, Carlsbad, CA, USA) for 60 cycles (95 °C for 15 s, 60 °C for 60 s and 72 °C for 60 s) after the initial 10 min

incubation at 95 °C. A Ct (cycle threshold) value for each reaction was calculated using Applied Biosystems' sequence detection software and the relative ratio of expression was determined. For statistical analysis, all experiments were performed at least in triplicate. Primers used to amplify specific targets are previously presented in Table 3.3.

4.4 Results and Discussion

4.4.1 AMP Dispersion in PLA Mixture

The dispersion of AMP w/o HSA in PLA mixture after 24 h setting in room temperature is shown in Figure 4-1. It is observed that AMP itself can be uniformly dispersed in PLA mixture without precipitation and HSA has no significant impacts on AMP dispersion.

Figure 4-1: Dispersion of AMP in (a) PLA and (b) PLA-HSA system after 24 hours

4.4.2 Physical Characterization

The XRD patterns of AMP particles, PLA pellets, PLA fibers, PLA–AMP fibers and PLA–AMP–HSA fibers are shown in Figure 4-2. PLA pellets examined by XRD showed high crystallinity with a strong peak observed at 16.5°. After electrospinning, PLA lost its crystallinity. On the other hand, the synthesized AMP particles are highly amorphous.

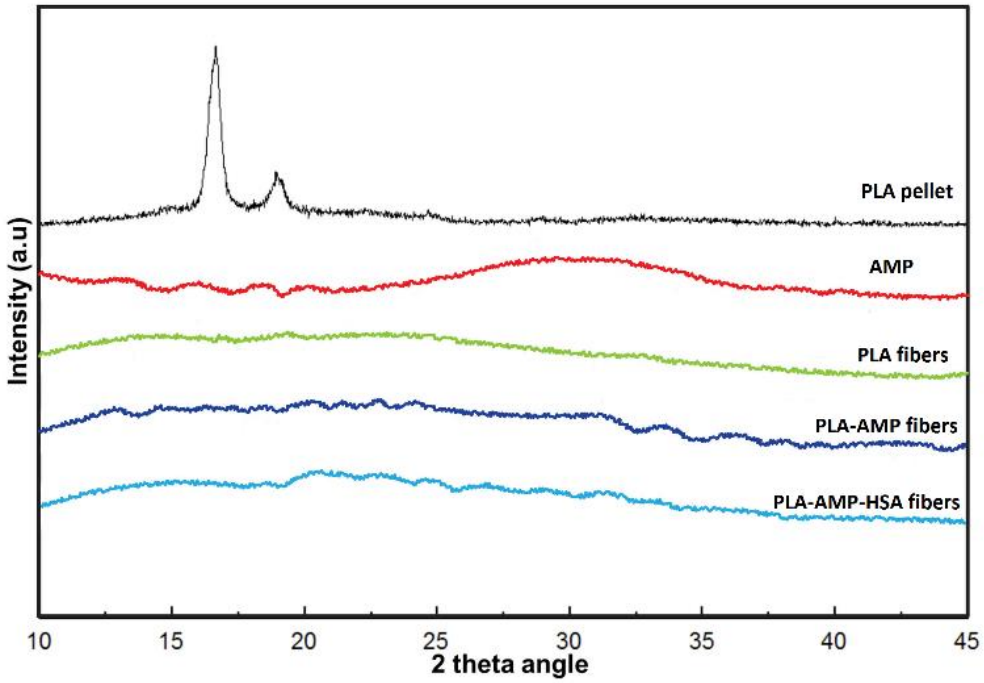

Figure 4-2: XRD patterns of PLA pellet, AMP, PLA fibers, PLA–AMP fibers and PLA–AMP–HSA fibers

The FTIR data of AMP, PLA fibers, PLA–AMP fibers, and PLA–AMP–HSA fibers are shown in Figure 4-3. From FTIR data of AMP, no absorption bands observed at 1470–1420 and 875 cm−1, indicating no presence of carbonate in AMP structure. The absorption band of PO_4^{3-}/HPO_4^{2-}that belonged to AMP at 1040–1020 cm^{-1} was also observed on FTIR data of PLA–AMP fibers, which confirmed the presence of AMP particles in PLA–

AMP fibers. PLA–AMP and PLA–AMP–HSA fibers also showed a new absorption peak that appeared at 1600 cm^{-1} as compared to PLA and AMP.

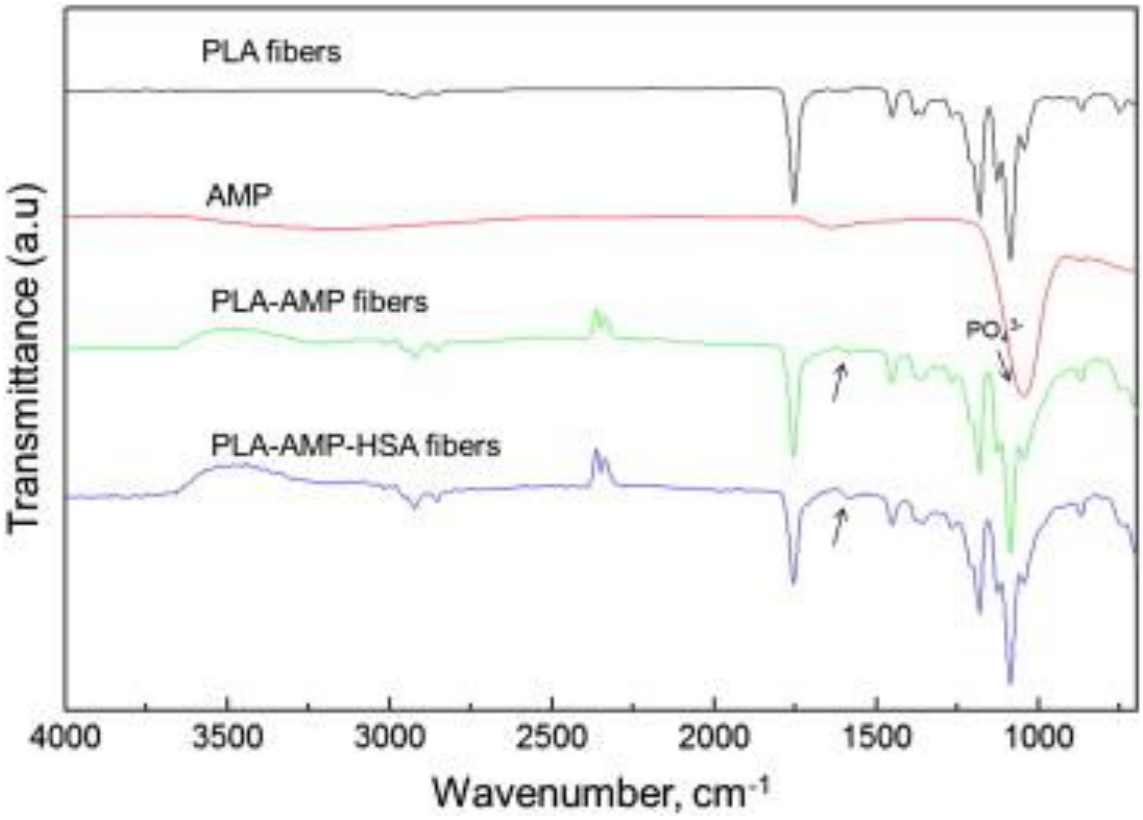

Figure 4-3: FTIR results of AMP, PLA fibers, PLA–AMP fibers and PLA–AMP–HSA fibers

The SEM results are shown in Figure 4-4. The as-synthesized AMP is nanospheres. The presence of Mg and P in the nanospheres was confirmed by EDS, with a Mg/P molar ratio of approximately 1.285±0.24. The SEM images show that the size of the fibers was decreased due to the incorporation of AMP fillers to PLA matrix. However, the addition of HSA showed no significant impacts on AMP dispersion in PLA fibers.

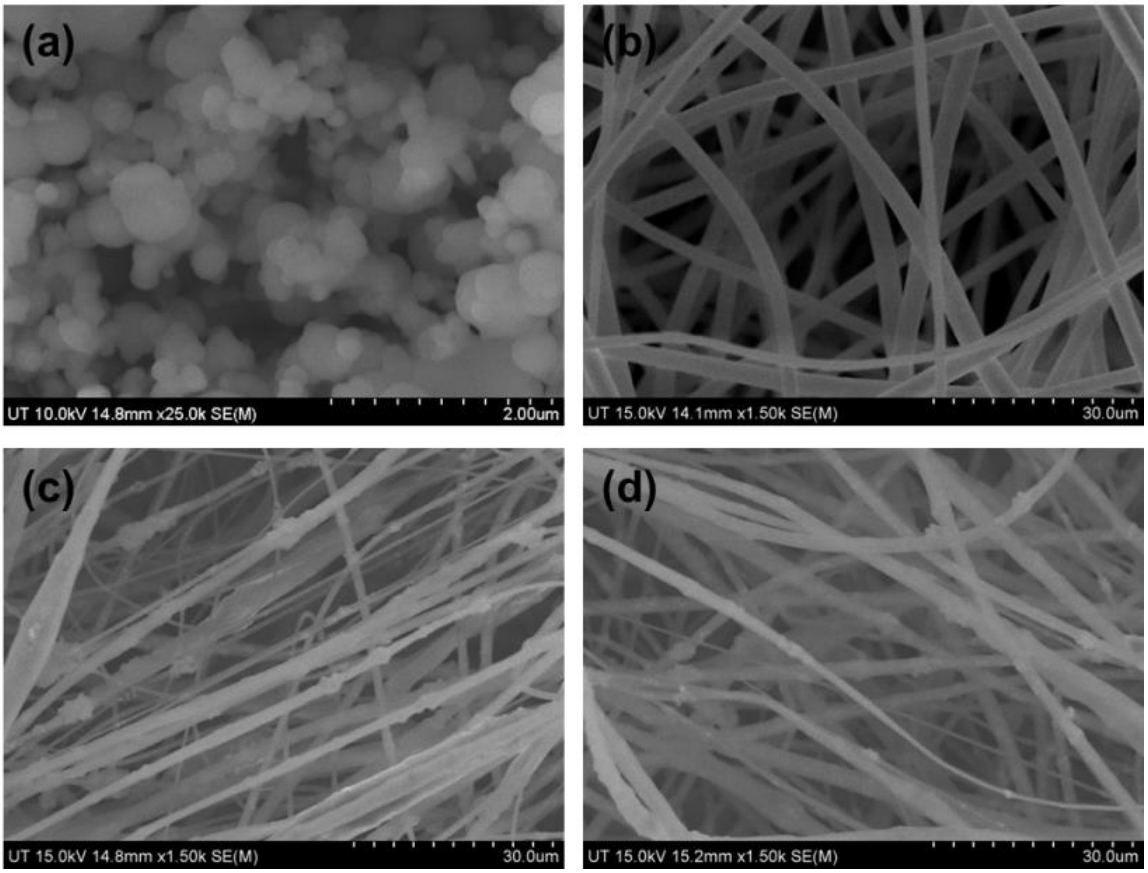

Figure 4-4: SEM images of (a) as-synthesized AMP nanospheres; (b) electrospun PLA fibers; (c) electrospun PLA–AMP fibers; and (d) electrospun PLA–AMP–HSA fibers

In TEM image, AMP nanospheres show a dense core (Figure 4-5 a), and they can agglomerate together due to the newly formed bonding between each spheres (Figure 4-5 b). AMP is randomly dispersed in the internal channel of PLA matrix as fillers (Figure 4-5 c and d).

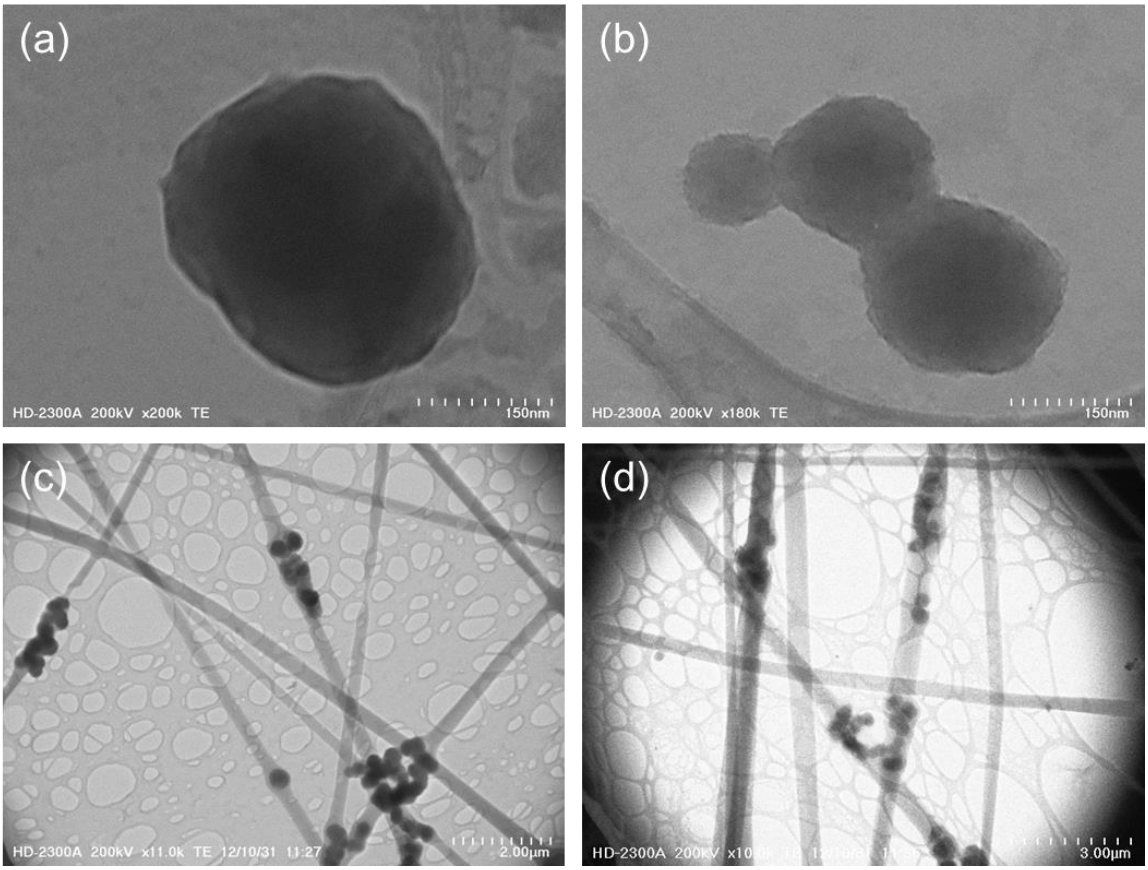

Figure 4-5: TEM of (a, b) AMP nanospheres, (c) PLA–AMP electrospun fiber, and (d) PLA–AMP–HSA electrospun fibers

Typical DSC traces of PLA pellets, PLA fibers, PLA–AMP fibers and PLA–AMP–HSA fibers are shown in Figure 4-6. The melting enthalpies of the PLA pellets, PLA fibers, PLA–AMP fibers and PLA–AMP–HSA fibers are 33.4 J/g, 27.1 J/g, 23.15 J/g and 27.09 J/g, respectively. The melting temperatures (Tm) of PLA pellets, PLA fibers, PLA–AMP fibers and PLA–AMP–HSA fibers are 170.1 °C, 170.1 °C, 167.42 °C, and 167.73 °C. The crystallization temperatures (Tc) of the PLA pellets, PLA fibers, PLA–AMP fibers and PLA–AMP–HSA fibers are 119 °C, 92.3 °C, 85.95 °C, and 85.95 °C. Besides, the glass

transition (Tg) of the PLA pellets, PLA fibers, PLA–AMP fibers and PLA–AMP–HSA fibers are 67.5 °C, 67.5 °C, 61.7 °C, and 62 °C, respectively.

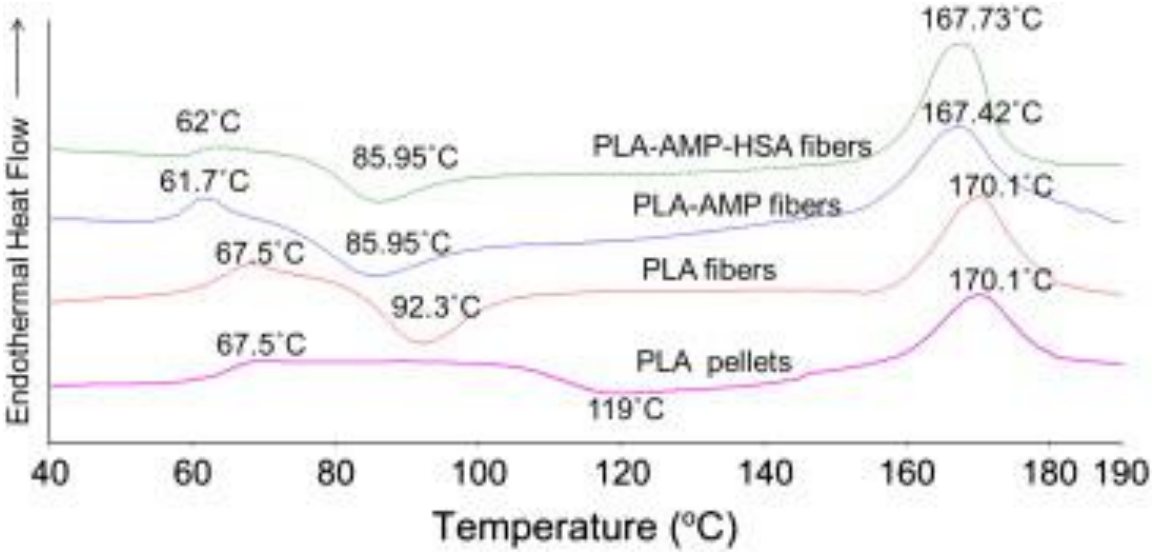

Figure 4-6: DSC of PLA pellets, PLA fibers, PLA–AMP fibers and PLA–AMP–HSA fibers

TGA analysis of PLA–AMP is shown in Figure 4-7. The final weight of PLA/AMP after 500 °C is approximately 17.5% of the total weight, and PLA/AMP/HSA after heating only has approximately 16.5% weight left.

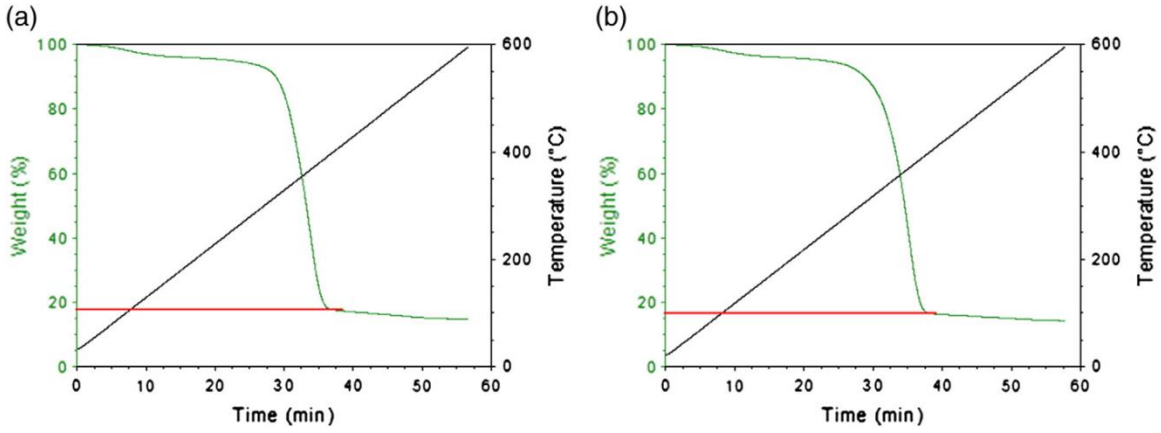

Figure 4-7: TGA results of (a) PLA–AMP fibers and (b) PLA–AMP–HSA fibers

4.4.3 In Vitro Degradation and Bioactivity Testing

The weight changes of samples with time are shown in Figure 4-8. PLA-AMP fibers show a significantly lower weight increase ($p < 0.05$) with time as compared to the control (PLA) after 1 week incubation in the SBF. Both PLA-AMP and PLA-AMP-HSA groups showed significantly lower ($p < 0.05$) weight increase after 2 and 3 weeks incubation in the SBF when compared to the control (PLA) group. After 4 weeks of SBF incubation PLA-AMP and PLA-AMP-HSA groups showed significantly lower ($p < 0.1$) and ($p < 0.05$) weight increase respectively when compared to the control (PLA) group.

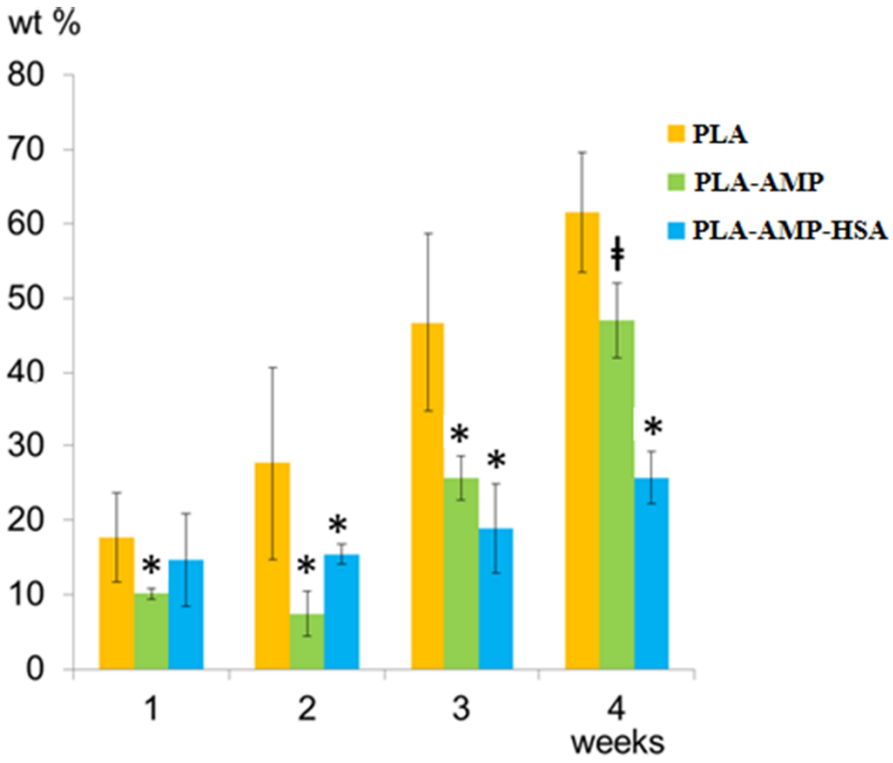

Figure 4-8: Weight change of PLA, PLA–AMP and PLA–AMP–HSA fibers with time after incubation in the SBF at 37 °C. Groups were studied in at least triplicates. PLA was used as the control group. Statistical analysis was performed using t-test. (*) indicates $p < 0.05$, (ǂ) indicates $p < 0.1$.

The fiber's surface features are shown in Figure 4-9. PLA–AMP fibers show the most uniform coating with highest thickness, the space between fibers is filled with deposited apatite. Conversely, PLA fibers show randomly deposited apatite on its surface with agglomerates of apatite present in its matrix.

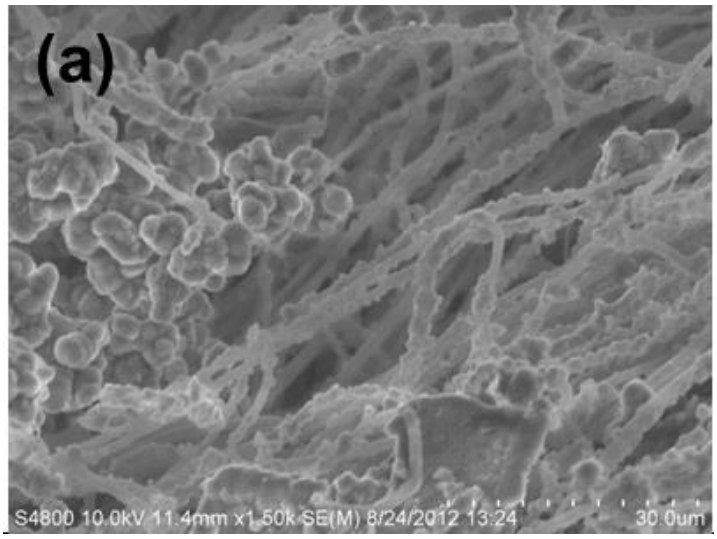

Figure 4-9: SEM images of (a) electrospun PLA fibers after 4 weeks incubation in SBF

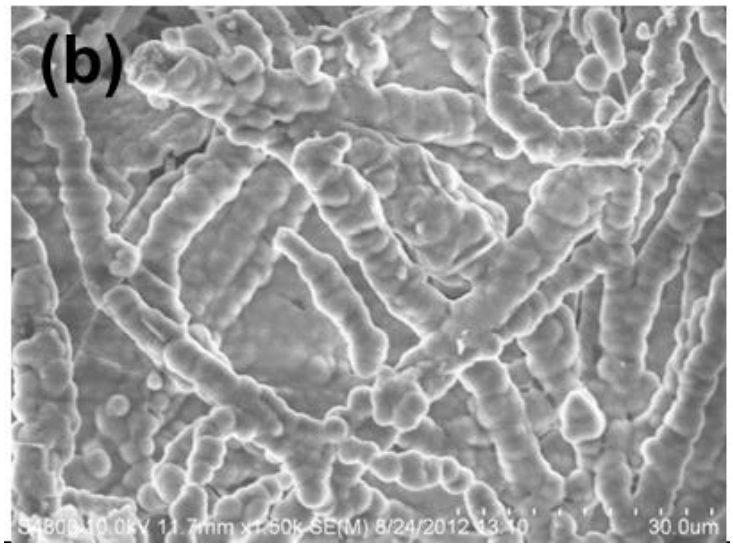

Figure 4-9: SEM images of (b) electrospun PLA–AMP fibers after 4 weeks incubation in SBF

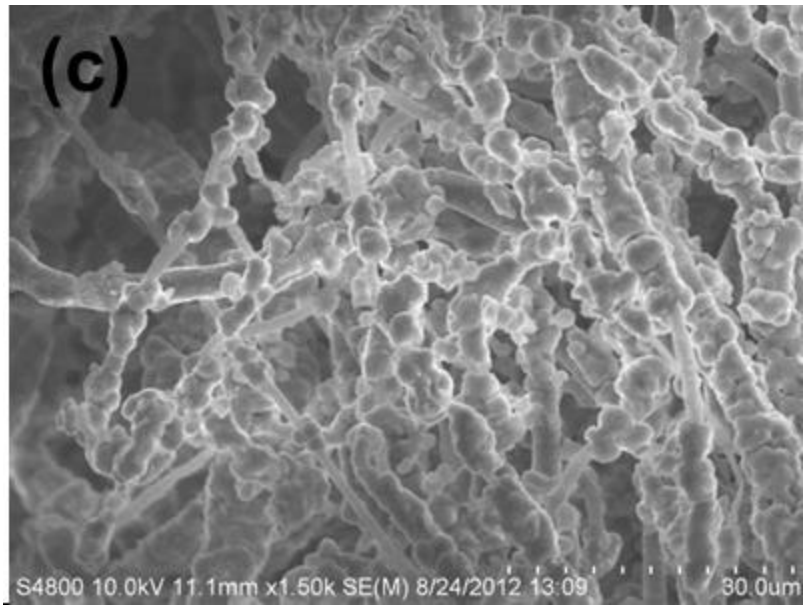

Figure 4-9: SEM images of (c) electrospun PLA–AMP–HSA fibers after 4 weeks incubation in SBF

4.4.4 Preosteoblast Culture

In vitro cell proliferation data are shown in Figure 4-10. Although cell proliferation rate was not significantly different between PLA-AMP and PLA-HA groups as compared to the control group (PLA), cell proliferation on PLA–AMP–HSA electrospun fibers was significantly lower ($p < 0.05$) than the PLA group. All other groups showed similar MC3T3-E1 cell proliferation.

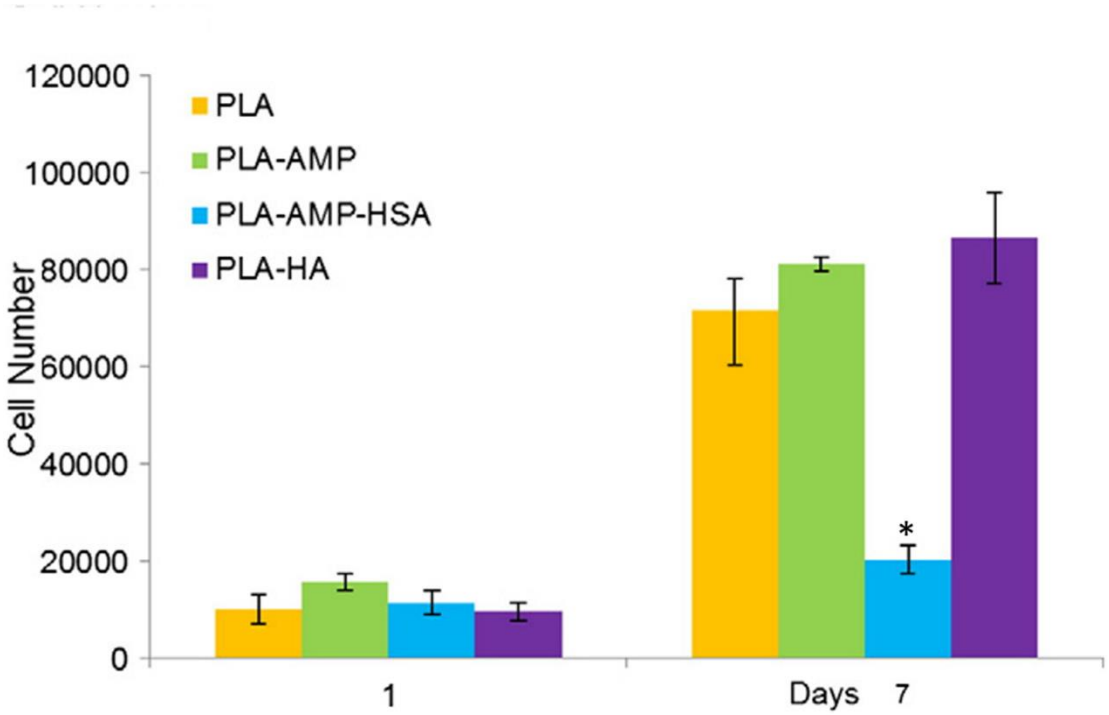

Figure 4-10: Number of MC3T3-E1 preosteoblast cells on PLA, PLA–AMP, PLA–AMP–HSA and PLA–HA fibers at day 1 and day 7. Groups were studied in at least triplicates. Statistical analysis was performed using t-test. PLA was used as the control group. Four studied groups were compared within the time periods of 1 and 7 days. (*) indicates $p < 0.05$, (ł) indicates $p < 0.1$.

Besides, MC3T3-E1 cell morphology on samples exhibited a flat appearance and was spread out over the surfaces of all samples (Figure 4-11). However, it is observed that MC3T3-E1 cells on PLA–AMP fibers synthesized higher matrix as compared to the PLA samples while MC3T3-E1 cells on PLA–AMP–HSA showed the poorest proliferation.

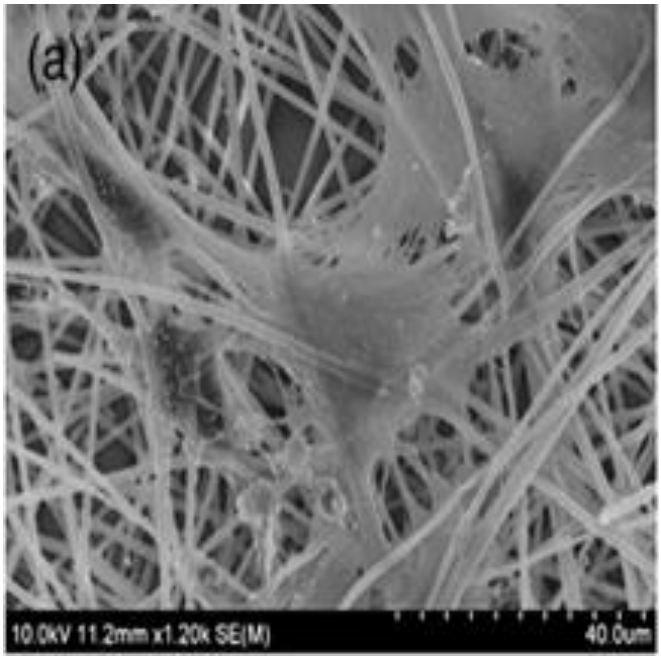

Figure 4-11: SEM images of MC3T3-E1 preosteoblast cells on (a) PLA electrospun fibers

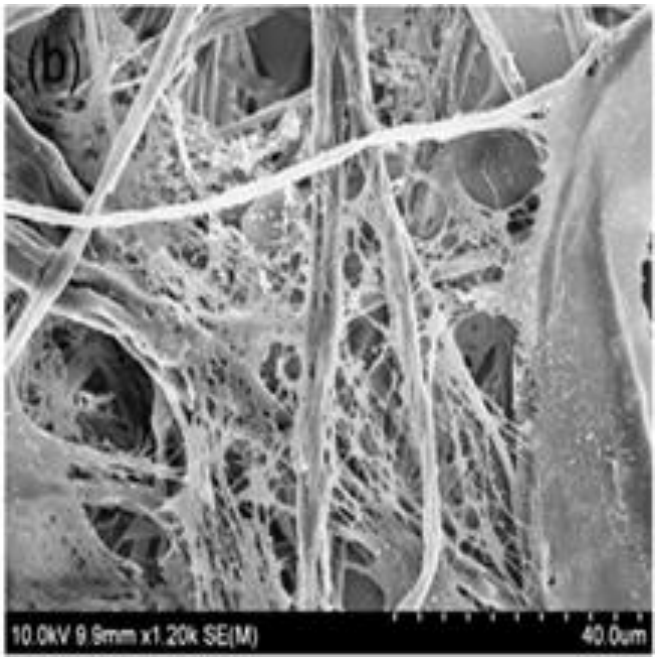

Figure 4-11: SEM images of MC3T3-E1 preosteoblast cells on (b) PLA–AMP electrospun fibers

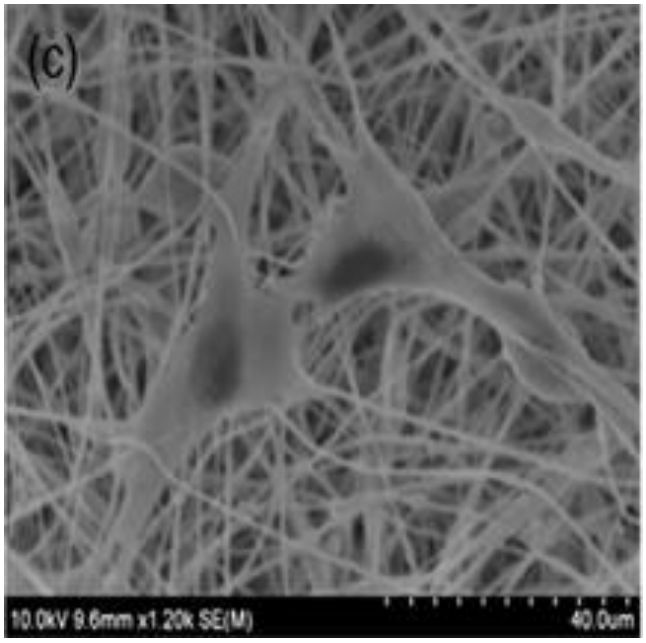

Figure 4-11: SEM images of MC3T3-E1 preosteoblast cells on (c) PLA–AMP–HSA electrospun fibers

Fold change in expression level of different genes grown on PLA–AMP and PLA–AMP–HSA fibers is shown in Figure 4-12. Data are normalized to the expression level of beta actin housekeeping gene for cells grown on PLA–AMP and PLA–AMP–HSA fibers. In the PLA-AMP group, OCN and OPN expression level significantly increased ($p < 0.05$), ALP expression level significantly decreased ($p < 0.05$), and COL I expression level did not significantly change as compared to the Beta actin expression level. In the PLA-AMP-HSA group OCN, ALP and COL I expression level significantly decreased ($p < 0.05$). Moreover, OPN expression level significantly decreased ($p < 0.1$).

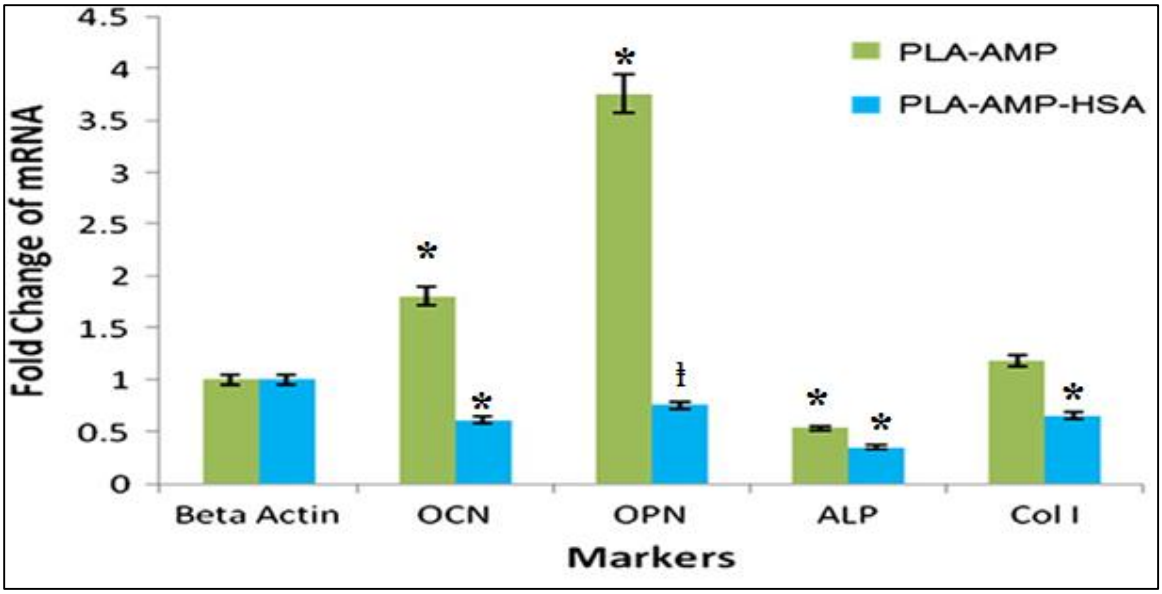

Figure 4-12: RT PCR results of expression level of OCN, OPN, ALP, and Col I in MC3T3-E1 preosteoblast cells grown on PLA–AMP and PLA–AMP–HSA electrospun fibers after 7 days. Data is normalized to the beta actin housekeeping gene expression level in cells grown on PLA–AMP and PLA–AMP–HSA fibers and illustrates the fold change in expression level. Groups were studied in at least triplicates. Statistical analysis was performed using t-test. (*) indicates $p < 0.05$, (ǂ) indicates $p < 0.1$.

.

Appropriate PCR products are confirmed by the gel electrophoresis image of OCN (146 bp), OPN (304 bp), ALP (105 bp), Col I (101 bp), and Beta actin (568 bp) (Figure 4-13).

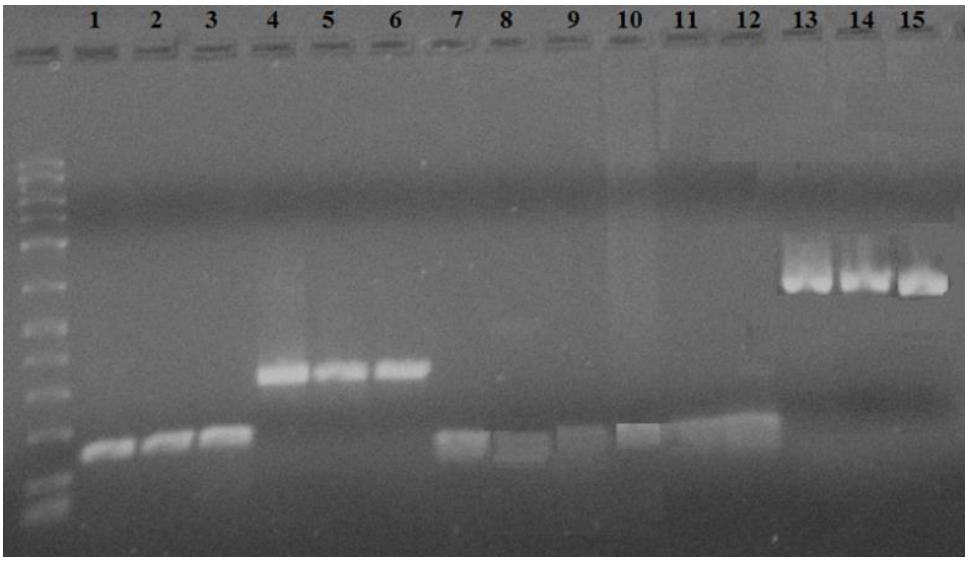

Figure 4-13: DNA gel electrophoresis image of monitored genes along with the DNA marker (Lonza, 50–2500 bp). Lanes 1, 4, 7, 10, and 13 illustrate expression level of OCN, OPN,ALP, Col I, and Beta actin genes of preosteoblast cells grown on PLA fibers respectively.Lanes 2, 5, 8, 11, and 14 illustrate expression level of OCN, OPN, ALP, Col I, and Beta actin genes of preosteoblast cells grown on PLA–AMP fibers respectively. Lanes 3, 6, 9, 12, and 15 illustrate expression level of OCN, OPN, ALP, Col I, and Beta actin genes of preosteoblast cells grown on PLA–AMP–HSA fibers respectively.

4.5 Discussion

The mechanism of synthesizing AMP nanospheres has been well demonstrated in our previous report [61]. Generally, the mechanism of formation can be attributed to the fact that AMP nanospheres, as the first phase to form in concentrated MgP solution under microwave irradiation, are the most energy favored crystal structure as compared to other mature MgP materials, such MgP phases include $MgHPO_4 \cdot 3H_2O$, $Mg_3PO_4 \cdot 5H_2O$, $Mg_3PO_4 \cdot 8H_2O$, and $Mg_3PO_4 \cdot 22H_2O$. Besides, with the continuing precipitation, the ionic concentration continually decreases, thus resulting in the formation of smaller AMP nanospheres.

One highlight of this study is the incorporation of AMP nanospheres into PLA matrix via electrospinning with the purpose of modifying the properties of fibrous bionanocomposite. Electrospinning is an ambient process to fabricate fibrous scaffold with high surface area and interconnected channels suitable for tissue regeneration. AMP nanospheres were successfully incorporated into the inner structure of PLA fibers. The incorporation of AMP to PLA matrix can decrease fiber diameter, which is related to the chemical bonding formed between AMP and PLA in PLA–AMP fibers. The new absorption band of PLA–AMP fibers observed on FTIR can be assigned to COO^- resulting from the interaction of COOH in PLA with $Mg2+$ in AMP lattice [221].

The PLA layer slowed down the fast dissolution of AMP and provided sustained release of Mg^{2+} to the environment.

There are some possible routes to provide better dispersion of nanospheres: 1) decreasing the ionic concentration and modifying the composition of reaction aqueous solution for the synthesis of AMP nanospheres; 2) providing a rapid cooling system such as using liquid nitrogen to limit the time for the bonding formation of separated AMP nanospheres; and 3) incorporating Ca^{2+} into AMP, not only to stabilize the structure of AMP, but also to provide Ca^{2+} to improve the biocompatibility of newly prepared materials.

The lowest melting enthalpy of PLA–AMP indicates that the composite has microcrystals produced by the compression force loaded between PLA fragmentary layers divided by AMP particles during the forging process, similar to what was reported on PLA–CaP electrospun fibers [221]. The melting enthalpy of PLA pellets is higher than PLA

fibers due to the fast solidification along with the volatilization of solvent during electrospinning, which hindered the crystallization of PLA. Besides, Tc value difference (PLA–AMP fibers<PLA filers<PLA pellets) was caused by two factors: 1) subjecting the mixture to electrospinning resulting in incomplete crystallization of PLA chains and 2) easing crystallization due to the presence of AMP nucleants. The incorporation of amorphous AMP decreases the Tg and Tm of matrix. However, the Tg and Tm of PLA–AMP–HSA are slightly higher than PLA–AMP fibers, possibly attributed to the incorporated HSA content, and better dispersion of AMP in PLA matrix.

The final weight of materials after TGA analysis is below 20% of total weight. This can be caused by the loss of water molecules of AMP structure during heating, as MgP materials have a high affinity to incorporate with waters to crystal structure. Another possibility is the decomposition of AMP with temperature. Consequently, the study of AMP in sintering will be a necessary work in future.

In the SBF incubation experiment, the weight increase is mainly caused by apatite deposition from SBF. The apatite formation on PLA surface is related to the hydrolysis of PLA, which results in a negatively charged PLA surface. The positively charged calcium ions in the solution are attracted to the hydrolyzed PLA surface and apatite forms through the attraction of phosphate groups from the solution. PLA fibers showed faster weight increase as compared to PLA–AMP and PLA–AMP–HSA fibers during incubation, which is a combined result of three factors. First, AMP itself is a highly degradable material. In an experiment reported by Loher et al. [222], pure PLGA matrix only had 0.5% mass loss and 2% water uptake after 6 weeks, while 30% a-TCP incorporation resulted in 7% mass loss and 14% water uptake after 6 weeks. The high degradation rate of α-TCP particles

generated pores in the composite to result in a larger polymer surface being exposed to the surrounding media to promote PLGA degradation. It is believed that the same mechanism is also applicable to PLA–AMP composite fibers. A larger section of PLA surface is exposed to the surrounding media due to the degradation of AMP. The accumulation of hydrophilic degradation products of AMP inside the PLA–AMP fibers, further draws media into PLA matrix during the whole degradation process. Second, the presence of Mg^{2+} released from incorporated AMP fillers induces the formation of amorphous calcium phosphate (ACP). After the sufficient deposition of ACP to matrix and the mature of AMP in SBF [61], these ACP materials play an active role, the precursors of apatite deposition. Consequently, after 2 weeks, the weight increase rate of PLA–AMP fibers improves significantly. Third, as shown in Figure 4-9, PLA fibers show the poorest coating, the deposition of apatite in PLA matrix contributed most of weight increase. This is because PLA itself has a poor hydrophilicity. However, the presence of AMP in PLA–AMP fibers can improve the hydrophilicity and inhibit the apatite agglomeration deposition to the matrix via release of Mg^{2+} to local area.

The addition of HSA to PLA–AMP fibers showed adverse effects, contrary the work of Kim et al. [217]. In their work, HSA was added to PLA–HA electrospun fibers to generate continuous and uniform fibers. Initial cellular assays showed excellent cell proliferation and also enhanced expression of alkaline phosphatase at7 days of culturing on PLA–HA fibers as compared to PLA fibers. However, in our experiment the presence of HSA decreased both the bioactivity and biocompatibility of PLA–AMP fibers. Future studies on the toxicity of HSA or a combined effect of HSA and Mg^{2+} to MC3T3-E1 is

necessary before its application in improving ceramic filler dispersion in biopolymer matrix.

As the biocompatibility testing clearly illustrates in Figure 4-10, AMP incorporation into the PLA fibers promotes cell growth while the addition of HSA into the PLA–AMP fibers reverses the benefits of the AMP as opposed to Kim et al. [217]. Although the cell growth was not significantly different between PLA, PLA-AMP, and PLA-AMP-HA groups after 7 days, significantly lower cell number was observed in the PLA-AMP-HSA ($p < 0.05$) when compared to the control (PLA). Not only cells growing on the PLA–AMP fibers showed higher growth rate at the 7th day compared to the PLA-AMP-HSA, but also many markers associated with the growth and bone formation of preosteoblasts showed higher expression level (Figure 4-12). As it is previously reported, OCN and ALP, two biochemical markers for bone formation [223, 224], Col I, a marker for bone proliferation [223, 224] and differentiation [225], and OPN, a marker for osteoblastic differentiation, are commonly used for measuring osteogenic activity [226]. In order to measure osteogenic activity of our cells, expression level of the above mentioned markers were monitored. Present results showed 80% increase in OCN, and more than 3 times higher expression level of OPN in preosteoblasts grown on PLA–AMP in comparison with the cells grown on the PLA fibers, therefore, confirming positive effect of AMP on bone formation. Collagen type I expression level was also up-regulated by 18% showing higher bone differentiation on cells grown on PLA–AMP fibers than those seeded on PLA fibers. Although ALP expression level showed a decline in samples grown on PLA–AMP fibers, and PLA–AMP–HSA fibers, the latter group showed a higher decline

rate. The lower ALP expression level in the presence of AMP is in quite contrast to those reported in Mg related drugs [227], magnesium incorporated CaP materials [2, 228], Mg coating [229] and Mg alloys [230]. One possible explanation is the fast release of magnesium from amorphous AMP to the environment especially in an environment of 5% CO2 in air which lowered the ALP of MC3T3-E1 cells, as reported by Kircelli et al. that high magnesium level inhibited the β-glycerophosphate (BGP) induced ALP activity as well as gene expression associated with the process of transdifferentiation of bovine vascular smooth muscle cells (BVSMCs) into osteoblast-like cells in vascular calcification study [231]. However, as observed in the study, the expressions of other gene markers related to bone differentiation and formation all show significant increase. Another possibility is the interactions between different gene markers, the increased expression of other markers lowered the expression of ALP at some level. For example, osteoblasts slow down proliferation as they begin to secrete extracellular matrix proteins [232]. The third hypothesis is the uptake of calcium by AMP nanospheres from medium during their growth to mature MgP particles, a phenomenon that was recently reported [61]. It is well known that both magnesium and calcium are essential elements to bone formation. Therefore the consumption of calcium during AMP activity can partially decrease the ALP activity of MC3T3-E1 cells, which may not significantly influence other gene markers on contrast. The fourth possibility is that AMP nanospheres have direct impacts to MC3T3-E1 cells because they can play roles in gene delivery. Bhakta et al. reported that MgP nanoparticles showed 100% transfection efficiency in delivering genes to HeLa cells [84]. Additionally, the magnesium ions present in the medium can also assist the polynucleotide into cells [233]. In such gene transfection, the activity of target cells can be adjusted. Therefore, in

the presence of AMP nanospheres the activity of cells can also be potentially changed. However, it is not clear on what is the main driving force resulting the ALP level lower than expected in this study, possibly a combined effect of different factors. A systematical study focusing on AMP nanoparticles is needed in the future.

Consequently, it was successfully shown that microwave assisted synthesized AMP nanospheres can be potential filler materials for biopolymers. Additionally, it is possible that the applied nanospheres can be expanded into alkaline earth phosphate materials in the future, such as calcium magnesium phosphate (CaMgP). This is because in microwave irradiation, alkaline earth ion molar ratio in formed nanospheres can be controlled by adjusting the composition of reaction solution. It is expected that the optimized combination of these alkaline earth ions can provide significant impacts on bone regeneration.

4.6 Conclusions

Fibrous composites of PLA and AMP nanospheres were fabricated via electrospinning. This study provided significant data regarding the physical and biological properties of PLA–AMP composites and their in vitro interaction with preosteoblast cells.The presence of AMP nanospheres in PLA matrix was beneficial to the bone formation via improving the gene expression of OCN, Col I and OPN of preosteoblast cells. Additionally, it was observed that HSA, a surfactant used to improve ceramic dispersion in polymer matrix, showed adverse effects to preosteoblast cells when present in conjunction with MgP (AMP). It is believed that AMP can be a potential candidate in bone tissue engineering applications.

Chapter 5

Amorphous Magnesium Phosphate Nanoparticles as Nonviral DNA Carriers

5.1 Abstract

Nonviral gene delivery has gained much attention due to its potential in combating the viral gene delivery limitations like unintentional mutagenesis. Different natural and synthetic materials such as polymers, lipids, and calcium phosphate particles have been developed as DNA carriers. However, there is still a need for development of highly efficient gene vehicles. Amorphous magnesium phosphate nanoparticles are potential candidates for biomedical applications as they are biocompatible, highly biodegradable, and lack cytotoxicity. Present study investigates the application of amorphous magnesium phosphate nanoparticles as nonviral DNA vehicles. Here, different plasmid DNA to amorphous magnesium phosphate nanoparticle (1:1, 1:100, and 1:200) ratios was examined, and determined the optimal concentration of cargo to carrier (1:200). Positively charged Mg^{+2} ions were suggested to significantly enhance the uptake of amorphous magnesium phosphate attached plasmid DNA by the osteoblasts. SEM and zeta potential were used to evaluate the morphology, and surface charge of the nanoparticles. pCMV6-

AC-GFP vectors were attached to the amorphous magnesium phosphate and were used as the cargo.

5.2 Introduction

Gene therapy is a developing medical field. The ability to transfer DNA molecules which are capable of encoding functional proteins and replacing the mutated genes with therapeutic genes creates great prospective for treatment of different diseases. As a result, delivery of genes in a safe and secure manner is extremely crucial. During the last few decades viral and nonviral gene delivery methods have been developed. Although viral method is commonly known as the most efficient way, it is not an entirely harmless method since insertion of viral DNA can increase the risk for unintentional mutagenesis and immune response [234]. Nonviral methods like synthetic lipids, peptides, dendrimers, and other polymers along with cationic complexation, electroporation, and magnetofection provide alternative ways for secure gene delivery [235, 236]; however, lower efficiency of this method is a drawback for therapeutic applications [237-240].

More recently nanoparticles have gained attention for secure gene delivery. Inorganic nanoparticles have been explored as the biomolecule vehicles as they offer great potential for encapsulating active compounds such as DNA molecules and drugs [241]. Resistance against microbial attack, high storage stability, inexpensive and relatively simple preparation procedures are some of the advantages that inorganic particles have over their organic counterparts [240].

Alkaline earth phosphates especially different phases of calcium phosphates such as tricalcium phosphate (TCP), biphasic calcium phosphate (BCP), and especially

hydroxyapatite (HA) have shown potential as DNA carriers. Bose *et al.* and Epple *et al.* reviewed applications of calcium phosphate nanoparticles in drug delivery and gene silencing [242, 243]. Initially calcium phosphate was used in a transfection procedure by Graham *et al.*in 1973 [244]. Graham *et al.* introduced a cheap, precipitation method to co-precipitate the negatively charged DNA and phosphates, and positively charged calcium using phosphate containing (HEPES-buffered saline solution) and calcium chloride solutions [244].

Magnesium phosphate particles, on the other hand, have not received much attention in gene delivery applications. This is mainly due to the lack of adequate studies on applications of magnesium phosphates. However, few researchers studied the magnesium nanoparticles as potential DNA vehicles. Bhakta *et al.* reported successful *in vitro* delivery of pSVβgal plasmids using magnesium and manganous phosphate nanoparticles [240]. Same group conducted a similar study *in vivo* and reported that the magnesium phosphate nanoparticles can effectively deliver vectors into different cell types for targeted gene delivery [85]. Their results demonstrated that magnesium phosphate nanoparticles could show approximately 100% transfection efficiency when compared to transfecting reagents like Polyfect® and previously examined nanoparticles such as calcium phosphate nanoparticles [85]. Chowdhury *et al.* incorporated Mg^{+2} into the structure of apatites, inhibited the growth of crystals, and synthesized Ca-Mg phosphate particles [245]. The Ca-Mg nanoparticles were then used to carry labeled DNA into the mammalian HeLa and NIH 3T3 cells in a highly effective manner [245]. Kumta *et al.* replaced calcium by 50% magnesium in the structure of tricalcium phosphate and created nanosized spheres of magnesium substituted brushite with high surface area (~200 m^2/g)

[110]. Kumta *et al.* showed that calcium phosphate with different (Ca/P) ratios were capable of transporting DNA molecules into MC3T3-E1 and HeLa cells, and suggested that the magnesium substituted brushite was also capable for nonviral gene delivery applications [110]. Hanifi *et al.* repo rted that incorporation of Mg^{+2} into hydroxyapatite increases the positive surface charge of HA crystals and consequently increases the DNA loading capacity of resulting particles [83]. Dasguptha *et al.* doped hydroxyapatite nanoparticles by Mg^{+2} ions and successfully controlled the release of bovine serum albumin proteins *in situ* [246]. They suggested that the same procedure can be applied in bone proliferation and drug release studies [246].

Our knowledge of the capability of the magnesium phosphate nanoparticles for various biomedical applications is still at an infancy level. This study aims to expand the general understanding of magnesium phosphate nanoparticles. Here, we show how different ratios of AMP nanoparticle to plasmid DNA, and available surface area can impact the efficiency of these particles in carrying large plasmid DNA via monitoring of the green fluorescent protein. We have previously reported the lack of cytotoxic effects in examined magnesium phosphate nanoparticles [247].

5.3 Experiments

5.3.1 Microwave Assisted Phosphate Synthesis

All chemicals were purchased from Fisher Scientific (Fair Lawn, NJ, USA) and used without further purification. AMP nanoparticles ($Mg(PO_3OH)•3(H_2O)$) were synthesized using microwave assisted method which has been reported in our previous

publication [185]. Briefly, the reaction solution was prepared by orderly stirring the reagents in Table 5.1.

Table 5.1: Compositions of reaction solutions

DI Water	**$NaHCO_3$ (g)**	**$MgCl_2.6H_2O$(g) (g)**	**KH_2PO_4 (g)**
10 mL	0.680	0.623	0.409

The solution was then placed in onto 10 × 10 × 1 cm alumina insulating fiberboards and covered with an upside down 250 ml glass beaker. The entire assembly was later placed into a household microwave (MW) oven (Emerson, 800 W, 2450 MHZ, Hackensack, NJ, USA) for 5 minutes. Once microwave heating was completed, the beakers were left to cool in the microwave for 15 minutes prior to the transportation to the cold water bath for further cooling. The precipitates were magnetically stirred at 400 rpm in 500 ml of de-ionized water until the entire precipitates were dissolved. Finally, the solution was washed with approximately 2 L of de-ionized water and filtered using a filter paper (Whatman Grade 4, 1004- 055). The filtrates were then placed in an 80^{o} C oven overnight to dry. The synthesized AMP powders were then crushed and used for the analysis. The Mg/P molar ratio in AMP solution was set to 1 since the Mg/P molar ratio in human plasma/serum ranges from 3/2 to 2/3 [18, 216] .

5.3.2 Production, Purification, and Isolation of Plasmid DNA

Plasmid production, purification, and isolation was executed following the previously published procedure by Wagner [235]. Briefly, 1.5 ml of electrocompetent

strain of DH5-α E.Coli frozen stock was thawed and inoculated with 100 ml of Super Broth (SB Broth) media. Table 5.2 shows the composition of SB media.

Table 5.2: Composition of SB media [235]

Chemical	**Amount**
Tryptone	32 g
Yeast Extract	20 g
NaCl	5 g
UltraPure Water	1000 mL
Additives	**Amount/500 mL**
Agar	7.5 g
2% glucose solution	50 mL
20% glucose solution	5 mL
Ampicillin - 25mg/ mL	0.5 mL
Ampicillin - 100mg/ mL	0.5 mL
Kanamycin - 50mg/ mL	0.5 mL

The bacterial culture was left to grow overnight in a water bath at 37º C and 130RPM. Later, to ensure that the bacterial culture was in the proper growth phase, 2 ml of the overnight culture was used to inoculate 100 ml of SB media. The new culture was grown for approximately 2.5 hours until the OD600 reading was ~0.5. 35 ml of the freshly cultured DH5-α E.Coli was centrifuged at 10,000RPMs for 10 minutes. The resulting pellet was washed gently with 35ml, 25ml, 20ml, 15ml, 10 ml, and 5ml of ultrapure water until the supernatant was clear. After each wash the pellet was resuspended in 2 ml of DI water and bacterial culture was centrifuged at 10,000RPMs for 10 minutes. Finally, the pellet was resuspended in 200µl of 10% glycerol. 40µl of the pellet was later placed in an electroporation cuvette along with 1µl of purified pCMV6-AC-GFP plasmid (Origene, Rockville, MD). Vector map of pCMV6-AC-GFP plasmid is shown in Figure 5-1.The vector was slightly modified since the ORF which encodes for human BMP-2 was added

to the pCMV6-AC-GFP plasmid (ORF is not shown). Bacterial cells were then electroporated at 1.5kV. Immediately after electroporation 1ml of SOC media was added to the cells and cells were transferred to a sterile culture tube. They were then incubated at 37º C and shaken at 130RPMs for 1.5 hours.

Table 5.3 shows the composition of SOC transformation media.

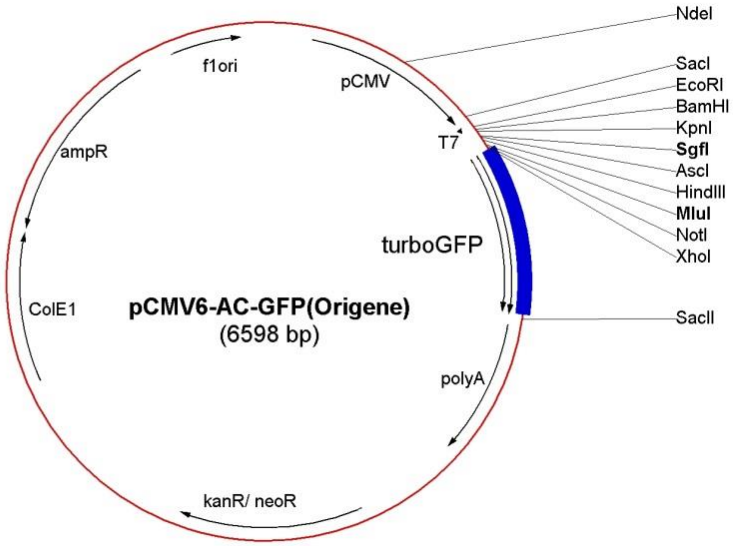

Figure 5-1: Map of pCMV6-AC-GFP vector [248]

Table 5.3: Composition of SOC transformation media

Chemical	**Amount**
Super Broth	980 mL
50x SOC	20 mL
Additives	**Amount/50 mL**
$MgCl_2$(10mM)	2.38 g
$MgSO_4$ (10mM)	3.01 g
Glucose (20mM)	9.01 g
Ultrapure Water	50 mL

To ensure the accuracy of transformation of the DH5-α bacteria with pCMV6-AC-GFP plasimds, 100µl of the culture was placed on Kanamycin and ampicillin resistant LB agar plates and allowed to grow overnight. Colonies present on the plate where successfully

transformed and contained the Kanamycin and ampicillin resistant gene from the pCMV6-AC-GFP vector. One single colony was then chosen from the Kanamycin and ampicillin resistant plate to inoculate with 100 ml SB Broth media with 50 μg/ml Kanamycin, and allowed to grow overnight at 37º C while shaking. Later, Qiagen's QIAprep Spin Miniprep Kit was used to purify the plasmids and stored in TE buffer. Purification accuracy was confirmed via 260/280nm spectrophotometer reading.

5.3.3 Attachment of pCMV6-AC-GFP Vectors to AMP Nanoparticles

pCMV6-AC-GFP vectors were mixed with AMP nanoparticles at different ratios. To determine the DNA attachment efficiency the supernatant was collected and read in the spectrophotometer (SpectraMax Plus, Molecular Devices) at 260/280nm . The DNA concentration was used to determine the total free DNA.

To test the attachment and transfection efficiency of pCMV6-AC-GFP DNA to AMP nanoparticles weight (w/w) ratios of 1, 100, and 200 were examined. AMP nanoparticles were mixed with 2.5M $MgCl_2$ at 1:1 ratio volume of nanoparticle. The mixture was spun down on a rotor at 15,000RPMs for 30 seconds. Later, the supernatant was removed and AMP nanoparticles were resuspended in deionized water. pCMV6-AC-GFP DNA was added to the AMP nanoparticles with relative (w/w) ratios, and left for 20 minutes. Later, the transfection mix was added in a dropwise manner to the MC3T3-E1 cells, which were seeded on the previous day at 5000 cells per well.

5.3.4 Zeta Potential Characterization of AMP Nanoparticles, Surface Charge and Particle Size

Surface charge of the AMP nanoparticles was measured using the Nicomp 380ZLS zeta potential/particle sizer (Particle sizer systems, Santa Barbara, CA). Particle sizes were determined using the freely available ImageJ program.

5.3.5 Transfection of Mouse Preosteoblasts with pCMV6-AC-GFP and AMP Nanoparticles

Mouse preosteoblast cells (MC3T3-E1, CRL-2593™, ATCC, USA) were used to study the transfection efficiency of pCMV6-AC-GFP and AMP nanoparticles. Preosteoblast cells were initially grown at 37 °C and 5% CO_2 complete media containing in alpha minimum essential medium (α-MEM, Thermo Scientific HyClone), augmented by 10% Fetal Bovine Serum (FBS, Thermo Scientific HyClone, USA), and 1% antimycin and penicillin (Sigma-Aldrich, USA). The culture medium was replenished every other day until the cell reached 90% confluency. A day prior to transfection, MC3T3-E1 cells were seeded to wells (Flacon™ 48 wells cell culture plates, BD Biosciences, USA) at a density of 5,000 cells per well. pCMV6-AC-GFP DNA vectors were attached to AMP nanoparticles with different ratios (1:1, 1:100, and 1:200). pCMV6-AC-GFP consisted of 6598 base pairs prior to addition of BMP2. Modified pCMV6-AC-GFP contains 7781 bp including an open reading frame (ORF) of 1191bp. Human BMP2 (NM_001200) is encoded by this ORF with a GFP tag at the C-terminus since the N-terminus sequences are crucial for localization to the endoplasmic reticulum (ER) [249]. 2 μg of pCMV6-AC-GFP DNA was mixed with 40 μl of Polyfect ® (Qiagen, Germnay) and was added to the cells and was used as the positive control group. Mixture of 2 μg of pCMV6-AC-GFP DNA and

320 µl of α-MEM media was added to the cells and was used as the negative control groups. In addition, blank cells containing only complete α-MEM media were used as the second negative control group. Furthermore, the media was removed from the cell culture wells and transfection media was added to the respective groups. Final volume was then brought to 2 ml by addition of complete α-MEM. The cells were returned to the incubator. After 48 hours, the transfection media was removed and fluorescent imaging was performed using an inverted fluorescent microscope.

5.3.6 Cytocompatibility Study

Cytotoxicity effects of AMP nanoparticles on MC3T3-E1 cells were determined using CytoTox 96® Non-Radioactive Cytotoxicity Assay kit (Promega, USA). Relative results were published in a previous study [247]. For statistical analysis, all experiments were performed at least in triplicate, and t-test analysis was applied for data analysis.

5.4 Results

5.4.1 Particle Size and Surface Charge Characterization of AMP Nanoparticles

Scanning electron microscopy images of the synthesized nanoparticles are illustrated in Figure 5-2. The microwave assisted apatite synthesis resulted in production of homogeneous nanosphere shaped AMP nanoparticles. Based on the SEM images and ImageJ program average diameter of nanospheres was 226 nm, and standard deviation was 97 nm. Particle size distribution of AMP nanoparticles are shown in Figure 5-3. Mean surface charge of nanoparticles was -19.3 mV.

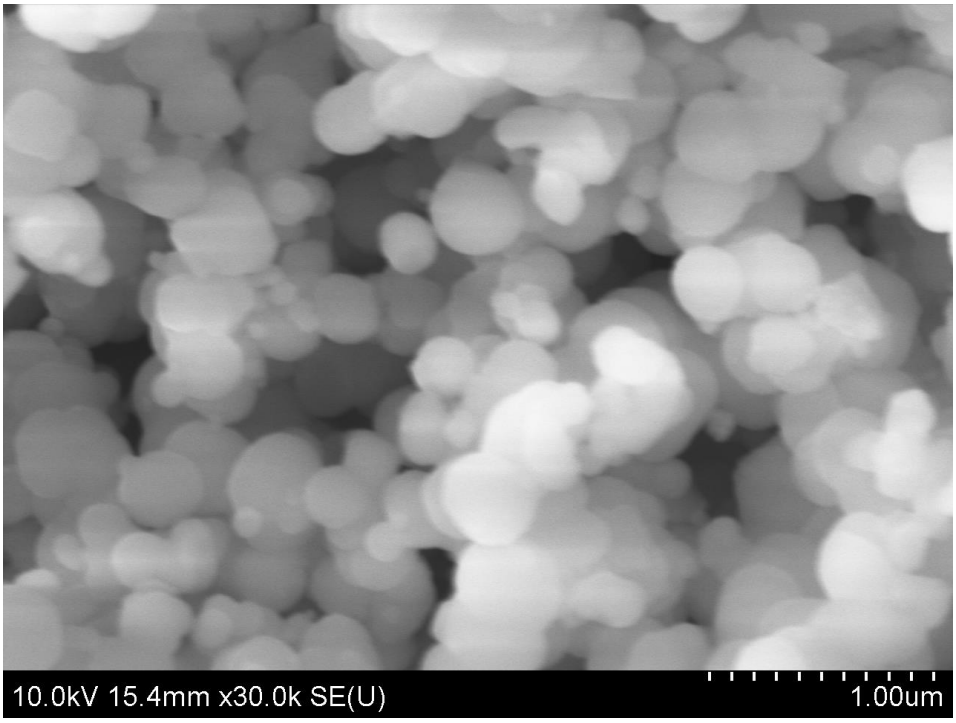

Figure 5-2: Scanning electron microscopy image of AMP nanoparticles (30K)

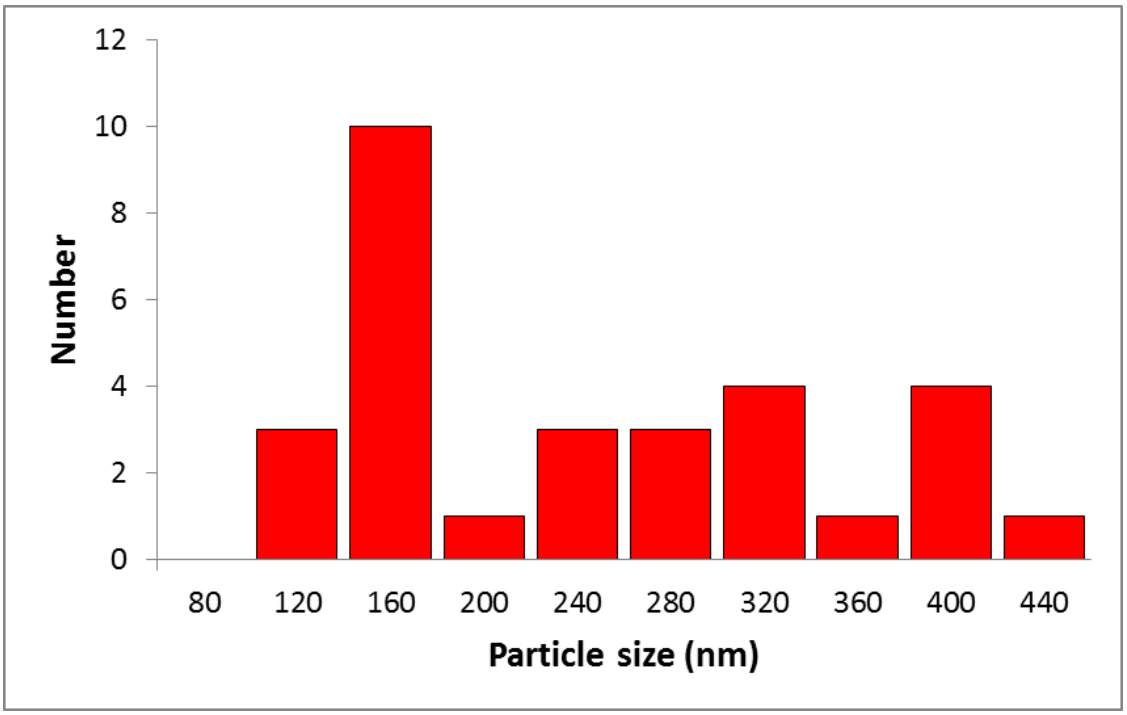

Figure 5-3: Particle size distribution of AMP nanoparticles

5.4.2 Transfection of Mouse Preosteoblasts with AMP Nanoparticles as DNA Carriers

Ability of AMP nanoparticles for transfecting MC3T3-E1 mouse preosteoblasts by large DNA molecules like pCMV6-AC-GFP was examined. Previous study by Wagner suggested that 1/100 w/w ratio was optimal for DNA to calcium phosphate nanowhiskers (CaPnw) [235]. Wagner used both g-wiz 5757bp and pCMV6-AC-GFP for transfection purposes. However, present study monitored ratios of 1/1, 1/100, and 1/200 w/w of DNA to AMPs. Here the pCMV6-AC-GFP and BMP-2 create a larger DNA molecule 7781bp compared to the g-wiz plasmid 5757bp. Table 5.4 illustrates the content composition of each group.

Table 5.4: Content composition of Plasmid/AMP (w/w) ratios

Group	**Plasmid:AMP (w/w)**	**Plasmid**	**Polyfect®**	**MC3T3-E1 cells per well**	**Number of Fluorescent Cells (Mean)**
1	1/1	Yes	No	5000	None
2	1/100	Yes	No	5000	51
3	1/200	Yes	No	5000	421
4	--	Yes	Yes	5000	2036
5	--	Yes	No	5000	None
6	--	No	No	5000	None

Bright field image of group 1 (1/1) is presented in Figure 5-4. It shows that the AMP nanoparticles are up taken by the preosteoblasts; however, the transfected cells did not fluoresce when exposed to fluorescent microscopy.

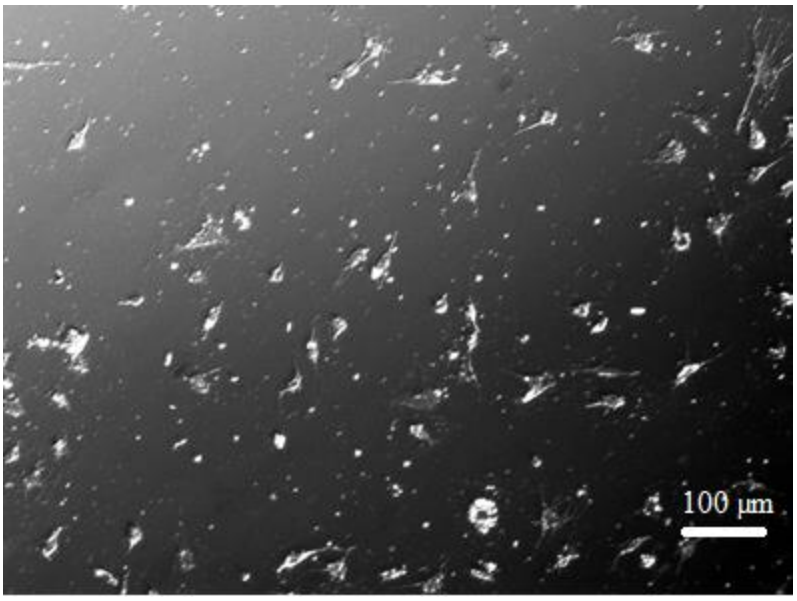

Figure 5-4: Bright field image of group 1 (1/1) (100X)

Successful transfection of MC3T3-E1 cells were determined by fluorescent microcopy images. Only images of the groups 2, 3, and 4 are presented in Figure 5-5, Figure 5-6, and Figure 5-7 since other groups did not show fluorescence.

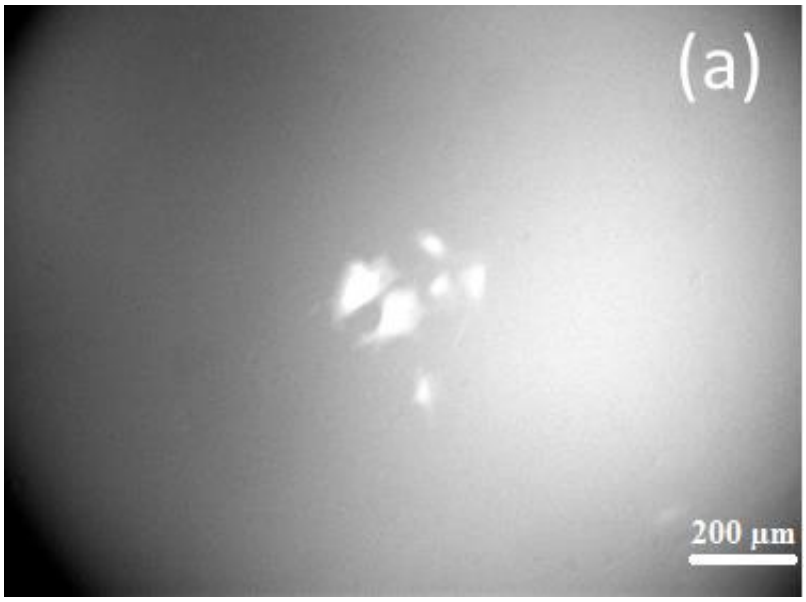

Figure 5-5: (a) Fluorescence microscopy image of group 2 (1/100) nanoparticles (200X) after 48 hours in culture

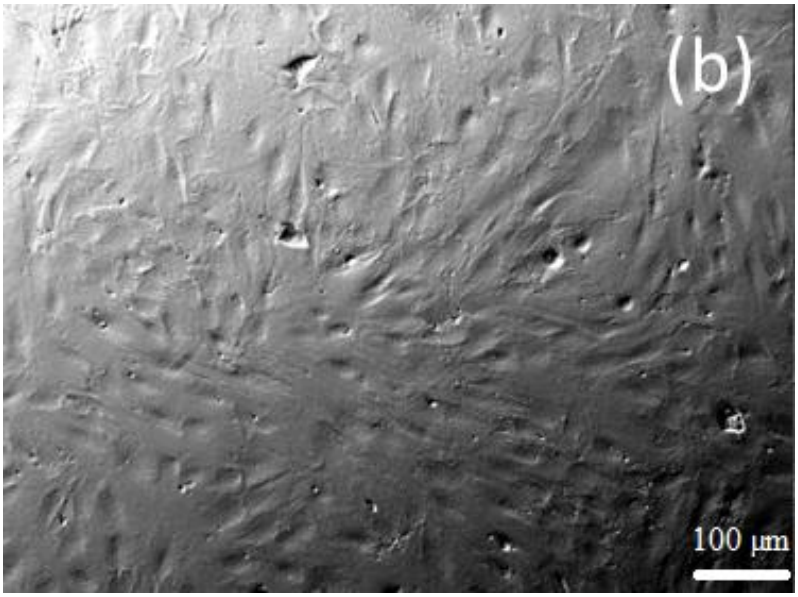

Figure 5-5: (b) Bright filed image of preosteoblasts transfected by plasmid DNA shows no disruption in cell growth (100X) after 48 hours in culture

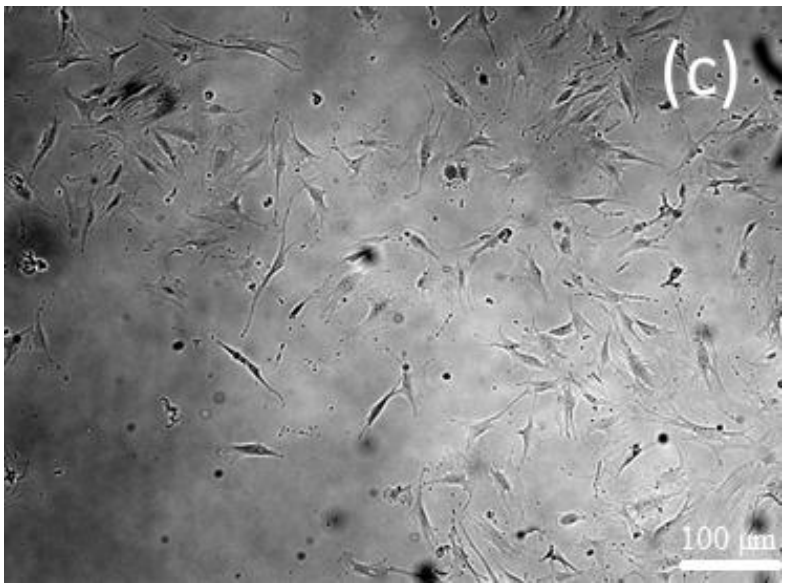

Figure 5-5: (c) no agglomeration of AMPs after 48 hours in culture

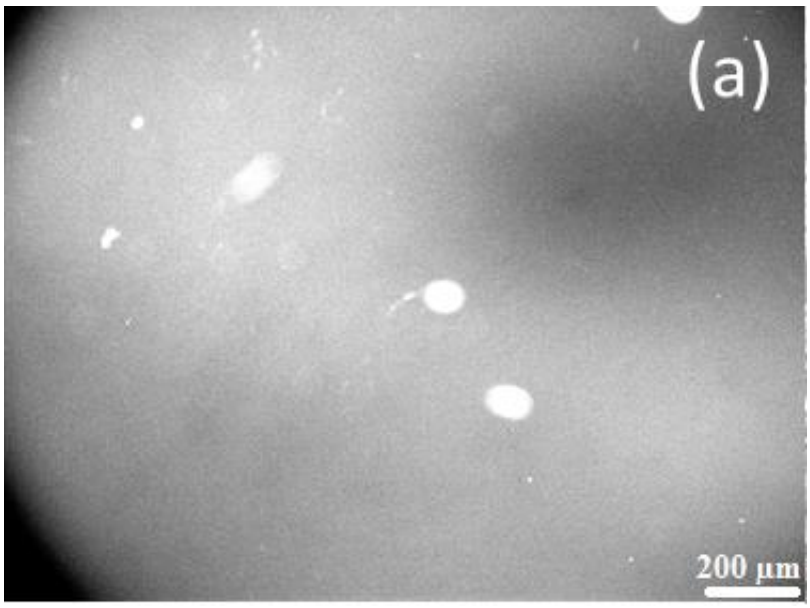

Figure 5-6: (a) Fluorescence microscopy image of group 3 (1/200) nanoparticles (200X) after 48 hours in culture

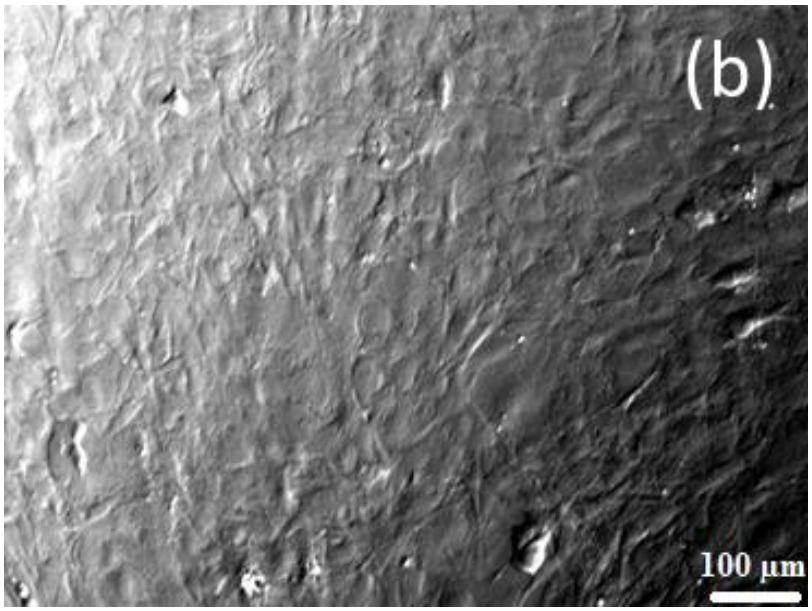

Figure 5-6: (b) Bright filed image of preosteoblasts transfected by plasmid DNA shows no disruption in cell growth (100X) after 48 hours in culture

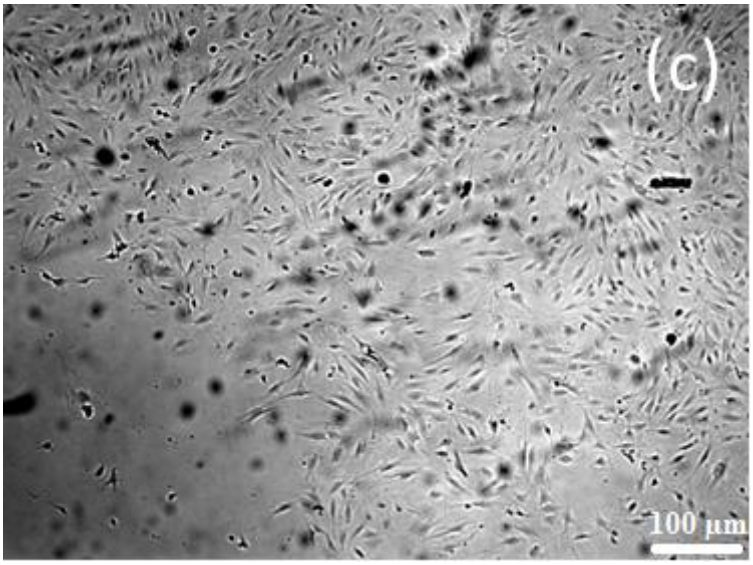

Figure 5-6: (c) no agglomeration of AMPs after 48 hours in culture

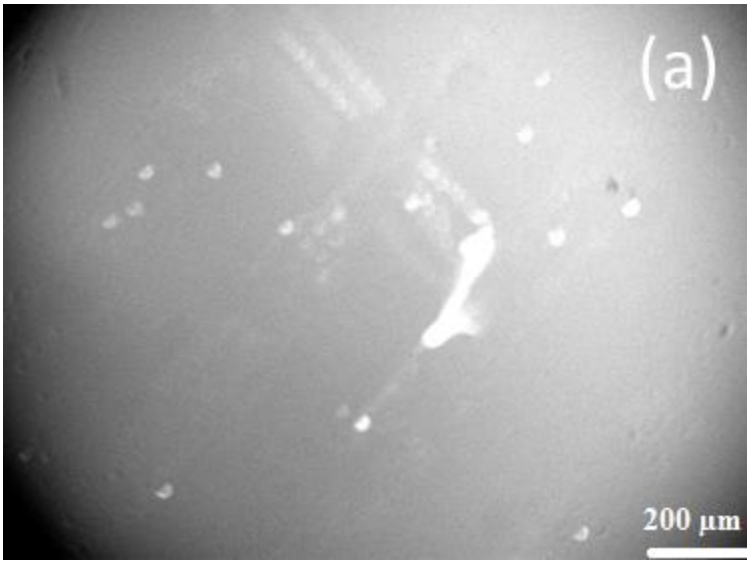

Figure 5-7: (a) Fluorescence microscopy image of group 4 (Polyfect) (200X) after 48 hours in culture

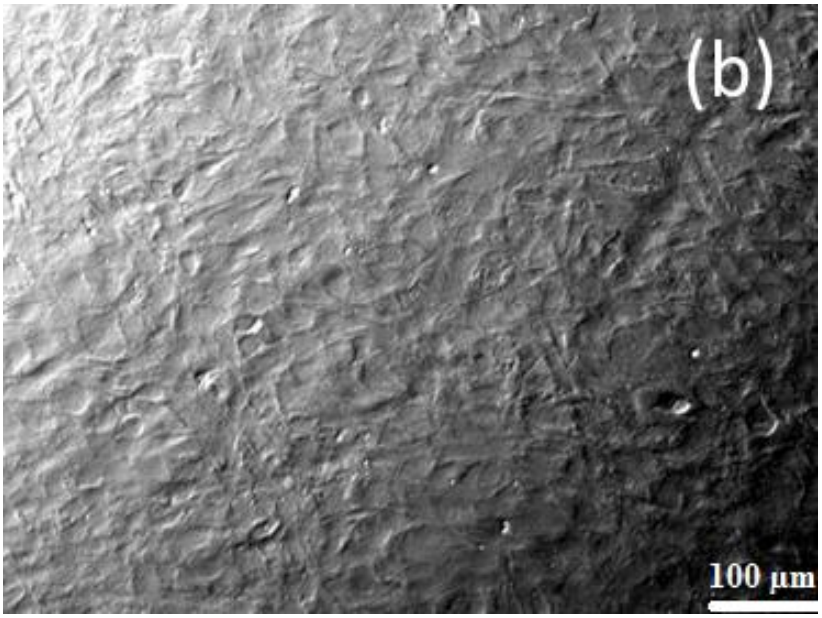

Figure 5-7: (b) Bright filed image of preosteoblasts transfected by polyfect shows no disruption in cell growth (100X) after 48 hours in culture

5.5 Discussion

The overall results suggest the ability of magnesium phosphate nanoparticles as gene delivery vehicles. The efficiency of transportation, however, depends on different parameters such as the cell type, shape and size of DNA carrier, DNA condensation etc. [250]. To monitor and quantify the efficiency of DNA uptake, previously several techniques such as flow cytometry, transmission electron microscopy, and fluorescent microscopy were used to investigate the mechanism of uptake in different cell lines [251]. Here, we used fluorescent microscopy to confirm the entry of nanoparticles and successful gene delivery.

This study suggested that the plasmid/AMP ratio, nanoparticle size and surface charge play crucial roles in the process of particle uptake by the examined cells. A

comparison between transfection efficiency of the AMP nanospheres with average diameter of 226 nm (Figure 5-2, Figure 5-3) with the previously synthesized magnesium phosphate particles by Bhakta *et al.*, which were reported to have the average diameter of 100-130 nm [84], indicates the importance of particle size in successful transfection of the target cells in addition to the differences in the nature of various cell lines. Bhakta *et al.* previously reported a 100% *in vitro* transfection efficiency of HeLa cells using magnesium phosphate nanoparticles [84]. This can be due to their smaller particle size which facilitates passage of the nanoparticles through the HeLa cell membrane. As formerly suggested by Panyam *et al.*, nanosized therapeutic particles offer many advantages over the larger particle sizes [252]. Their results demonstrated that 100 nm size nanoparticles showed 2.5 fold higher uptakes in Caco-2 cell line when compared to 1μm particles [253]. This ratio is much higher when nanoparticles are compared to larger particle sizes.

The exact uptake mechanism of nanoparticle attached DNA molecules is unclear, however the endocytotic pathway can offer an uptake mechanism. In this method nucleotides make a complex with the cationic molecules which will be attracted to the negative charges on the cell membrane. The positively charged complex later binds to the negatively charged cell membrane and is endocytosed [254]. We suggest that despite the slightly negative surface charge of the AMP nanoparticles, the positively charged magnesium ions (Mg^{+2}) ionically bond to the negatively charged phosphate (PO_4^{-3}) groups of plasmid DNA. Similar to results reported by Jiang *et al.* [250] and Wagner [235] addition of $MgCl_2$ provides the AMP-DNA compound with more Mg^{+2} and positive charges and facilitates transportation of the entire assembly across the plasma membrane. Furthermore, addition of solvent polarity expedites the DNA condensation which further assists the

transportation mechanism. Moreover, Mg^{+2} ions shield and protect the plasmid DNA from cytoplasmic nuclease activities. This process justifies the fluorescent signals observed in AMP-DNA complexes verses the naked DNA. Figure 5-8 provides a schematic presentation of the AMP-DNA uptake.

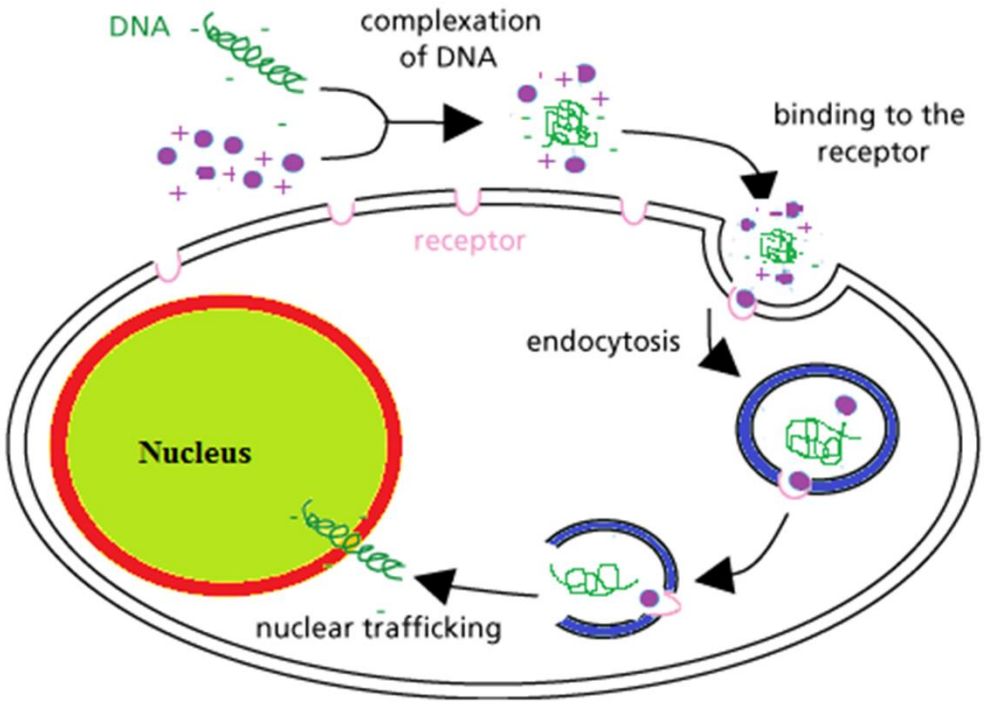

Figure 5-8: Schematic presentation of the AMP-DNA uptake in osteoblastic cells [255]

After the DNA molecules are uptaken by the cell, an endosome encapsulates the complex. Later, endosomal pH causes the solubilization to proceed [256]. It is crucial for the non-viral vectors to protect the DNA molecules from degradation while in the endosome [84, 254]. Due to the influx of protons and the following charge gradient between the endosome and the cytosol, water enters the endosome which leads to the swelling and rupture of the endosome. Consequently, nucleotide-vector complexes are

ejected into the cytoplasm. Once in the cytoplasm the nucleotides travel towards the nucleus via diffusion and the use of cytoskeletal pathways. Due to the high viscosity of the cytosol active transportation of endocytotic vesicles like endosomes and lysosomes towards the nucleus is observed. Upon reaching the nucleus, the nucleotides are taken into the nucleus with the help of nuclear localization signals (NLS) [254, 257, 258] via nuclear pore complexes (NPC) [259]. Three different mechanisms including passive diffusion (<10 kDa), calcium regulated transport (10-70 kDa), and active transport (>70 kDa) [254, 260] are used to transfer molecules across the nuclear membrane. Once in the nucleus DNA is transcribed to mRNA. mRNA later is translated into proteins. In this study expression of the green fluorescent protein (GFP) as the ultimate product can be monitored via fluorescent microscopy.

Small particle size, and presence of Mg^{+2} ions facilitates the effective uptake of AMP attached DNA nanoparticles into the cytoplasm, and the transportation of plasmid DNA via AMP nanoparticles to the nucleus [261]. As shown above, lower plasmid/AMP w/w ratio (1/1) is still capable of delivering some plasmid DNA into the cytoplasm (Figure 5-4); however, the low amount of available AMP surface area limits the transportation of plasmid DNA and AMP nanoparticles into the nucleus. As a result, DNA molecules are exposed to the cytoplasmic nucleases. Consequently, group 1 (1/1) ratio shows no fluorescent imaging which is similar to the group 5 (naked DNA) (results are not shown). We suggest that the higher available surface areas and readily available Mg^{+2} ions enhance the effectiveness of DNA delivery by AMP nanoparticles. Larger plasmid/AMP (w/w) ratio of (1/100), and (1/200), (Figure 5-5, Figure 5-6 and respectively) resulted into higher observance when exposed to the fluorescent microscopy imaging. As a result, higher

available surface areas and available positive charges are necessary for the attachment and delivery of large plasmid molecules via AMP nanoparticles.

5.6 Conclusions

This study presents, for the first time, the ability of AMP nanoparticles as large DNA molecule carriers. Here, we provide valuable evidence on importance of particle size, available surface area, and positive charge for attachment and transportation of DNA molecules via AMP nanoparticles across the plasma membrane. We suggest that shielding effect of Mg^{2+} facilitates the transportation and protection of AMP attached DNA molecules across the cytoplasm and into the osteoblastic nuclei.

Chapter 6

Conclusion and Future Directions

6.1 Conclusions

Investigation of the orthopedic applications of the magnesium phosphate nanoparticles was the primary goal of this dissertation. To clearly understand the properties of different magnesium based bioceramics and accordingly applying them in various biomedical fields, three important classes of Mg-containing bioceramics were reviewed including: 1) $MgO–P_2O_5$ resulting in magnesium phosphates; 2) $CaO\text{-}MgO\text{-}P_2O_5$ resulting in calcium magnesium phosphates; and $MgO\text{-}SiO_2$ representing the magnesium silicate glasses.

Calcium magnesium phosphate and magnesium phosphate nanoparticles were further studied in the subsequent chapters. Both groups were successfully synthesized using the microwave assisted method. Chapter 3 provided valuable evidence on crucial role of Mg^{2+} and Ca^{2+} ions in proliferation, differentiation, and mineralization of preosteoblasts via regulation of osteoblastic genes.

Chapter 4 demonstrated the successful fabrication of fibrous composites of PLA and AMP nanospheres via electrospinning. Moreover, physical and biological properties of PLA–AMP composites and their in vitro interaction with preosteoblast cells were

investigated. The results indicated that the presence of AMP nanospheres in PLA matrix is beneficial to the bone formation via increasing the osteoblastic gene expression level of preosteoblast cells.

Chapter 5 further demonstrated the ability of AMP nanoparticles as plasmid DNA molecule vehicles and provided evidence on importance of available surface area for attachment and transportation of DNA molecules via AMP nanoparticles across the plasma membrane. Mg^{2+} shielding was suggested to facilitate the transportation and protection of AMP attached DNA molecules across the cytoplasm and into the osteoblastic nuclei.

6.2 Future Directions

Similar to CaPs, magnesium phosphates can be doped with different luminescent materials. Dopants such europium (Eu) and Yttrium (Y) have been previously used to track calcium phosphates such as hydroxyapatites [262] and chlorapatites [263]. These dopants have shown to improve biocompatibility, promote of cell growth, mechanical and thermal enhancement of calcium phosphates, and fluorescent properties of calcium phosphate nanoparticles. Similar methods can be applied to track the magnesium phosphate nanoparticles. MgP dopants can be beneficial for *in vivo* studies and in physiological conditions. Future studies can investigate the degradation rate of MgPs *in vivo* and compare it with the traditional bone substitutes like hydroxyapatites.

Amorphous magnesium phosphates can be further applied in delivery of DNA molecules and various drugs in different cell lines. Drug attachment and release efficiency of AMPs and other magnesium phosphate compositions are some of the other unexplored avenues.

References

[1] Yang G, Liu J, Li F, Pan Z, Ni X, Shen Y, et al. Bioactive calcium sulfate/magnesium phosphate cement for bone substitute applications. Materials science & engineering C, Materials for biological applications 2014;35:70-6.

[2] Jia J, Zhou H, Wei J, Jiang X, Hua H, Chen F, et al. Development of magnesium calcium phosphate biocement for bone regeneration. J R Soc Interface 2010;7:1171-80.

[3] Klammert U, Ignatius A, Wolfram U, Reuther T, Gbureck U. In vivo degradation of low temperature calcium and magnesium phosphate ceramics in a heterotopic model. Acta Biomater 2011;7:3469-75.

[4] Zhou H, Agarwal AK, Goel VK, Bhaduri SB. Microwave assisted preparation of magnesium phosphate cement (MPC) for orthopedic applications: A novel solution to the exothermicity problem. Materials Science and Engineering: C 2013;33:4288-94.

[5] Navarro M, Michiardi A, Castaño O, Planell JA. Biomaterials in orthopaedics. J Roy Soc Interface 2008;5:1137-58.

[6] Zhou H, Lawrence JG, Bhaduri SB. Fabrication aspects of PLA-CaP/PLGA-CaP composites for orthopedic applications: A review. Acta Biomater 2012;8:1999-2016.

[7] Stevens MM. Biomaterials for bone tissue engineering. Mater Today 2008;11:18-25.

[8] Keating JF, McQueen MM. Substitutes for autologous bone graft in orthopaedic trauma. J Bone & Joint Surg, Brit Vol 2001;83-B:3-8.

[9] Damien CJ, Parsons JR. Bone graft and bone graft substitutes: A review of current technology and applications. J Appl Biomat 1991;2:187-208.

[10] Lord CF, Gebhardt MC, Tomford WW, Mankin HJ. Infection in bone allografts. Incidence, nature, and treatment. J Bone and Joint Surg - Ser A 1988;70:369-76.

[11] Logeart-Avramoglou D, Anagnostou F, Bizios R, Petite H. Engineering bone: challenges and obstacles. J Cell Mol Med 2005;9:72-84.

[12] Hench LL, Polak JM. Third-generation biomedical materials. Sci 2002;295:1014-7.

[13] Langer R, Vacanti JP. Tissue engineering. Sci 1993;14:920-6.

[14] Zeng R, Dietzel W, Witte F, Hort N, Blawert C. Progress and challenge for magnesium alloys as biomaterials. Adv eng mater 2008;10:3-14.

[15] Zhang Y, Gu X. Research activities of biomedical magnesium alloys in china. JOM 2011;63:105-8.

[16] Scopus. 2014.

[17] Walker J, Shadanbaz S, Woodfield TB, Staiger MP, Dias GJ. Magnesium biomaterials for orthopedic application: a review from a biological perspective. J Bio Med Mater Res B Appl Biomater 2014;102:1316-31.

[18] Weisinger J, Bellorín-Font E. Magnesium and phosphorus. Lancet 1998;352:391-6.

[19] Wolf FI, Cittadini A. Chemistry and biochemistry of magnesium. Mol Asp Med 2003;24:3-9.

[20] Wolf FI, Trapani V. Cell(patho)physiology of magnesium. Clin Sci 2008;114:27-35.

[21] Maquire ME, Cowan JA. Magnesium chemistry and biochemistry. Biometals 2002;15:203-10.

[22] Diba M, Tapia F, Boccaccini A, Strobel L. Magnesium-containing bioactive glasses for biomedical applications. Int J Appl Glass Sci 2012;3:221-53.

[23] Vormann J. Magnesium: nutrition and metabolism. Mol Asp Med 2003;24:27-37.

[24] Staiger MP, Pietak AM, Huadmai J, Dias G. Magnesium and its alloys as orthopedic biomaterials: A review. Biomaterials 2006;27:1728-34.

[25] Witte F, Hort N, Vogt C, Cohen S, Kainer KU, Willumeit R, et al. Degradable biomaterials based on magnesium corrosion. Curr Opin Solid State Mater Sci 2008;12:63-72.

[26] Witte F. The history of biodegradable magnesium implants: a review. Acta Biomater 2010;6:1680-92.

[27] Flatman P. Magnesium transport across cell membranes. J Membr Biol 1984;80:1-14.

[28] Simon DB, Lu Y, Choate KA, Velazquez H, Al-Sabban E, Praga M, et al. Paracellin-1, a renal tight junction protein required for paracellular mg2+ resorption. Sci 1999;285:103-6.

[29] Baker SB, Worthley LI. The essentials of calcium, magnesium and phosphate metabolism: part II. Disorders. Crit Care Resus: J Austr Acad Crit Care Med 2002;4:307-15.

[30] Rude RK, Gruber HE, Wei LY, Frausto A, Mills BG. Magnesium deficiency: Effect on bone and mineral metabolism in the mouse. Calcif Tis Int 2003;72:32-41.

[31] Dorozhkin SE, M. Biological and medical significance of calcium phosphates. Ang Chem Int Ed 2002;41:3130-46.

[32] Rude RK, Singer FR, Gruber HE. Skeletal and hormonal effects of magnesium deficiecy. J Ameri Col Nut 2009;28:131-41.

[33] Gronowicz G, McCarthy MB. Response of human osteoblasts to implant materials: Integrin-mediated adhesion. J Orth Res 1996;14:878-87.

[34] Zreiqat H, Howlett CR, Zannettino A, Evans P, Schulze-Tanzil G, Knabe C, et al. Mechanisms of magnesium-stimulated adhesion of osteoblastic cells to commonly used orthopaedic implants. J Biom Mat Res 2002;62:175-84.

[35] Gailit J, Ruoslahti E. Regulation of the fibronectin receptor affinity by divalent cations. J Bio Chem 1988;263:12927-32.

[36] Kingery W. Fundamental study of phosphate bonding in refractories: I. J Am Ceram Soc 1950;33:239-41.

[37] Kingery W. Fundamental study of phosphate bonding in refractories: II. J Am Ceram Soc 1950;33:242-50.

[38] Shashkova I, Kitikova N, Rat'ko A, D'yachenko A. Preparation of calcium and magnesium hydrogen phosphates from natural dolomite and their sorptive properties. Inorg Mat 2000;36:826-9.

[39] Aramendía MaA, Borau V, Jiménez C, Marinas JMa, Romero FJ. Synthesis and characterization of magnesium phosphates and their catalytic properties in the conversion of 2-hexanol. J Coll Int Sci 1999;217:288-98.

[40] Sugiyama S, Moffat JB. Oxidative coupling of methane on salts of magnesium doped by alkali carbonates. Energy & Fuels 1994;8:463-9.

[41] Seehra SS, Gupta S, Kumar S. Rapid setting magnesium phosphate cement for quick repair of concrete pavements — characterisation and durability aspects. Cem Concr Res 1993;23:254-66.

[42] Yang Q, Zhu B, Wu X. Characteristics and durability test of magnesium phosphate cement-based material for rapid repair of concrete. Mat Str 2000;33:229-34.

[43] Vesna BI, Jasminka K, Damir K, Ljerka B. Precipitation diagrams of struvite and dissolution kinetics of different struvite morphologies. Croat chem acta 2002;75:89-106.

[44] Wagh A. Chemically bonded phosphate ceramics:twenty-first century materials with diverse applications.: Elsevier; 2005.

[45] Bartl H, Catti M, Joswig W, Ferraris G. Investigation of the crystal structure of newberyite, MgHPO4·3H2O, by single crystal neutron diffraction. Tscher Mineral Petro Mit 1983;32:187-94.

[46] Abbona F, Calleri M, Ivaldi G. Synthetic struvite, MgNH4PO4.6H2O: correct polarity and surface features of some complementary forms. Acta Crystall Sec B 1984;40:223-7.

[47] Schroeder LW, Mathew M, Brown WE. XO4n- ion hydration. The crystal structure of Mg3(PHO4)2.22H2O. J Phy Chem 1978;82:2335-40.

[48] Takagi S, Mathew M, Brown WE. Crystal structures of bobierrite and synthetic Mg3(PO4)2(H2O)8. Amer Mineral 1986;71:1229-33.

[49] Brown P, Gulick J, Dumm J. The System MgO-P2O5-H2O at 25°C. J Amer Ceram Soc 1993;76:1558-62.

[50] Chau C, Qiao F, Li Z. Potentiometric study of the formation of magnesium potassium phosphate hexahydrate. J Mater Civil Eng 2012;24:586-91.

[51] Belposky A, Shpunt S, Shulgina M. Physiochemical researches in the field of magnesium phosphates. J Appl Chem 1950;23:873-84.

[52] Shpunt S, Belposky A, Shulgina M. The polytherm of the MgO-P2O5-H2O. J Appl Chem 1951;24:439-47.

[53] Brown P. Phase relationships in the ternary system Ca0-P2O5-H2O at 25C J Am Ceram Soc 1992;75:17-22.

[54] Mousa S. Study on synthesis of magnesium phosphate materials. Phosph Res Bull 2010;24:16-21.

[55] Sales BC, Chakoumakos BC, Boatner LA, Ramey JO. Structural properties of the amorphous phases produced by heating crystalline MgHPO4·3H2O. J Non-Cry Sol 1993;159:121-39.

[56] Mathew M, Kingsbury P, Takagi S, Brown WE. A new struvite-type compound, magnesium sodium phosphate heptahydrate. Acta Crys Sec B 1982;38:40-4.

[57] Chau CK, Qiao F, Li Z. Microstructure of magnesium potassium phosphate cement. Cons Buil Mat 2011;25:2911-7.

[58] Vinokurov SE, Kulyako YM, Slyunchev OM, Rovnyi SI, Wagh AS, Maloney MD, et al. Magnesium potassium phosphate matrices for immobilization of high-level liquid wastes. Radiochem 2009;51:65-72.

[59] Abdelrazig BEI, Sharp JH. Phase changes on heating ammonium magnesium phosphate hydrates. Therm Acta 1988;129:197-215.

[60] Tamimi F, Nihouannen DL, Bassett DC, Ibasco S, Gbureck U, Knowles J, et al. Biocompatibility of magnesium phosphate minerals and their stability under physiological conditions. Acta Biomater 2011;7:2678-85.

[61] Zhou H, Luchini TF, Bhaduri S. Microwave assisted synthesis of amorphous magnesium phosphate nanospheres. J Mat Sci: Mat Med 2012;23:2831-7.

[62] Sarkar A. Phosphate cement-based fast-setting binders. Amer Cer Soc Bull 1990;69:234-8.

[63] Wainer E, Solomon A. Quick Setting Cement. US Patent No 2,391,493, April 21, 1942 1942.

[64] Abdelrazig BEI, Sharp JH, Siddy PA, El-Jazairi B. Chemical reactions in magnesia-phosphate cement. Proc Br Ceram Soc 1984;35:141-54.

[65] Popovics S, Rajendran N, Penko M. Rapid hardening cements for repair of concrete. Aci J 1987;84:64-73.

[66] Soudée E, Péra J. Mechanism of setting reaction in magnesia-phosphate cements. Cem Concr Res 2000;30:315-21.

[67] Neiman R, Sarma A. Setting and thermal reactions of phosphate investments. J Dent Res 1980;59:1478-85.

[68] Wagh A, Jeong S. Chemically bonded phosphate ceramics: I. A dissolution model of formation. J Am Ceram Soc 2003;86:1838–44.

[69] Wagh A, Jeong S. Chemically bonded phosphate ceramics: II. Warm temperature process for alumina ceramics. J Am Ceram Soc 2003;86:1845–49.

[70] Sugama T, Kukacka L. Magnesium monophosphate cements derived from diammonium phosphate solutions. Cem Concr Res 1983;13:407-16.

[71] Sugama T, Kukacka L. Characteristics of magnesium polyphosphate cements derived from ammonium polyphosphate solutions. Cem Concr Res 1983;13:499-506.

[72] Stierli F, Gaidis J, Clayton C. Control of setting time in magnesia-phosphate cement. In: patent U, editor. England1978.

[73] Hall D, Stevens R. Effect of water content on the structure and mechanical properties of magnesia-phosphate cement mortar. J Am Ceram Soc 1998;81:1550-56.

[74] Vondran E, Ewald A, Miller F, Zorn K, Kufner A, Gburek U. Formation and properties of magnesium-ammonium phosphate hexahydrate biocements in the Ca-Mg-PO4 system. Journal of materials science Materials in medicine 2011;22:429-36.

[75] Driessens FCM, Boltong MG, Zapatero MI, Verbeeck RMH, Bonfield W, Bérmúdez O, et al. In vivo behaviour of three calcium phosphate cements and a magnesium phosphate cement. J Mat Sci: Mat Med 1995;6:272-8.

[76] Waselau M, Samii VF, Weisbrode SE, Litsky AS, Bertone AL. Effects of a magnesium adhesive cement on bone stability and healing following a metatarsal osteotomy in horses. Amer J Vet Res 2007;68:370-8.

[77] Moseke C, Saratsis V, Gbureck U. Injectability and mechanical properties of magnesium phosphate cements. J Mat Sci: Mat Med 2011;22:2591-8.

[78] Mestres G, Ginebra M. Novel magnesium phosphate cements with high early strength and antibacterial properties. Acta Biomater 2011;7:1853-61.

[79] Mestres G AM, Bowles W, Huang SH, Aparacio C, Gorr SU, Ginebra MP. Novel cements with high early strength and antibacterial properties and dentin bonding strength of magnesium phosphate cements. Acta Biomater 2013;9:8384-93.

[80] Zhou H, Agarwal AK, Goel VK, Bhaduri SB. Microwave assisted preparation of magnesium phosphate cement (MPC) for orthopedic applications: a novel solution to the exothermicity problem. Materials science & engineering C, Materials for biological applications 2013;33:4288-94.

[81] Yu Y, Wang J, Liu C, Zhang B, Chen H, Guo H, et al. Evaluation of inherent toxicology and biocompatibility of magnesium phosphate bone cement. Coll Surf B: Biointerfaces 2010;76:496-504.

[82] Ewald A, Helmschrott K, Knebl G, Mehrban N, Grover L, Gbureck U. Effect of cold-setting calcium- and magnesium phosphate matrices on protein expression in osteoblastic cells. Journal of biomedical materials research Part B, Applied biomaterials 2011;96:326-32.

[83] Hanifi A, Fathi M, Mir Mohammad Sadeghi H, Varshosaz J. Mg2+ substituted calcium phosphate nano particles synthesis for non viral gene delivery application. J Mat Sci: Mat Med 2010;21:2393-401.

[84] Bhakta G, Mitra S, Maitra A. DNA encapsulated magnesium and manganous phosphate nanoparticles: potential non-viral vectors for gene delivery. Biomaterials 2005;26:2157-63.

[85] Bhakta G, Shrivastava A, Maitra A. Magnesium phosphate nanoparticles can be efficiently used in vitro and in vivo as non-viral vectors for targeted gene delivery. J Biomedl Nanotechnol 2009;5:106-14.

[86] Bhakta G, Nurcombe V, Maitra A, Shrivastava A. DNA-encapsulated magnesium phosphate nanoparticles elicit both humoral and cellular immune responses in mice. Resul Immunol 2014;4:46-53.

[87] Lee J, Farag M, Park E, Lim J, Yun H. A simultaneous process of 3D magnesium phosphate scaffold fabrication and bioactive substance loading for hard tissue regeneration. Materials science & engineering C, Materials for biological applications 2014;36:252-60.

[88] Chen Z, Mao X, Tan L, Friis T, Wu C, Crawford R, et al. Osteoimmunomodulatory properties of magnesium scaffolds coated with β-tricalcium phosphate. Biomaterials 2014;35:8553-65.

[89] Burnell J, Teubner E, Miller A. Normal maturational changes in bone matrix, mineral, and crystal size in the rat. Calcif Tis Int 1980;31:13-9.

[90] Bigi A, Foresti E, Gregorini R, Ripamonti A, Roveri N, Shah J. The role of magnesium on the structure of biological apatites. Calcif Tis Int 1992;50:439-44.

[91] Amjad Z, Koutsoukos P, Nancollas G. The crystallization of hydroxyapatite and fluorapatite in the presence of magnesium ions. J Coll Interface Sci 1984;101:250-6.

[92] Eanes E, Rattner S. The effect of magnesium on apatite formation in seeded supersaturated solutions at pH 7.4. J Dent Res 1981;60:1719-23.

[93] Salimi M, Heughebaert J, Nancollas G. Crystal growth of calcium phosphates in the presence of magnesium ions. Langmuir 1985;1:119-22.

[94] Boskey A, Posner A. Magnesium stabilization of amorphous calcium phosphate: A kinetic study. Mat Res Bull 1974;9:907-16.

[95] Tung M, Tomazic B, Brown W. The effects of magnesium and fluoride on the hydrolysis of octacalcium phosphate. Arch Oral Biol 1992;37:585-91.

[96] Zhou H, Bhaduri S. Novel microwave synthesis of amorphous calcium phosphate nanospheres. J Biomed Mat Res Part B: Appli Biomater 2012;100B:1142-50.

[97] Abbona F, Baronnet A. A XRD and TEM study on the transformation of amorphous calcium phosphate in the presence of magnesium. J Crys Grow 1996;165:98-105.

[98] Boistelle R, Lopez-Valero I, Abbona F. Crystallization of calcium phosphate in the presence of magnesium. Nephrologie 1993;14:265-9.

[99] Cheng P, Grabher J, LeGeros R. Effects of magnesium on calcium phosphate formation. Magnesium 1988;7:123-32.

[100] Bigi A, Falini G, Foresti E, Gazzano M, Ripamonti A, Roveri N. Rietveld Structure Refinements of Calcium Hydroxylapatite Containing Magnesium. Acta Crystallog Sec B: Struct Sci 1996;52:87-92.

[101] Yasukawa A, Ouchi S, Kandori K, Ishikawa T. Preparation and characterization of magnesium-calcium hydroxyapatites. J Mat Chem 1996;6:1401-5.

[102] Boanini E, Gazzano M, Bigi A. Ionic substitutions in calcium phosphates synthesized at low temperature. Acta Biomater 2010;6:1882-94.

[103] Landi E, Logroscino G, Proietti L, Tampieri A, Sandri M, Sprio S. Biomimetic Mg-substituted hydroxyapatite: From synthesis to in vivo behaviour. J Mat Sci: Mat Med 2008;19:239-47.

[104] Bertinetti L, Drouet C, Combes C, Rey C, Tampieri A, Coluccia S, et al. Surface characteristics of nanocrystalline apatites: Effect of Mg surface enrichment on morphology, surface hydration species, and cationic environments. Langmuir 2009;25:5647-54.

[105] Aina V, Lusvardi G, Annaz B, Gibson I, Imrie F, Malavasi G, et al. Magnesium- and strontium-co-substituted hydroxyapatite: the effects of doped-ions on the structure and chemico-physical properties. J Mat Sci: Mat Med 2012;23:2867-79.

[106] Cacciotti I, Bianco A, Lombardi M, Montanaro L. Mg-substituted hydroxyapatite nanopowders: Synthesis, thermal stability and sintering behaviour. J Eur Cer Soc 2009;29:2969-78.

[107] Ioanovici T, Monchau F, Berdich K, Hivart P, Traisnel M, Bereteu L. Influence of magnesium doping on synthesized hydroxyapatite using the wet precipitation method. E-Health Bioeng Conf (EHB), 2011. p. 1-4.

[108] Cacciotti I, Bianco A. High thermally stable Mg-substituted tricalcium phosphate via precipitation. Cer Int 2011;37:127-37.

[109] Ryu H, Hong KS, Lee J, Kim D. Variations of structure and composition in magnesium incorporated hydroxyapatite/β-tricalcium phosphate. J Mat Res 2006;21:428-36.

[110] Kumta P, Sfeir C, Lee D, Olton D, Choi D. Nanostructured calcium phosphates for biomedical applications: novel synthesis and characterization. Acta Biomater 2005;1:65-83.

[111] Legeros R. Calcium phosphates in oral biology and medicine. Basel: Karger 1991.

[112] Xue W, Dahlquist K, Banerjee A, Bandyopadhyay A, Bose S. Synthesis and characterization of tricalcium phosphate with Zn and Mg based dopants. J Mat Sci: Mat Med 2008;19:2669-77.

[113] Lee D, Kumta P. Chemical synthesis and stabilization of magnesium substituted brushite. Mat Sci Eng: C 2010;30:934-43.

[114] Le Geros R. Properties of osteoconductive biomaterials: calcium phosphates. Clin Orthop 2002;39:81-98.

[115] Fan W, Jie W, Han G, Fangping C, Hua H, Changsheng L. Self-setting bioactive calcium–magnesium phosphate cement with high strength and degradability for bone regeneration. Acta Biomater 2008;4:1873–84.

[116] Klammert U, Ignatius A, Wolfram U, Reuther T, Gbureck U. In vivo degradation of low temperature calcium and magnesium phosphate ceramics in a heterotopic model. Acta Biomater 2011;7:3469–75.

[117] Kim D, Kim T, Lee J, Shin K, Jung J, Hwang K, et al. Preparation and in vitro and in vivo performance of magnesium ion substituted biphasic calcium phosphate

spherical microscaffolds as human adipose tissue-derived mesenchymal stem cell microcarriers. J Nanomaterials 2013:9.

[118] Wei J, Jia J, Wu F, Wei S, Zhou H, Zhang H, et al. Hierarchically microporous/macroporous scaffold of magnesium–calcium phosphate for bone tissue regeneration. Biomaterals 2010;31:1260–9.

[119] Li X, Niu Y, Guo H, Chen H, Li F, Zhang J, et al. Preparation and osteogenic properties of magnesium calcium phosphate biocement scaffolds for bone regeneration. J inst 2012;8.

[120] Hussain A, Bessho K, Takahashi K, Tabata Y. Magnesium calcium phosphate as a novel component enhances mechanical/physical properties of gelatin scaffold and osteogenic differentiation of bone marrow mesenchymal stem cells. Tissue Eng Part A 2012;18:768-74.

[121] Mroz W, Budner B, Syroka R, Niedzielski K, Golanski G, Slosarczyk A, et al. In vivo implantation of porous titanium alloy implants coated with magnesium-doped octacalcium phosphate and hydroxyapatite thin films using pulsed laser depostion. Journal of biomedical materials research Part B, Applied biomaterials 2014.

[122] Borges R, Ribeiro S, Marchi J, Yoshimura H. Mechanical characterization of tricalcium phosphate ceramics doped with magnesium. In: Castanho SM, Acchar W, Hotza D, editors. Brazil ceram conf 57: Material Science Forum; 2014. p. 454-9.

[123] Qi G, Zhang S, Khor K, Lye S, Zeng X, Weng W, et al. Osteoblastic cell response on magnesium-incorporated apatite coatings. Appli Surf Sci 2008;225:304–7.

[124] Park J, Ko H, Jang J, Kang H, Suh J. Increased new bone formation with a surface magnesium-incorporated deproteinized porcine bone substitute in rabbit calvarial defects. J Biomed Mater Res 2012;100:834–40.

[125] Zreiqat H, Howlett C, Zannettino A, Evans P, Schulze-Tanzil G, Knabe C, et al. Mechanisms of magnesium-stimulated adhesion of osteoblastic cells to commonly used orthopaedic implants. J Biomed Mater Res 2002;62:175–84.

[126] Revell P, Damien E, Zhang X, Evans P, Howlett C. The effect of magnesium ions on bone bonding to hydroxyapatite coating on titanium alloy implants Key Eng Mat 2004;254-256:447-50.

[127] Chowdhury E, Akaike T. Fibronectin-coated nano-precipitates of calcium-magnesium phosphate for integrin-targeted gene delivery. J Contr Release 2006;116:68-9.

[128] Zhou H, Nedley M, Bhaduri S. The impacts of Mg2+ on strontium phosphate: A preliminary study. Mat Let 2013;113:63-6.

[129] Diba M, Goudouri O, Tapia F, Boccaccini A. Magnesium-containing bioactive polycrystalline silicate-based ceramics and glass-ceramics for biomedical applications. Cur Opi Sol Stat Mat Sci 2014;18:147-67.

[130] George A, Stebbins J. Structure and dynamics of magnesium in silicate melts: a high-temperature Mg-25 NMR study. Am Mineral 1998;83:1022–9.

[131] Oliveira J, Correia R, Fernandes M. Effects of Si speciation on the in vitro bioactivity of glasses. Biomaterials 2002;23:371-9.

[132] Shimoda K, Tobu Y, Hatakeyama M, Nemoto T, Saito K. Structural investigation of Mg local environments in silicate glasses by ultra-high field Mg-25 3QMAS NMR spectroscopy. Am Mineral 2007;92:695–8.

[133] Watts S, Hill R, O'Donnell M, Law R. Influence of magnesia on the structure and properties of bioactive glasses. J Non-Cryst Solids 2010;356:517–24.

[134] Hand R, Tadjiev D. Mechanical properties of silicate glasses as a function of composition. J Non-Cryst Solids 2010;356:2417-23.

[135] Deriano S, Rouxel T, LeFloch M, Beuneu B. Structure and mechanical properties of alkali-alkaline earth-silicate glasses. Phys Chem Glasses 2004;45:37-44.

[136] Verne E. Early stage reactivity and in vitro behavior of silica-based bioactive glasses and glass-ceramics. J Mater Sci: Mater Med 2009;20:75–87.

[137] Albelda SB, CA. Integrins and other cell-adhesion molecules. FASEB J 1990;4:2868–80.

[138] Zhang D. Antibacterial effects and dissolution Behavior of six bioactive glasses. J Biomed Mater Res, Part A 2010;93:475-83.

[139] Dietrich E, Oudadesse H, Lucas-Girot A, Le Gal Y, Jeanne S, Cathelineau G. Effects of Mg and Zn on the surface of doped melt-derived glass for biomaterials applications. Appl Surf Sci 2008;255:391-5.

[140] Erol M, Ozyuguran A, Celebican O. Synthesis, characterization, and in vitro bioactivity of Sol-Gel-derived Zn, Mg, and Zn-Mg Co-doped bioactive glasses. Chem Eng Technol 2010;33:1066-74.

[141] Saboori A. Sol-Gel preparation, characterisation and in vitro bioactivity of Mg containing bioactive glass. Adv Appl Ceram 2009;108:155-61.

[142] Ma J, Chen C, Wang D, Jiao Y, Sh J. Effect of magnesia on the degradability and bioactivity of Sol-Gel derived SiO2–CaO–MgO–P2O5 system glasses. Colloids Surf B 2010;81:87-95.

[143] Tulyaganov D. Synthesis, bioactivity and preliminary biocompatibility studies of glasses in the system CaO–MgO–SiO2–Na2O–P2O5–CaF2. J Mater Sci: Mater Med 2011;22:217–27.

[144] Goel A, Rajagopal R, Ferreira J. Influence of strontium on structure, sintering and biodegradation behaviour of CaO–MgO–SrO–SiO2–P2O5–CaF2 glasses. Acta Biomater 2011;7:4071–80.

[145] Varanasi V, Owyoung J, Saiz E, Marshall S, Marshall G, Loomer P. The ionic products of bioactive glass particle dissolution enhance periodontal ligament fibroblast osteocalcin expression and enhance early mineralized tissue devel development. J Biomed Mater Res, Part A 2011;98:177–84.

[146] Vedel E, Arstila H, Yla nen H, Hupa L, Hupa M. Predicting physical and chemical properties of bioactive glasses from chemical composition. part 1: viscosity characteristics. Glass Technol: Eur J Glass Sci Technol, Part A 2008;49:251–9.

[147] Cacaina D, Yla nen H, Hupa M, Simon S. Study of yttrium containing bioactive glasses behaviour in simulated body fluid. J Mater Sci: Mater Med 2006;17:709–16.

[148] Covani U. Biomaterials for orthopedics: a roughness analysis by atomic force microscopy. J Biomed Mater Res, Part A, 2007;82:723-30.

[149] Josset Y. Influence of physicochemical reactions of bioactive glass on the behavior and activity of human osteoblasts in vitro. J Biomed Mater Res, Part A 2003;67:1205-18.

[150] Balamurugan A, Balossier G, Michel J, Kannan S, Benhayoune H, Rebelo A, et al. Sol gel derived SiO(2)-CaO-MgO-P(2)O(5) bioglass system-preparation and in vitro characterization. Journal of biomedical materials research Part B, Applied biomaterials 2007;83:546-53.

[151] Cao W, Hench L. Bioactive Materials. Ceram Int 1996;22:493-507.

[152] Janning C. Magnesium hydroxide temporarily enhancing osteoblast activity and decreasing the osteoclast number in peri-implant bone remodelling. Acta Biomater 2010;6:1861–8.

[153] Chen G, Ushida T, Tateishi T. Scaffold design for tissue engineering. Macromolec Biosci 2002;2:67-77.

[154] Murugan R, Ramakrishna S. Design strategies of tissue engineering scaffolds with controlled fiber orientation. Tissue Eng 2007;13:1845–66.

[155] Rezwan K, Chen Q, Blaker J, Boccaccini A. Biodegradable and bioactive porous polymer/inorganic composite scaffolds for bone tissue engineering. Biomaterials 2006;27:3413–31.

[156] Bretcanu O, Chatzistavrou X, Paraskevopoulos K, Conradt R, Thompson I, Boccaccini A. Sintering and Crystallisation of 45S5 Bioglass (R) Powder. J Eur Ceram Soc 2009;29:3299–306.

[157] Brink M, Turunen T, Happonen R, Yli-Urpo A. Compositional dependence of bioactivity of glasses in the system Na2O–K2O–MgO–CaO–B2O3–P2O5–SiO2. J Biomed Mater Res 1997;37:114-21.

[158] Salinas A, Roman J, Vallet-Regi M, Oliveira J, Correia R, Fernandes M. In vitro bioactivity of glass and glass-ceramics of the 3CaO x P2O5-CaO x SiO2-CaO x MgO x 2SiO2 system. Biomaterials 2000;21:251–7.

[159] Tamura J. Mechanical and biological properties of two types of bioactive bone cements containing MgO–CaO–SiO2–P2O5–CaF2 glass and glass-ceramic powder. J Biomed Mater Res 1996;30:89-94.

[160] Shinzato S, Nakamura T, Tamura J, Kokubo T, Kitamura Y. Bioactive bone cement: effects of phosphoric ester monomer on mechanical properties and osteoconductivity. J Biomed Mater Res 2001;56:571-7.

[161] Boesel L, Fernandes M, Reis R. The behavior of novel hydrophilic composite bone cements in simulated body fluids. J Biomed Mater Res, Part B 2004;70:368-77.

[162] Shinzato S, Nakamura T, Kawanabe K, Kokubo T. PMMA-based bioactive cement: Effect of caf2 on osteoconductivity and histological change with time. J Biomed Mater Res, Part B 2003;65:262-71.

[163] Yoshihara S, Kokubo T, Nishimura N, Yamamuro T, Nakamura T. Effects of glass composition on compressive strength of bioactive cement-based on Cao–Sio2–P2o5 glass powders. J Mater Sci: Mater Med 1994;5:123-9.

[164] Matsuya S, Matsuya Y, Ohta M. Structure of bioactive glass and its application to glass ionomer cement. Dent Mater J 1999;18:155-66.

[165] Oliveira J, Correia R, Fernandes M. Surface modifications of a glass and a glass-ceramic of the MgO-3CaO.P2O5-SiO2 system in a simulated body fluid. Biomaterials 1995;16:849–54.

[166] Kolan K, Leu M, Hilmas G, Brown R, Velez M. Fabrication of 13-93 bioactive glass scaffolds for bone tissue engineering using indirect selective laser sintering. Biofabrication 2011;3:025004.

[167] Brown R, Day D, Day T, Jung S, Rahaman M, Fu Q. Growth and differentiation of osteoblastic cells on 13-93 bioactive glass fibers and scaffolds. Acta Biomater 2008;4:387–96.

[168] Fu Q, Rahaman M, Bal B, Huang W, Day D. Preparation and bioactive characteristics of a porous 13-93 glass, and fabrication into the articulating surface of a proximal tibia. J Biomed Mater Res, Part A 2007;82:222-9.

[169] Fu Q, Rahaman M, Fu H, Liu X. Silicate, borosilicate, and borate bioactive glass scaffolds with controllable degradation rate for bone tissue engineering applications. I. preparation and in vitro degradation. J Biomed Mater Res, Part A 2010;95:164-71.

[170] Fu Q, Rahaman M, Bal B, Kuroki K, Brown R. In vivo evaluation of 13-93 bioactive glass scaffolds with trabecular and oriented microstructures in a subcutaneous rat Implantation model. J Biomed Mater Res, Part A 2010;95:235-44.

[171] Doiphode N, Huang T, Leu M, Rahaman M, Day D. Freeze extrusion fabrication of 13-93 bioactive glass scaffolds for bone repair. Journal of materials science Materials in medicine 2011;22:515-23.

[172] Liu X, Rahaman M, Fu Q, Tomsia A. Porous and strong bioactive glass (13–93) scaffolds prepared by unidirectional freezing of camphene-based suspensions. Acta Biomater 2012;8:415-23.

[173] Wang X, Li X, Ito A, Sogo Y. Synthesis and characterization of hierarchically macroporous and mesoporous CaO-MO-SiO(2)-P(2)O(5)(M=Mg, Zn, Sr) bioactive glass scaffolds. Acta Biomater 2011;7:3638-44.

[174] Russias J. Fabrication and in vitro characterization of three-dimensional organic/inorganic scaffolds by robocasting. J Biomed Mater Res, Part A 2007;83:434–45.

[175] Moimas L, De Rosa G, Sergo V, Schmid C. Bioactive porous scaffolds for tissue engineering applications: investigation on the degradation process by raman spectroscopy and scanning electron microscopy. J Appl Biomater Biomech 2006;4:102–9.

[176] Hench L, Andersoon O. Bioactive glass coatings. An introd bioceram 1993:239–60.

[177] Lopez-Esteban S, Saiz E, Fujino S, Oku T, Suganuma K, Tomsia A. Bioactive Glass Coatings for Orthopedic Metallic Implants. J Eur Ceram Soc 2003;23:2921–30.

[178] Keranen P, Moritz N, Alm J, Ylanen H, Kommonen B, Aro H. Bioactive glass microspheres as osteopromotive inlays in macrotextured surfaces of Ti and CoCr alloy bone implants: trapezoidal surface grooves without inlay most efficient in resisting torsional forces. J Mech Behav Biomed 2011;4:1483–91.

[179] Lotfibakhshaiesh N, Brauer D, Hill R. Bioactive glass engineered coatings for Ti6Al4V alloys: influence of strontium substitution for calcium on sintering behaviour. J Non-Cryst Solids 2010;356:2583-90.

[180] Zhao Y, Song M, Liu J. Characteristics of bioactive glass coatings obtained by pulsed laser deposition. Surf Interface Anal 2008;40:1463–8.

[181] Pazo A, Saiz E, Tomsia A. Silicate glass coatings on ti-based implants. Acta Mater 1998;46:2551–8.

[182] Gomez-Vega J. Novel bioactive functionally graded coatings on Ti6Al4V. Adv Mater 2000;12:894–8.

[183] Liu X, Xie Z, Zhang C, Pan H, Rahaman M, Zhang X, et al. Bioactive borate glass scaffolds: in vitro and in vivo evaluation for use as a drug delivery system in the treatment of bone infection. Journal of materials science Materials in medicine 2010;21:575-82.

[184] Vallet-Regí M, Ragel C, Salinas A. Glasses with medical applications. Eur Jou Ino Chem 2003;2003.

[185] Zhou H, Nabiyouni M, Lin B, Bhaduri SB. Fabrication of novel poly(lactic acid)/amorphous magnesium phosphate bionanocomposite fibers for tissue engineering applications via electrospinning. Materials science & engineering C, Materials for biological applications 2013;33:2302-10.

[186] Blanc V, Henderson JO, Newberry EP, Kennedy S, Luo J, Davidson NO. Targeted deletion of the murine apobec-1 complementation factor (acf) gene results in embryonic lethality. Molecular and cellular biology 2005;25:7260-9.

[187] Matsubara T, Kida K, Yamaguchi A, Hata K, Ichida F, Meguro H, et al. BMP2 regulates Osterix through Msx2 and Runx2 during osteoblast differentiation. J Biol Chem 2008;283:29119-25.

[188] Oujo B, Munoz-Felix JM, Arevalo M, Nunez-Gomez E, Perez-Roque L, Pericacho M, et al. L-endoglin overexpression increases renal fibrosis after unilateral ureteral obstruction. PloS one 2014;9:e110365.

[189] Hsieh YH, Juliana MM, Hicks PH, Feng G, Elmets C, Liaw L, et al. Papilloma development is delayed in osteopontin-null mice: implicating an antiapoptosis role for osteopontin. Cancer research 2006;66:7119-27.

[190] Gaur T, Hussain S, Mudhasani R, Parulkar I, Colby JL, Frederick D, et al. Dicer inactivation in osteoprogenitor cells compromises fetal survival and bone formation, while excision in differentiated osteoblasts increases bone mass in the adult mouse. Developmental biology 2010;340:10-21.

[191] Roberts SJ, Ng BY, Filler RB, Lewis J, Glusac EJ, Hayday AC, et al. Characterizing tumor-promoting T cells in chemically induced cutaneous carcinogenesis. Proceedings of the National Academy of Sciences of the United States of America 2007;104:6770-5.

[192] Zhou H, Touny AH, Bhaduri SB. Fabrication of novel PLA/CDHA bionanocomposite fibers for tissue engineering applications via electrospinning. Journal of materials science Materials in medicine 2011;22:1183-93.

[193] Darder M, Aranda P, Ruiz-Hitzky E. Bionanocomposites: A New Concept of Ecological, Bioinspired, and Functional Hybrid Materials. Adv Mater 2007;19:1309-19.

[194] Maguire ME, Cowan JA. Magnesium chemistry and biochemistry. Biometals 2002;15:203-10.

[195] Witte F, Kaese V, Haferkamp H, Switzer E, Meyer-Lindenberg A, Wirth CJ, et al. In vivo corrosion of four magnesium alloys and the associated bone response. Biomaterials 2005;26:3557-63.

[196] Zhang E, Xu L, Yu G, Pan F, Yang K. In vivo evaluation of biodegradable magnesium alloy bone implant in the first 6 months implantation. Journal of biomedical materials research Part A 2009;90:882-93.

[197] Ishizaki T, Kudo R, Omi T, Teshima K, Sonoda T, Shigematsu I, et al. Magnesium hydroxide/magnesium phosphate compounds composite coating for corrosion protection of magnesium alloy by a combination process of chemical conversion and steam curing. Mater Lett 2012;68:122-5.

[198] Bai K, Zhang Y, Fu Z, Zhang C, Cui X, Meng E, et al. Fabrication of chitosan/magnesium phosphate composite coating and the in vitro degradation properties of coated magnesium alloy. Mat Let 2012;73:59-61.

[199] Lu J, Wei J, Yan Y, Li H, Jia J, Wei S, et al. Preparation and preliminary cytocompatibility of magnesium doped apatite cement with degradability for bone regeneration. Journal of materials science Materials in medicine 2011;22:607-15.

[200] Wu F, Wei J, Guo H, Chen F, Hong H, Liu C. Self-setting bioactive calcium-magnesium phosphate cement with high strength and degradability for bone regeneration. Acta Biomater 2008;4:1873-84.

[201] Paul W, Sharma CP. Effect of calcium, zinc and magnesium on the attachment and spreading of osteoblast like cells onto ceramic matrices. Journal of materials science Materials in medicine 2007;18:699-703.

[202] Landi E, Tampieri A, Mattioli-Belmonte G, Celotti M, Sandri M, Gigante A, et al. Biomimetic Mg-and Mg, CO3-substituted hydroxyapatites: synthesis characterization and in vitro behaviour. J Eur Cer Soc 2006;26:2593-601.

[203] Roy M, Bose S. Osteoclastogenesis and osteoclastic resorption of tricalcium phosphate: effect of strontium and magnesium doping. Journal of biomedical materials research Part A 2012;100:2450-61.

[204] Combes C, Rey C. Amorphous calcium phosphates: Synthesis, properties and uses in biomaterials. Acta Biomater 2010;6:3362-78.

[205] Dorozhkin S. Amorphous calcium (ortho)phosphates. Acta Biomater 2010;6:4457-75.

[206] Simon C, Antonucci J, Liu D, Skrtic D, Bioact J. In vitro cytotoxicity of amorphous calcium phosphate composites. J Bioact Compat Polym 2005;20:279-95.

[207] Ma Z, Chen F, Zhu Y, Cui T, Liu X. Amorphous calcium phosphate/poly(d,l-lactic acid) composite nanofibers: Electrospinning preparation and biomineralization. J Colloid Interface Sci 2011;359:371-9.

[208] Boskey A, Posner A. Conversion of amorphous calcium phosphate to microcrystalline hydroxyapatite. A pH-dependent, solution-mediated, solid-solid conversion. J Phys Chem 1973;77:2313-7.

[209] Posner A, Betts F. Synthetic amorphous calcium phosphate and its relation to bone mineral structure. Acc Chem Res 1975;8:273-81.

[210] Blumenthal N, Betts F, Posner A. Stabilization of amorphous calcium phosphate by Mg and ATP. Calcif Tis Res 1977;23:245-50.

[211] Kurtulus G, Tas A. Transformations of neat and heated struvite (MgNH4PO4·6H2O). Mater Lett 2011;65:2883-6.

[212] Shive M, Anderson J. Biodegradation and biocompatibility of PLA and PLGA microspheres. Advanced drug delivery reviews 1997;28:5-24.

[213] Wuisman P, Smit T. Bioresorbable polymers: heading for a new generation of spinal cages. Eur Spine J 2006;15:133-48.

[214] Denti M, Randelli P, Vetere D, Moioli M, Tagliabue M. Bioabsorbable interference screws for bone-patellar tendon-bone anterior cruciate ligament reconstruction: clinical and computerized tomography results of four different models. A prospective study. J Orthop Traumatol 2004;5:151-5.

[215] Schiffmana J, Schauera C. A Review: Electrospinning of Biopolymer Nanofibers and their Applications. Polym Rev 2008;48:317-52.

[216] A. Oyane H-MK, T. Furuya, T. Kokubo, T. Miyazaki, and T. Nakamura. Preparation and assessment of revised simulated body fluids. J Biomed Mater Res A May 2003;65A:188-95.

[217] Kim H, Lee H, Knowles J. Electrospinning biomedical nanocomposite fibers of hydroxyapatite/poly(lactic acid) for bone regeneration. Journal of biomedical materials research Part A 2006;79A:643-9.

[218] Jalota S, Bhaduri S, Tas A. Using a synthetic body fluid (SBF) solution of 27 mM HCO3− to make bone substitutes more osteointegrative. Mater Sci Eng C 2008;28:129-40.

[219] Zhou H, Lawrence L, Touny A, Bhaduri S. Biomimetic coating of bisphosphonate incorporated CDHA on Ti6Al4V. Journal of materials science Materials in medicine 2012;23:365-74.

[220] Zhou H, Bhaduri S. J Biomater Sci Polym Ed 2012:1-13.

[221] Deng XL, Sui G, Zhao ML, Chen GQ, Yang XP. Poly(L-lactic acid)/hydroxyapatite hybrid nanofibrous scaffolds prepared by electrospinning. J Biomater Sci Polym Ed 2007;18:117-30.

[222] Loher S, Reboul V, Brunner T, Simonet M, Dora C, Neuenschwander P, et al. Improved degradation and bioactivity of amorphous aerosol derived tricalcium phosphate nanoparticles in poly(lactide-co-glycolide). Nanotechnology 2006;17:2054-61.

[223] Yoon K, Cho D, Yu S, Kim K, Jeon Y, Sung J. The Change of Bone Metabolism in Ovariectomized Rats : Analyses of MicroCT Scan and Biochemical Markers of Bone Turnover. J Korean Neurosurg Soc 2012;51:323-7.

[224] Lutz LJ, Karl JP, Rood JC, Cable SJ, Williams KW, Young AJ, et al. Vitamin D status, dietary intake, and bone turnover in female Soldiers during military training: a longitudinal study. Journal of the International Society of Sports Nutrition 2012;9:38.

[225] Jeon E, Yun YR, Kang W, Lee S, Koh YH, Kim HW, et al. Investigating the role of FGF18 in the cultivation and osteogenic differentiation of mesenchymal stem cells. PloS one 2012;7:e43982.

[226] Okamoto H, Matsumi Y, Hoshikawa Y, Takubo K, Ryoke K, Shiota G. Involvement of microRNAs in regulation of osteoblastic differentiation in mouse induced pluripotent stem cells. PloS one 2012;7:e43800.

[227] Lai CC, Singer L, Armstrong WD. Bone composition and phosphatase activity in magnesium deficiency in rats. The Journal of bone and joint surgery American volume 1975;57:516-22.

[228] Zhao SF, Jiang QH, Peel S, Wang XX, He FM. Effects of magnesium-substituted nanohydroxyapatite coating on implant osseointegration. Clinical oral implants research 2013;24 Suppl A100:34-41.

[229] Park JW, Kim YJ, Jang JH, Song H. Osteoblast response to magnesium ion-incorporated nanoporous titanium oxide surfaces. Clinical oral implants research 2010;21:1278-87.

[230] Pietak A, Mahoney P, Dias GJ, Staiger MP. Bone-like matrix formation on magnesium and magnesium alloys. Journal of materials science Materials in medicine 2008;19:407-15.

[231] Kircelli F, Peter ME, Sevinc Ok E, Celenk FG, Yilmaz M, Steppan S, et al. Magnesium reduces calcification in bovine vascular smooth muscle cells in a dose-dependent manner. Nephrology, dialysis, transplantation : official publication of the European Dialysis and Transplant Association - European Renal Association 2012;27:514-21.

[232] Liu H. World Scientific Publishing Co Pte Ltd 2007:1-51.

[233] Braun S. USA2005.

[234] Donahue RE, Kessler SW, Bodine D, McDonagh K, Dunbar C, Goodman S, et al. Helper virus induced T cell lymphoma in nonhuman primates after retroviral mediated gene transfer. The Journal of experimental medicine 1992;176:1125-35.

[235] Wagner D. calcium phosphate nanoparticles synthesis and manufacture using microwave processing for biomedical applications. Toledo, Ohio: University of Toledo; 2011.

[236] Feigner JHK, R.; Sridhar, C.N.; Wheeler, C.J.; Tsai, Y.J.; Border, R.; Ramsey, P.; Martin, M.; Feigner, P. L. Enhanced gene delivery and mechanism studies with a novel series of cationic lipid formulations. The journal of biological chemistry 1994;269:2550-61.

[237] Leong KW, Mao HQ, Truong-Le VL, Roy K, Walsh SM, August JT. DNA-polycation nanospheres as non-viral gene delivery vehicles. J Control Release 1998;53:183-93.

[238] Niidome T, Huang L. Gene therapy progress and prospects: nonviral vectors. Gene therapy 2002;9:1647-52.

[239] Ogris M, Wagner E. Tumor-targeted gene transfer with DNA polyplexes. Somatic cell and molecular genetics 2002;27:85-95.

[240] Bhakta GM, S.;Maitra, A. DNA encapsulated magnesium and manganous phosphate nanoparticles: potential non-viral vectors for gene delivery. Biomaterials 2004;26:2157-63.

[241] Jain TKR, I.; De, T.K.; Maitra, A.N. Nanometer silica particles encapsulating active compounds: a novel ceramic drug carrier. J Am Chem Soc 1998;120:11092-5.

[242] Bose S, Tarafder S. Calcium phosphate ceramic systems in growth factor and drug delivery for bone tissue engineering: a review. Acta Biomater 2012;8:1401-21.

[243] Epple MG, K.; Heumann R.; Klesing J.; Kovtun, A.; Neumann, S.; Sokolova, V. Application of calcium phosphate nanoparticles in biomedicine. J Mate Chem 2009;20:18-23.

[244] Graham FL, van der Eb AJ. A new technique for the assay of infectivity of human adenovirus 5 DNA. Virology 1973;52:456-67.

[245] Chowdhury EH, Kunou M, Nagaoka M, Kundu AK, Hoshiba T, Akaike T. High-efficiency gene delivery for expression in mammalian cells by nanoprecipitates of Ca-Mg phosphate. Gene 2004;341:77-82.

[246] Dasgupta S, Banerjee SS, Bandyopadhyay A, Bose S. Zn- and Mg-doped hydroxyapatite nanoparticles for controlled release of protein. Langmuir 2010;26:4958-64.

[247] Nabiyouni M, Bhaduri S. Magnesium substitution in the structure of orthopedic nanoparticle: a comparison between amorphous magnesium phosphates, calcium magnesium phosphates, and hydroxyapatites. 2014.

[248] Aldevron. 2013.

[249] Felin JE, Mayo JL, Loos TJ, Jensen JD, Sperry DK, Gaufin SL, et al. Nuclear variants of bone morphogenetic proteins. BMC cell biology 2010;11:20.

[250] Jiang X, Qu W, Pan D, Ren Y, Williford JM, Cui H, et al. Plasmid-templated shape control of condensed DNA-block copolymer nanoparticles. Adv Mater 2013;25:227-32.

[251] Slowing, II, Vivero-Escoto JL, Wu CW, Lin VS. Mesoporous silica nanoparticles as controlled release drug delivery and gene transfection carriers. Advanced drug delivery reviews 2008;60:1278-88.

[252] Panyam J, Labhasetwar V. Biodegradable nanoparticles for drug and gene delivery to cells and tissue. Advanced drug delivery reviews 2003;55:329-47.

[253] Desai MP, Labhasetwar V, Walter E, Levy RJ, Amidon GL. The mechanism of uptake of biodegradable microparticles in Caco-2 cells is size dependent. Pharmaceutical research 1997;14:1568-73.

[254] Maitra A. Calcium phosphate nanoparticles: second-generation nonviral vectors in gene therapy. Expert review of molecular diagnostics 2005;5:893-905.

[255] Chenoweth W, Maginnis E, Rayburn D, Williams S. Materials for Non-Viral Gene Delivery. 2009.

[256] Chowdhury EH, Maruyama A, Kano A, Nagaoka M, Kotaka M, Hirose S, et al. pH-sensing nano-crystals of carbonate apatite: effects on intracellular delivery and release of DNA for efficient expression into mammalian cells. Gene 2006;376:87-94.

[257] Pouton CW, Wagstaff KM, Roth DM, Moseley GW, Jans DA. Targeted delivery to the nucleus. Advanced drug delivery reviews 2007;59:698-717.

[258] Dean DA, Strong DD, Zimmer WE. Nuclear entry of nonviral vectors. Gene therapy 2005;12:881-90.

[259] van der Aa MA, Mastrobattista E, Oosting RS, Hennink WE, Koning GA, Crommelin DJ. The nuclear pore complex: the gateway to successful nonviral gene delivery. Pharmaceutical research 2006;23:447-59.

[260] Yang W, Musser SM. Visualizing single molecules interacting with nuclear pore complexes by narrow-field epifluorescence microscopy. Methods 2006;39:316-28.

[261] Roy I, Ohulchanskyy TY, Bharali DJ, Pudavar HE, Mistretta RA, Kaur N, et al. Optical tracking of organically modified silica nanoparticles as DNA carriers: a nonviral, nanomedicine approach for gene delivery. Proceedings of the National Academy of Sciences of the United States of America 2005;102:279-84.

[262] Iconaru S, Motelica-Heino M, Predoi D. Study on europium-doped hydroxyapatite nanoparticles by fourier transform infrared spectroscopy and their antimicrobial properties. J Spectroscopy 2013;2013:10.

[263] Nabiyouni M, Zhou H, Bhaduri S. Microwave assisted solution combustion synthesis (MASCS) of europium (Eu) doped chlorapatite nanowhiskers. Mat Let 2013;108:54-7.